USE STABLE ISOTOPES TO INVESTIGATE MICROBIAL H_2 AND N_2O PRODUCTION

By

Hui Yang

A DISSERTATION

Submitted to
Michigan State University
in partial fulfillment of the requirements
for the degree of

Biochemistry and Molecular Biology - Doctor of Philosophy

2015

ABSTRACT

USE STABLE ISOTOPES TO INVESTIGATE MICROBIAL H_2 AND N_2O PRODUCTION

By

Hui Yang

Stable isotopes can be a useful tool in studying the basic processes involved in enzymatic catalysis. Isotope effects are quantifiable values related to the substitution of isotopes. It derives from the difference in zero-point energies. In contrast to non-catalyzed reactions, enzyme-catalyzed reactions involve multiple steps, the overall isotope effects are the sum of the isotope effects in each step. There are two major kinds of isotope effects, equilibrium isotope effects (EIEs) and kinetic isotope effects (KIEs). Each of them can provide us insights into different states in the reaction. This thesis describes several researches related to using the stable isotopes to study microbial metabolism.

It is demonstrated in Chapter 2 that a method is developed for the measurement of H isotope fractionation patterns in hydrogenases. After the development of the method, a detailed study of the H_2 metabolism catalyzed by different hydrogenases is presented in Chapter 3. The methods developed in hydrogenase studies were deployed in nitric oxide reductase-catalyzed N_2O production studies, which is described in Chapter 4.

TABLE OF CONTENTS

LIST OF TABLES

LIST OF FIGURES

CHAPTER 1

INTRODUCTION

In 1929 Giauque et al. discovered that the oxygen atom has two heavy isotopes, ^{17}O and ^{18}O.[1] This finding led to speculation that hydrogen must also have a heavy isotope based on the accurate determination of the molecular weight of H_2O.[2] Indeed, in 1932 Urey et al. reported spectroscopic evidence of deuterium for the first time.[3] These experiments served as the foundation for the discovery of pure heavy water[4] and the formation of the theory of zero-point energy and isotope effects,[5] which set the cornerstone for an explosion of research into the usage of isotopes and ultimately a Nobel Prize for Urey.

Isotopes are atoms of the same element that behave similarly in chemical reactions but have a different mass due to the different numbers of neutrons they are carrying. Stable isotopes are valuable tools in chemistry, biology, and biogeochemistry as tracers, internal standards, and mechanistic probes.[6] Many of the studies involve using different isotopes at enriched levels or radioactive isotopes, which are easy to detect. However, as the sensitivity of mass spectrometers increases, one can perform experiments using stable isotopes at natural abundance levels to study chemical and biochemical problems. In this chapter, the theory of isotope effects is briefly introduced, followed by a summary of key applications of stable isotopes in various research applications.

Nomenclature

The abundance of low-mass isotopes (H, O, N and S) in a compound is normally reported as the δ (delta) value in parts per thousand (‰ or permil). The δ value is calculated by the following equation (Equation 1):[7]

$$\delta = (R_x/R_s - 1)*1000 \quad (1)$$

where R_x and R_s are the ratios of the heavy to light isotope in the sample and standard, respectively. Table 1 lists the isotopes used in our research and their corresponding standards.

Table 1: The isotopes and their respective standards used in our studies.

Isotope	Ratios measured	Standard	Absolute abundance ratio (R) of standard
H	$^{2}H/^{1}H$	VSMOW[a]	$1.5575*10^{-4}$
N	$^{15}N/^{14}N$	Atmospheric N_2	$3.677*10^{-3}$
O	$^{18}O/^{16}O$	VSMOW[a]	$2.0052*10^{-3}$

[a]VSMOW (Vienna Standard Mean Ocean Water) is used as a standard for both H and O isotopes.[8]

The basics of isotope effects

In a chemical reaction, the phenomenon of isotopically-substituted molecules reacting at different rates and therefore fractionating[1] is known as the isotope effect. Although substitution of one isotope with the other changes the reaction rate, it will not alter the reaction coordinate (Figure 1), whose curvature depicts the potential energies of the substrate, transition state(s), and product. Isotope effects arise because of the nature of all chemical bonds, which can be described as harmonic oscillators. The energy of a chemical bond is equal to:

[1] Fractionation is the change in the relative proportions of various isotopes in molecules during a reaction.

$$E = \tfrac{1}{2}(\hbar\nu) \quad (2)$$

where $\hbar$ is Planck's constant over 2π ($h/2\pi$) and ν is the vibrational frequency. In addition, the vibrational frequency of a bond is inversely proportional to the square root of the reduced mass (i.e. $\nu \propto \frac{1}{\sqrt{\mu}}$) where

$$\mu = m_1m_2/(m_1+m_2) \quad (3)$$

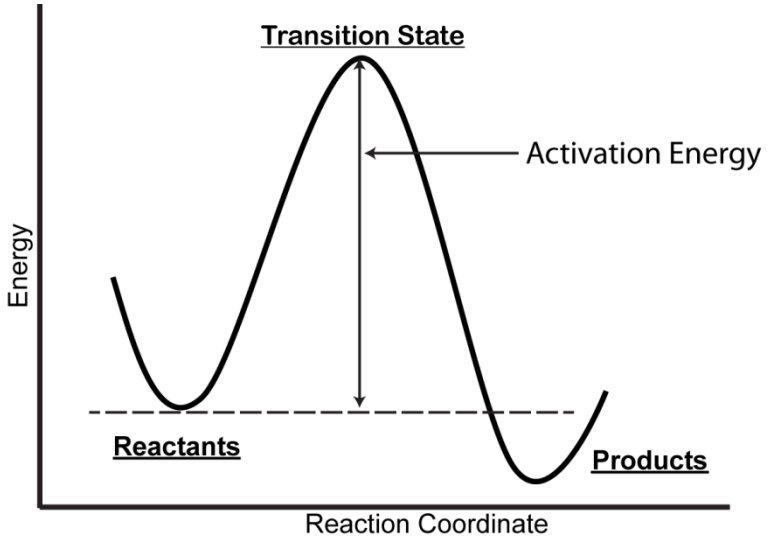

Figure 1: A simplified characterization of a hypothetical reaction coordinate representing progress along a reaction pathway. Isotopic substitution does not change the shape of the reaction coordinate.

Because heavy isotopes give rise to larger reduced masses, which in turn lead to lower vibrational frequencies, chemical bonds with heavy isotopes will have lower zero-point energies (ZPE, Figure 2).[9] It is this difference in zero-point energy that is the basis for isotope effects.

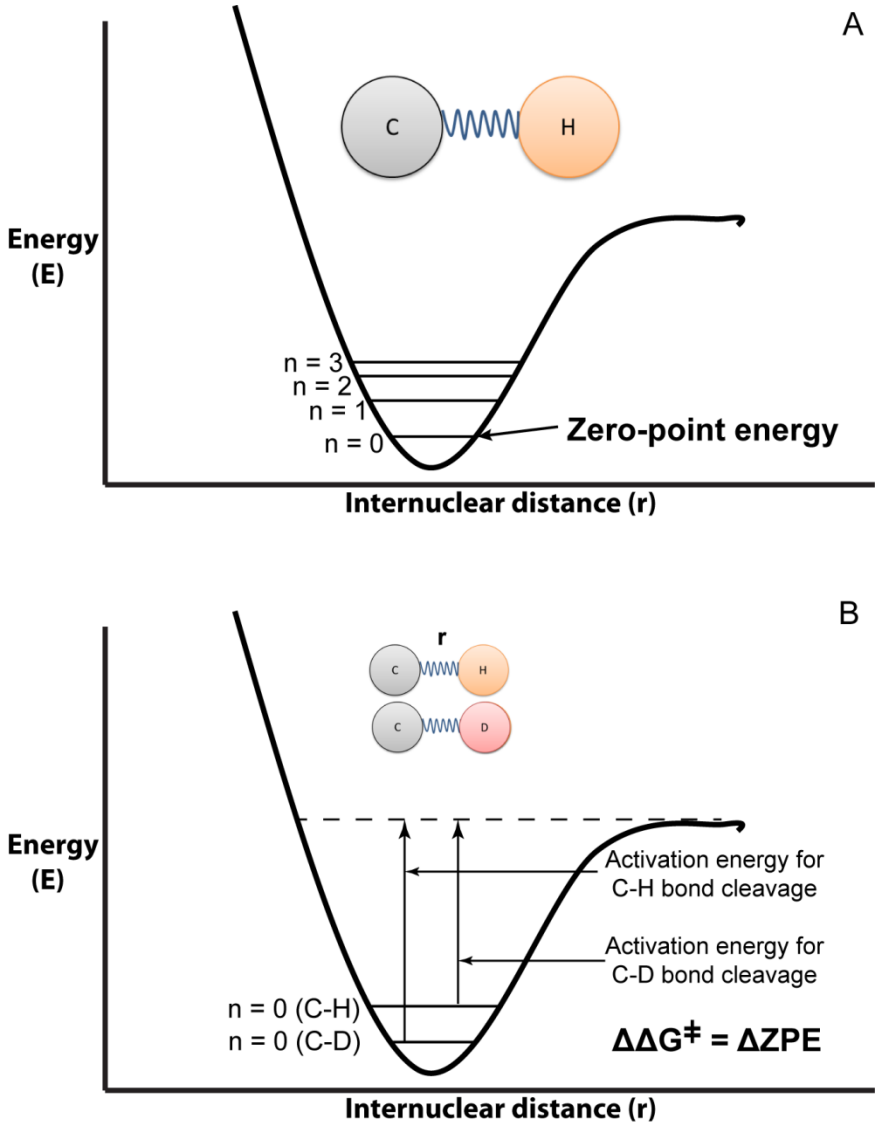

Figure 2: A picture depicting the zero-point energy and its causal relationship with the kinetic isotope effects. 2A shows the different quantum energy states of a typical C-H bond; the lowest possible energy level is called zero-point energy. In 2B, the hypothetical cleavage of a C-H and C-D bond is compared to highlight that the difference in activation energies between the two events is a result of the difference in zero-point energies of the two bonds.

There are two fundamentally different types of isotope effects – equilibrium isotope effects and kinetic isotope effects. Equilibrium isotope effects (EIEs) are the differences between $R_{substrate}$ and $R_{product}$ and arise from the differences in zero-point energies between the substrate and the product (Figure 3A), which, in turn, result in a change in the ratio of the equilibrium constants for the heavy and light isotopes (Equation 4).[10] Conversely, kinetic isotope effects (KIEs) are caused by the differences of zero-point energies between the ground state and the transition state, which give rise to the change in rate constants of the heavy and light isotopes (Equation 5).[7]

$$\text{EIE} = K_{light}/K_{heavy} \quad (4)$$

$$\text{KIE} = k_{light}/k_{heavy} \quad (5)$$

where K_{light} and K_{heavy} are the equilibrium constants of the light and heavy isotopes, respectively, and k_{light} and k_{heavy} are the rate constants for the light and heavy isotopes, respectively. Because the KIE and EIE are closely associated with the transition states and intermediates, isotope effects can be a valuable tool in elucidating the reaction mechanism. It should be noted, however, that due to the possibility of atom tunneling (especially for hydrogen), some isotope effects cannot be explained simply by classical transition state theory. For additional information on hydrogen atom tunneling, please refer to a review published by Kohen et al.[11]

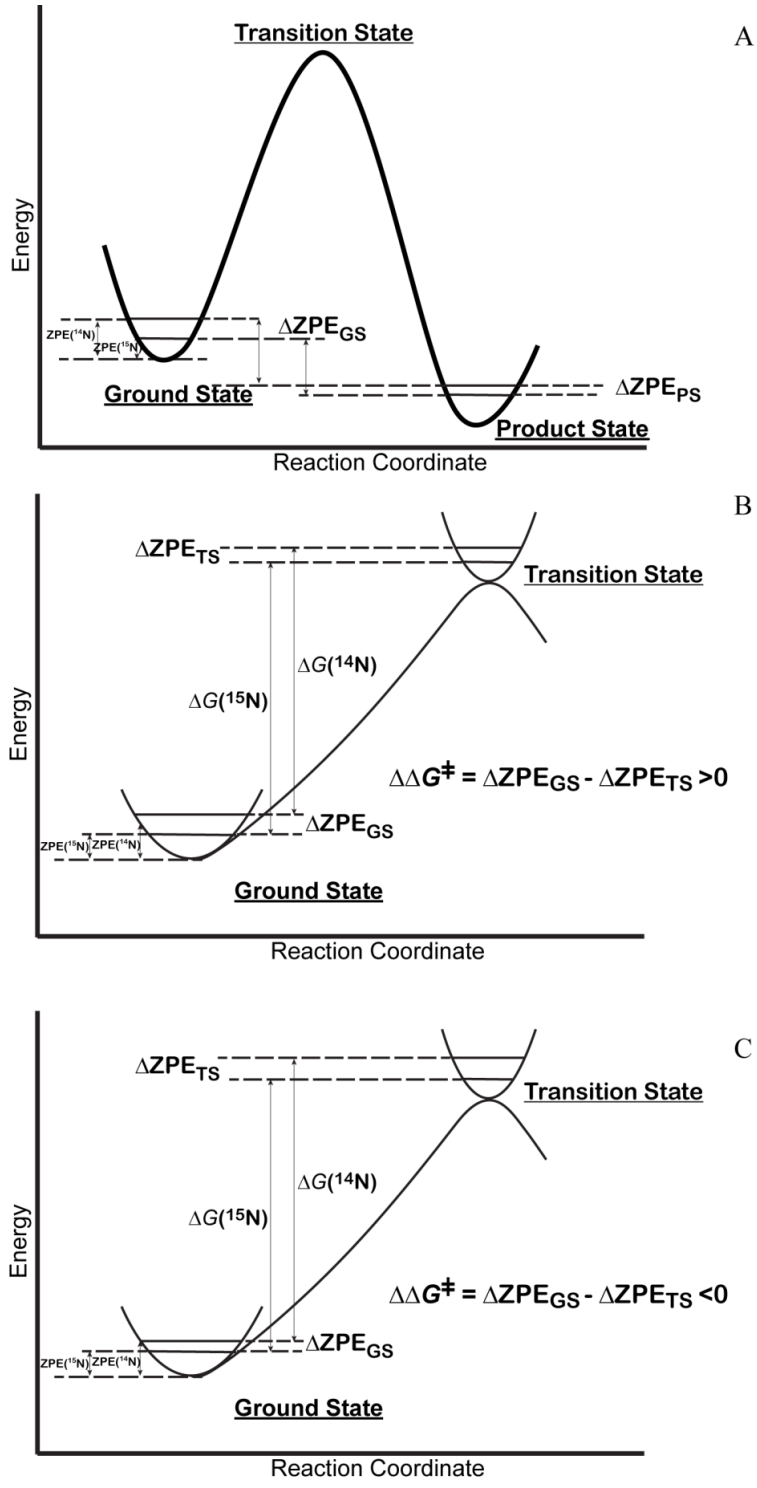

Figure 3: A picture depicting the potential energy curves for the normal equilibrium isotope effect (3A), the normal kinetic isotope effects (3B), and the inverse kinetic isotope effect (3C). Zero-point energies are represented on the graph of hypothetical reaction

coordinates. When the difference of zero-point energies in the ground state is larger than those in the transition state, there is a normal kinetic isotope effect. Conversely, an inverse kinetic isotope effect is observed when the difference of zero-point energies in the transition state is larger than those in the ground state. An equilibrium isotope effect is generated due to a difference in the zero-point energies between the substrates and the products.

Because isotope effects are calculated as a ratio, they are often compared to 1. If a kinetic isotope effect value is larger than 1 (i.e. the light isotope reacts more quickly than the heavy isotope, and the substrate therefore becomes enriched in heavy isotopes over time), it is considered to be a "normal" isotope effect (Figure 3B). Normal isotope effects are widely observed in both biochemical and chemical reactions. In some instances, however, the isotope effect value can be smaller than 1 (i.e. the heavy isotope reacts more quickly than the light isotope, and the substrate therefore becomes depleted in heavy isotopes over time), in which case it is termed an "inverse" kinetic isotope effect (Figure 3C).

The presence of inverse kinetic isotope effects may seem counterintuitive since it implies that a heavy atom is "preferred" over the light atom even though the bond with the heavy isotope will have the lower zero-point energy. This apparent conundrum can be easily explained, however, by recognizing that the magnitude and type (i.e. normal or inverse) of the isotope effect is determined by the relative differences in ΔZPEs in the ground state, transition state, and product state. In other words, any factors that contribute to changes in the ΔΔZPE between the ground state and transition state (for KIEs), or the ΔΔZPE between the ground state and the product state (for EIEs), will affect the magnitude (and potentially the type) of isotope effect. For example,

the steepness of an energy potential well in a reaction coordinate is determined by the bond strength between the two connected atoms, with stronger bonds leading to steeper wells. Because steeper wells lead to greater differences in the ΔZPE, anything that alters the bond order, and therefore the bond strength, will have a significant impact on the value of the isotope effect.

In the field of biogeochemistry, people often use different terminology to describe the isotopic fractionation process. Fractionation factors (α) and enrichment factors (ε) are two of the most widely used terms. The fractionation factor is calculated as the ratio of the isotope ratio of the product versus the substrate (Equation 6).

$$\alpha = R_{product}/R_{substrate} \quad (6)$$

The enrichment factor is a highly related expression and is simply the difference of the isotope ratios between the product and substrate (Equation 7).

$$\varepsilon = \delta_{product} - \delta_{substrate} \quad (7)$$

The fractionation factor and enrichment factor are mathematically related (Equation 8),

$$\alpha = \varepsilon/1000 + 1 \quad (8)$$

and both terms are quantitatively related to kinetic isotope effects, as shown in Equation 9,

$$\alpha = (KIE)^{-1} \quad (9)$$

where KIE is defined as the ratio of the rate constants of the light and heavy isotopes, i.e. k_L/k_H.

Enzyme-catalyzed versus uncatalyzed kinetic isotope effects

Uncatalyzed reactions often occur in a single step, while enzyme-catalyzed reactions are always composed of multiple steps. The steps involved in enzyme catalysis include: (1) the binding of substrate to the enzyme, (2) conversion of substrate into product, and (3) release of the product from the enzyme active site. In addition, the conversion of substrate into product can itself be a multistep process involving multiple transition states and intermediates.[12] In this process, a complex enzymatic reaction can be thought of as a series of individual steps, with each step having its own reactants, products, and activation energies. In theory, this can lead to KIEs and EIEs for each individual step. The observed KIE and EIE for a complex reaction is a combination of all of the individual steps. For uncatalyzed reactions, the rate determining step, which dictates the magnitude of the KIE, is determined by the nature of the bond-breaking and/or bond-forming steps. For enzyme-catalyzed reactions, however, processes other than the actual substrate bond-breaking or bond-forming steps (such as substrate binding or product release) can be rate-determining. In addition, by definition catalyzed reactions have lower energy transition states than uncatalyzed reactions. For this reason, enzyme-catalyzed reactions typically have a different kinetic isotope effect compared to their corresponding uncatalyzed reactions.

Magnitude of the observed isotope effect in enzyme-catalyzed reactions and the commitment to catalysis

Because enzyme-catalyzed reactions are complex, the isotope effects measured are often not controlled by one single rate-determining step, but rather by several partially rate-determining steps. In other words, there is a difference between the 'observed' fractionation factor (isotope effects directly measured in an experiment) and the 'intrinsic' fractionation factor (isotope

effects caused only by the actual enzyme-catalyzed step). While the observed fractionation factor can be affected by processes other than the isotopically sensitive step and display a broad range of values depending on different experimental conditions (e.g. substrate concentrations, experimental designs, etc.), the intrinsic fractionation factor represents the full isotope effect imposed on the isotopically sensitive step and is a single value. Therefore, to interpret an enzyme mechanism in terms of transition-state theory, it is important to separate the intrinsic isotope effect from the observed isotope effect.

According to Northrop,[13] the observed isotope effect and intrinsic isotope effect are mathematically related. Two of the important parameters that can affect the mathematical relationship between observed and intrinsic isotope effects are the forward commitment to catalysis (C_f) and the reverse commitment to catalysis (C_r). In this representation, C_f represents the tendency of the enzyme complex to continue forward to product and C_r represents the tendency of the enzyme complex following the isotopically sensitive step to follow reverse catalysis toward reactants.[14]

There are two general methods to measure isotope effects. In the classical method, substrates are largely isotopically substituted and V_{max}/K_m (maximum reaction rate versus Michaelis constant) values for different isotopic species are compared. In this thesis, I employ a different method in which isotope fractionation/distribution in the products and reactants are measured in systems containing near natural abundance isotope ratios. This is a competitive method in which the substrate is trace-labeled so there is limited isotope effect on reaction rate if observed directly, and the isotope effects are obtained by monitoring the rate of isotopic enrichment (or depletion) in the substrate or product during the initial phase of the reaction. For the traditional method, the isotope effect observed is proportional to the extent of how rate-limiting the isotopically

sensitive step is, as the commitment of catalysis will not alter the overall rate of the reaction. However, for the competitive method presented in this thesis, the commitment to catalysis factor might affect the observed isotope effect (Figure 4), because the unpreferred isotopic species can be accumulated at the isotopically sensitive step and go through the reverse catalysis, therefore changing the observed results. In essence, depending on the value of commitment to catalysis, the observed results in the latter case could be a combination of the forward kinetic isotope effect, the reverse kinetic isotope effect, and the equilibrium isotope effect. If the commitment to catalysis of the reaction is 1 (i.e. the reaction is irreversible), there is no isotope effect observed in the competitive method. If, however, the commitment to catalysis is 0 (i.e. the reaction is fully reversible), the observed isotope effect is equivalent to the intrinsic isotope effect in the competitive method utilized in this thesis.

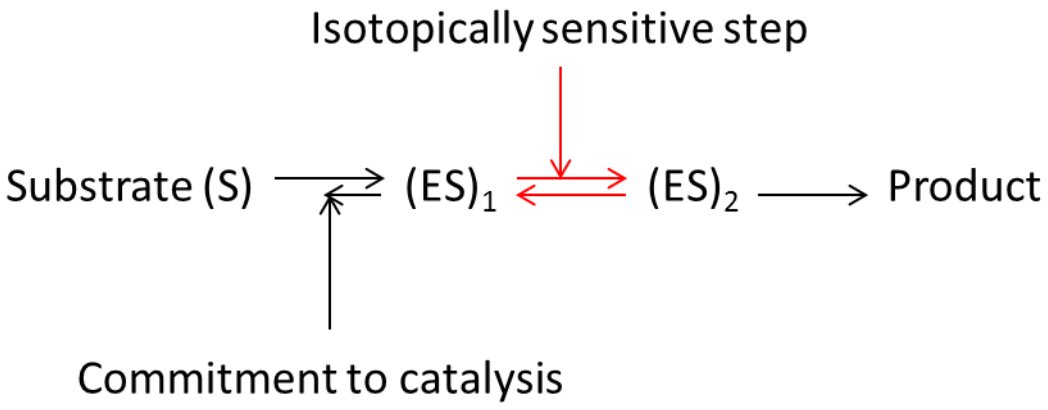

Figure 4: A simple reaction illustrating a hypothetical progression from the substrate to the product. In this figure, the commitment to catalysis step is before the isotopically sensitive step, which will lead to different observed isotope effects depending on the methods used.

Applications of stable isotopes in chemistry and biology

Stable isotopes can be employed to chemical and biochemical research in a couple of different ways. In the first application, stable isotopes are employed as a mechanistic probe to help elucidate the detailed reaction mechanism. For instance, stable C isotopes (^{12}C and ^{13}C) are often used to probe enzymatic reaction mechanisms related to central metabolism. In one example, Schmidt et al. determined the KIEs of the pyruvate dehydrogenase-catalyzed reactions by comparing the reaction rates of ^{13}C-labeled and unlabeled substrates.[15] As mentioned in the previous section, to determine the intrinsic isotope effect, they assumed appropriate values for the values like forward and reverse commitment to catalysis based on past studies and stripped these factors away from the observed isotope effect. The intrinsic isotope effect was then used to interpret the enzyme catalysis mechanism in terms of transition-state theory. In the following reaction,

$H_3CCOCO_2H \rightarrow H_3CCOSCoA + CO_2$

the KIE at C-2 position was $^{12}k/^{13}k = 1.0232$ while the KIE at C-1 position was 1.051. These results indicate that, as expected, C-C bond cleavage is at least partially rate determining. In addition, the smaller KIE value at the C-2 position than the C-1 position indicates that in the transition state, the loss of bond order at C-2 due to the cleavage of the C-C bond is partially compensated by bond formation.[16]

In another example, Waldrop et al analyzed kinetic isotope effects to probe the mechanism of aspartate transcarbamoylase.[17] Specifically, using ^{15}N isotope this group tested whether the reaction went through a cyanic acid or tetrahedral intermediate (Figure 5).[17] By comparing the measured intrinsic ^{15}N KIE (1.0024-1.0027) with the measured KIEs from two model

compounds (one utilizing a tetrahedral adduct mechanism (KIE = 1.0028) and the other a cyanide acid mechanism (KIE = 1.0105)), Waldrop et al. deduced that the enzyme-catalyzed reaction mechanism utilizes a tetrahedral intermediate.

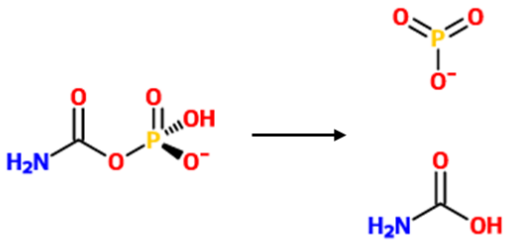

Scheme I

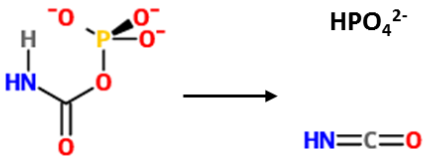

Scheme II

Figure 5: Two proposed reaction mechanisms for the aspartate transcarbamoylase catalyzed reaction. Scheme I is the tetrahedral intermediate mechanism and Scheme II is the cyanide intermediate mechanism.

The second broad application employs stable isotopes as tracers. In other words, stable isotopes are added into specific molecules to quantitatively determine the fluxes of a certain atom/metabolite in a particular pathway. By analyzing the quantitative input and output of the

labeled molecules, one can obtain a dynamic picture of the different fluxes of the metabolites in one or multiple pathways. For example, by incorporating stable isotopes into key substrates such as glucose, one can monitor, quantify, and compare metabolic fluxes in the glycolic pathway in different tissues. Using this approach, Fan et al.[18] were able to obtain a better understanding of lung cancer metabolomics. In particular, by comparing the flux of Krebs cycle metabolites in cancerous and non-cancerous lung tissue, they determined that glycolysis was upregulated in cancerous tissue. This discovery suggested new cancer treatment strategies[18] and led to the development biomarkers based on glycolytic and Krebs cycle intermediates to check for abnormal glucose metabolism in potentially pre-cancerous tissue.[19]

In addition, stable isotopes can also be used as tracers in environmental studies or ecology, where they can be a powerful tool in tracking the migration of animals and the untangling of various food-web interactions. For example, Hasson et al. analyzed stable N isotopes to assess the diets of fish within the food-web structures of coastal sea areas, thereby allowing them to ascertain their migration pattern.[20] Another example is that by measuring and comparing the C isotope ratios in soils at different sites, one can determine whether the landscape was covered by grasses or forest trees in the past, as well as whether the land was disturbed by human activities or left undisturbed.[21]

Application of stable isotopes in biogeochemistry

The application of stable isotopes in biogeochemistry is in essence the same as in the fields of chemistry and biology, where stable isotopes can be used both as tracers and as mechanistic probes. Because of the uniqueness of biogeochemistry, however, the nomenclature and the processes are expressed slightly differently.

The Rayleigh equation

The Rayleigh equations we use today originated from the Rayleigh distillation equation, which is described by:

$$R/R_0 = (X_L/X_L^0)^{\alpha-1} \quad (9)$$

where R and R_0 are the isotope ratios of the reactant at a certain time and the reactant at the start of the reaction, respectively, X_L and X_L^0 are the concentration of the light isotope at a certain time and the initial concentration of the light isotope, and α is the fractionation factor. Rearrangement of Equation 6 leads to the following equation[22]:

$$\delta p = \delta s_0 - \varepsilon_{p/s}[f*\ln f/(1-f)] \quad (10)$$

where δp and δs_0 describe the isotope ratio of the product and initial substrate, respectively, $\varepsilon_{p/s}$ is the difference of the isotope values between the product versus the substrate (i.e. $\delta_{product}-\delta_{substrate}$), and f is the fraction of the substrate remaining in a reaction.

Strictly speaking, the Rayleigh equation describes the isotopic change in a chemically open system, assuming that the isotopic species removed at any instant is in equilibrium with those remaining in the system. Such ideal case rarely exists, however, and the Rayleigh equation is often used to approximate kinetic fractionations in closed systems.

Although closed systems and open systems are quite different, the mathematical relationships derived from analysis of open systems are often applied to closed systems. Closed systems where the Rayleigh equation can be safely utilized are unidirectional reactions in which the atoms are transferred from one reservoir (substrate) to the second reservoir (product) under constant isotopic equilibrium. (For limitations to this approximation, see Kendall et al.[23])

Generally, most biological and geochemical systems have normal kinetic isotope effects (i.e. the light isotope reacts more quickly than the heavy isotope). In such systems, when the substrate is limited it gradually becomes enriched in the heavy isotope as the reaction proceeds. Concomitantly there is a slow enrichment of the heavy isotopes in the final product over time because of the gradual enrichment of the heavy isotopes in the substrate pool (Figure 6). In an open system where the substrate is infinite, the isotope ratio of the substrate does not change over the time, and the fractionation between the substrate and product (instantaneous or accumulated) is a constant value defined as the enrichment factor (ε). In essence, this concept can be expanded and can be applied to the closed systems where the substrate and product pools are constantly equilibrating. Therefore, at all times in the closed system, the fractionation between the substrate and the *instantaneous* product also equals ε.

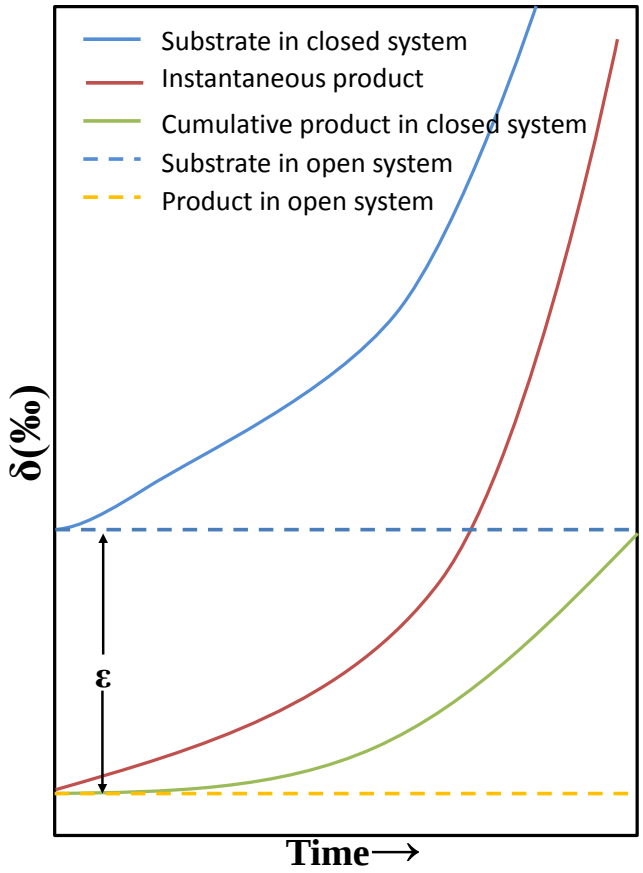

Figure 6: Changes of isotope ratios of the substrate, the instantaneous product, and the accumulated product in both open and closed systems. Modified from Kendall, 1998.[23]

Conclusion

Stable isotopes have been widely used by researches in biology, chemistry, and geochemistry. There are two major applications of stable isotopes. One of the applications is to use them as tracers to track the fluxes of certain molecules in metabolic pathways. In addition, stable isotopes can be used as a mechanistic probe by measuring the intrinsic kinetic isotope effect, which in turn can provide information about the reaction mechanism. The field of

biogeochemistry utilizes stable isotopes in similar applications, albeit presented in a different form because of the distinct expressions and terminology.

In this thesis, I employed stable isotopes as both tracers and mechanistic probes to study the microbial metabolism of two important gases. In Chapter 2, a method to study and quantify the isotope fractionation related to hydrogenases (H_2-producing enzymes) is presented, which provides the basis for the studies in the next chapter. In Chapter 3, an exhaustive study is presented where the isotope fractionation related to various reactions catalyzed by different hydrogenases were quantified and compared. The isotope effects determined in this study not only provided us with important mechanistic information, especially in the H_2 formation reaction, they also enabled future studies that can utilize these fractionation factors as signatures to quantify the activity of hydrogenases in complex microbial communities. In Chapter 4, isotope fractionation by a fungal N_2O-producing enzyme (the nitric oxide reductase P450nor) is described. The observed inverse isotope effect with the N^{β} provided key information about the binding of the first NO molecule to the enzyme active site and the formation of the crucial intermediate in the enzyme mechanism. In addition, I calculated the site preference (SP) values from the observed fractionation patters, and these SP values can, in turn, be used as a tool to trace the source of N_2O in the atmosphere.

BIBLIOGRAPHY

BIBLIOGRAPHY

1. Giauque, W. F.; Johnston, H. L., An isotope of oxygen, mass 18. *Nature (London, U. K.)* **1929,** *123* (Copyright (C) 2014 American Chemical Society (ACS). All Rights Reserved.), 318.

2. Birge, R. T.; Menzel, D. H., The Relative Abundance of the Oxygen Isotopes, and the Basis of the Atomic Weight System. *Physical Review* **1931,** *37* (12), 1669-1671.

3. Urey, H. C.; Murphy, G. M.; Duncan, J. A., A HYDROGEN DISCHARGE TUBE FOR THE CONTINUOUS ULTRAVIOLET SPECTRUM. *Review of Scientific Instruments* **1932,** *3* (9), 497-498.

4. Lewis, G. N.; Macdonald, R. T., Concentration of H2 Isotope. *The Journal of Chemical Physics* **1933,** *1* (6), 341-344.

5. (a) Cremer, E.; Polanyi, M., Test of "tunnel" theory of heterogeneous catalysis on hydrogenation of styrene. *Z. physik. Chem.* **1932,** *B19* (Copyright (C) 2014 American Chemical Society (ACS). All Rights Reserved.), 443-50; (b) Eyring, H., The zero point energy and the separation of isotopes. *Proc. Natl. Acad. Sci. U.S.A.* **1933,** *19* (1), 78-81.

6. Klein, F. S., Isotope Effects in Chemical Kinetics. *Annual Review of Physical Chemistry* **1975,** *26* (1), 191-210.

7. Bigeleisen, J.; Wolfsberg, M., Theoretical and Experimental Aspects of Isotope Effects in Chemical Kinetics. In *Advances in Chemical Physics*, John Wiley & Sons, Inc.: 2007; pp 15-76.

8. Hornberger, G. M., New manuscript guidelines for the reporting of stable hydrogen, carbon, and oxygen isotope ratio data. *Water Resources Research* **1995,** *31* (12), 2895-2895.

9. Hennig, C.; Oswald, R. B.; Schmatz, S., Secondary Kinetic Isotope Effect in Nucleophilic Substitution: A Quantum-Mechanical Approach†. *The Journal of Physical Chemistry A* **2006,** *110* (9), 3071-3079.

10. Bigeleisen, J.; Lee, M. W.; Mandel, F., Equilibrium Isotope Effects. *Annual Review of Physical* Chemistry **1973,** *24* (1), 407-440.

11. Kohen, A.; Klinman, J. P., Hydrogen tunneling in biology. *Chemistry & Biology* **1999,** *6* (7), R191-R198.

12. Cleland, W. W., Use of isotope effects to determine enzyme mechanisms. *Journal of Labelled Compounds and Radiopharmaceuticals* **2007,** *50* (11-12), 1006-1015.

13. Northrop, D. B., The Expression of Isotope Effects on Enzyme-Catalyzed Reactions. *Annual Review of Biochemistry* **1981,** *50* (1), 103-131.

14. Northrop, D. B., Steady-state analysis of kinetic isotope effects in enzymic reactions. *Biochemistry* **1975,** *14* (12), 2644-2651.

15. Melzer, E.; Schmidt, H. L., Carbon isotope effects on the pyruvate dehydrogenase reaction and their importance for relative carbon-13 depletion in lipids. *Journal of Biological Chemistry* **1987,** *262* (17), 8159-64.

16. Klinman, J. P., The power of integrating kinetic isotope effects into the formalism of the Michaelis–Menten equation. *FEBS Journal* **2014,** *281* (2), 489-497.

17. Waldrop, G. L.; Urbauer, J. L.; Cleland, W. W., Nitrogen-15 isotope effects on nonenzymic and aspartate transcarbamylase catalyzed reactions of carbamyl phosphate. *Journal of the American Chemical Society* **1992,** *114* (15), 5941-5945.

18. Fan, T.; Lane, A.; Higashi, R.; Farag, M.; Gao, H.; Bousamra, M.; Miller, D., Altered regulation of metabolic pathways in human lung cancer discerned by 13C stable isotope-resolved metabolomics (SIRM). *Molecular Cancer* **2009,** *8* (1), 41.

19. Vermeersch, K. A.; Styczynski, M. P., Applications of metabolomics in cancer research. *Journal of* Carcinogenesis **2013,** *12*, 9.

20. Hansson, S.; Hobbie, J. E.; Elmgren, R.; Larsson, U.; Fry, B.; Johansson, S., THE STABLE NITROGEN ISOTOPE RATIO AS A MARKER OF FOOD-WEB INTERACTIONS AND FISH MIGRATION. *Ecology* **1997,** *78* (7), 2249-2257.

21. Delègue, M.-A.; Fuhr, M.; Schwartz, D.; Mariotti, A.; Nasi, R., Recent origin of a large part of the forest cover in the Gabon coastal area based on stable carbon isotope data. *Oecologia* **2001,** *129* (1), 106-113.

22. Scott, K. M.; Lu, X.; Cavanaugh, C. M.; Liu, J. S., Optimal methods for estimating kinetic isotope effects from different forms of the Rayleigh distillation equation 1. *Geochimica et Cosmochimica Acta* **2004,** *68* (3), 433-442.

23. Kendall, C.; Caldwell, E. A., Chapter 2 - Fundamentals of Isotope Geochemistry. In *Isotope Tracers in Catchment Hydrology*, McDonnell, C. K. J., Ed. Elsevier: Amsterdam, 1998; pp 51-86.

CHAPTER 2

USING GAS CHROMATOGRAPHY-ISOTOPE RATIO MASS SPECTROMETRY TO DETERMINE THE FRACTIONATION FACTOR FOR H_2 PRODUCTION BY HYDROGENASES

This chapter is modified from *Rapid Communications in Mass Spectrometry* 26(1): 61-68 (2012) by Hui Yang, Hasand Gandhi, Liang Shi, Helen W. Kreuzer, Nathaniel E. Ostrom, and Eric L. Hegg.

Hasand Gandhi and Nathaniel Ostrom designed the gas chromatography-isotope ratio mass spectrometry system and Hasand Gandhi additionally helped with the measurements. Liang Shi provided the purified enzyme sample. Helen W. Kreuzer provided key instructions, and Nathaniel Ostrom and Eric Hegg helped analyze data and directed the research.

ABSTRACT

Hydrogenases catalyze the reversible formation of H_2, and they are key enzymes in the biological cycling of H_2. H isotopes have the potential to be a very useful tool in quantifying hydrogen ion trafficking in biological H_2 production processes, but there are several obstacles that have thus far limited the application of this tool. In this manuscript, we describe a new method that overcomes some of these barriers and is specifically designed to measure isotopic fractionation during enzyme-catalyzed H_2 evolution. A key feature of this technique is that purified hydrogenases are employed, allowing precise control over the reaction conditions and therefore a high level of precision. In addition, a custom-designed high-throughput gas chromatography-isotope ratio mass spectrometer is employed to measure the isotope ratio of the H_2. Using our new approach, we determined that the fractionation factor for H_2 production by the [NiFe]-hydrogenase from *Desulfovibrio fructosovorans* is 0.273 ± 0.006. This result indicates that, as expected, protons are highly favored over deuterium ions during H_2 evolution. Potential applications of this newly developed method are discussed.

Key Words

Hydrogenase; H_2 production; fractionation factor; isotope ratio mass spectrometry

INTRODUCTION

Economic and environmental concerns over the world's ever increasing energy consumption have led to considerable interest in alternative fuels.[1,2] H_2 is one attractive substitute due to its high energy content and the fact that it produces only water as the byproduct of combustion.[3] Currently H_2 is a critical chemical feedstock, but 96% of the H_2 produced today is derived from fossil fuels.[3] Conversely, microbially-produced H_2 is both renewable and carbon neutral, and the biological production of H_2 therefore has enormous potential to provide an environmentally friendly and sustainable source of energy.

Although considerable progress has been made in elucidating the metabolic pathways involved in H_2 metabolism, many uncertainties remain.[4,5] One major impediment to improving our understanding of H_2 metabolism is our inability to define adequately the regulation of and the flux through key pathways involved in H_2 production.[6,7] In addition to producing H_2, a number of microorganisms consume H_2, and this biotic cycling plays a vital role in the anaerobic metabolism of many microbial communities.[8-10] Being able to quantify the biotic cycling of H_2 is critical to our understanding of H_2 metabolism and our ability to maximize biological H_2 production.[2,7,11]

Hydrogenases are found in many microbes where they catalyze the reversible reduction of protons to form H_2:

$$2\ H^+ + 2\ e^- \leftrightarrow H_2$$

The two classes of hydrogenases that are particularly important in H_2 cycling are the [NiFe]- and [FeFe]-hydrogenases.[5] There is no evolutionary relationship between these two different

classes of hydrogenases, and as their name implies, they differ in the metal content at their active site.[12-14] Often organisms contain more than one hydrogenase, and it can therefore be difficult to ascertain the source and/or fate of biological H_2 in living systems.[15] Stable isotopes can be a powerful tool to trace fluxes through metabolic pathways,[8,16,17] and hydrogen isotopes have been used to study the abiotic cycling of H_2.[18] Thus far, however, there are relatively few examples of using hydrogen isotopes to improve our knowledge of H_2 metabolism.[19-22]

Fractionation factors for enzymes involved in H_2 metabolism can be used to help quantify the fluxes through different metabolic pathways. There are two strategies for measuring fractionation factors (α) associated with H_2 metabolism (defined as $\alpha = R_{H2}/R_{H2O}$)[2]: *in vivo* analysis in which one measures the isotope ratio of the H_2 produced or consumed by a whole organism, and *in vitro* analysis in which the fractionation factor is determined directly from purified hydrogenases. Recently the composite fractionation factor for H_2 uptake and H_2-H_2O exchange was measured for five different organisms,[23] but the fractionation factor for H_2 production was not reported. One of the major challenges in obtaining the *in vivo* fractionation factor for H_2 production is that the isotope ratio of the H_2 formed is dependent on the isotope ratio of the substrate, i.e. the hydrogen ions in intracellular water. Previously it was generally assumed that intracellular and extracellular water were effectively in complete equilibrium, and that bulk water was therefore the source of the hydrogen ions in H_2. Our results, however, indicated that intracellular can be quite distinct from extracellular water due to the flux of hydrogen ions from organic substrates into intracellular water during metabolic processing.[24]

[2] The fractionation factor (α) is defined as R_A/R_B where R_A and R_B are the isotope ratio of the rare atom versus the abundant atom in the products and reactants, respectively. Thus, in our studies of H_2 metabolism, $\alpha = R_{H2}/R_{H2O}$ where $R = {}^2H/{}^1H$.

Thus, to determine the *in vivo* fractionation factor for H_2 production, one must first measure the isotope ratio of intracellular water.

Determining the *in vitro* fractionation factor of H_2 production presents many challenges as well, some of which are also encountered when calculating the *in vivo* values. First and foremost, the hydrogenase-catalyzed formation of H_2 is readily reversible.[13] Even under conditions in which H_2 formation is favored (e.g. very low partial pressures of H_2 or the presence of reducing agents), some H_2 uptake can be still be observed.[25-28] Hydrogenases also catalyze a non-productive H_2-H_2O exchange reaction in which the H atoms of H_2 exchange with H_2O with no net formation or consumption of H_2. Because both H_2 consumption and H_2-H_2O exchange of H_2 will alter the isotope ratio of H_2 in the headspace, these reactions will perturb the calculated fractionation factor for H_2 formation. Thus, care must be taken to ascertain the extent to which these other reactions are occurring, and correct for them if needed. A second challenge encountered when determining the *in vitro* fractionation factors is that both [NiFe]- and [FeFe]-hydrogenases are inactivated by O_2, necessitating anaerobic purification and activity assays.

In this paper, we describe an experimental protocol designed to measure the fractionation factors of H_2 production catalyzed by purified hydrogenases from microbial organisms. As an important proof of concept, we calculated the fractionation factor of [NiFe]-hydrogenase from *Desulfovibrio fructosovorans*. To our knowledge, this is the first reported example of a fraction factor determined for a purified hydrogenase.

EXPERIMENTAL

H_2 Evolution Assay.

Enzyme purification. The [NiFe]-hydrogenase from *D. fructosovorans* used in this experiment was purified from the native organism according to a modified literature procedure.[16] Briefly, *D. fructosovorans* was obtained from ATCC (ATCC 49200; Manassas, VA, USA) and cultured anaerobically in SOS medium[29] at 37 ℃ for 72 h. Following cell lysis and ultracentrifugation, the supernatant was loaded on a DEAE column (Bio-Rad, Hercules, CA, USA) equilibrated with Tris buffer A (10 mM Tris, pH 7.6), washed with Buffer A, and eluted with a gradient of 0-500 mM NaCl. The brown colored hydrogenase fraction eluted at about 70 mM NaCl, as confirmed by the hydrogen uptake activity assay.[29] The active fractions were pooled and subsequently loaded to a pre-packed ceramic hydroxyapatite column (Bio-Rad, Hercules, CA, USA) equilibrated with 5 mM phosphate buffer saline (PBS). The column was washed with 5 mM PBS and eluted with a stepwise gradient of 5 to 150 mM PBS. Hydrogenase eluted at the end of the gradient. The fractions with hydrogenase activity were pooled and filtered through a HiPrep 16/60 Sephacryl S-200 HR gel filtration column with Tris buffer B (50 mM Tris, pH 8, and 150 mM NaCl) by means of an AKTA Explorer fast protein liquid chromatography system (GE Healthcare, Piscataway, NJ, USA). The active fractions were pooled, concentrated, and stored in Tris buffer B with 10% (vol/vol) glycerol at -20 ℃. The purity of the isolated hydrogenase was confirmed by sodium dodecyl sulfate-polyacrylamide gel electrophoresis.

Sample preparation. In an anaerobic Coy chamber containing approximately 3% H_2 and 97% N_2, 50 mL of anaerobic H_2 evolution buffer (10 mM methyl viologen, 80 mM $Na_2S_2O_4$, 500 mM NaCl in 50 mL of 50 mM HEPES buffer, pH 7) was transferred to a 125 mL borosilicate-glass serum vial (Wheaton Science Products, Millville, NJ, USA). The vial was sealed with a gas-tight stopper (Bellco Glass, Vineland, NJ, USA) and crimped with an aluminum seal. The vial was evacuated and refilled with Ar on a Schlenk line several times to remove H_2 and N_2 from the

headspace. Purified hydrogenase in Ni-NTA buffer (100 mM Tris-HCl, pH 8, 100 mM imidazole, 200 mM NaCl, and 5% glycerol) was treated in an analogous manner.

Measuring H_2 evolution. A 1 mL syringe was used to inject 100 μL of purified enzyme into the vial containing the H_2 evolution buffer. The reaction vial was then inverted and incubated at room temperature for 2 h, and the isotope ratio of the H_2 formed was measured via GC-isotope ratio mass spectrometry (GC-IRMS). The amount of H_2 produced was quantified from the peak height (ion beam intensity at *m*/*z* 2) using a standard curve. The concentration of H_2 in the headspace never exceeded 5%, thereby limiting nonproductive hydrogen ion exchange with water and H_2 uptake. To verify that the isotope ratio of the H_2 in the headspace was not significantly affected by the competing reactions, the ratio was monitored for 3 h, and no changes in δ^2H over time were observed.

IRMS Measurements

IRMS Instrument setup. In this experiment, we use a new continuous flow design for measuring the δ^2H of H_2 (δ^2H_{H2}) to enable determination of fractionation factors. Our system maintains the high throughput capacity expected of continuous flow IRMS, while at the same time providing a high level of both precision (error of less than 3‰ in repeated measurements) and sensitivity (as low as 0.6 μmol gaseous H_2 while maintaining a precision of 3‰ or better). Figure 7 depicts the continuous-flow gas chromatography isotope-ratio mass spectrometry (CF-GC-IRMS) system for the measurement of δ^2H_{H2}. The gas chromatograph (Hewlett-Packard # 5890 Series II, Palo Alto, CA, USA) is interfaced to an Elementar Isoprime stable isotope ratio mass spectrometer (Isoprime Limited, Cheadle, UK). An ascarite trap is used to remove water before the sample gas is introduced into a sample loop and then into the gas chromatograph and isotope ratio mass

spectrometer. A liquid N_2 trap was placed prior to the vacuum pump to facilitate water-removal between sample injections. In the sample loading position (Figure 7A), the inlet system (consisting of the sample loop, tubing and injection port) is completely evacuated, and it is then isolated from the vacuum pump by closing stopcock 2. The sample is injected via a gastight syringe into the inlet system on the gas chromatograph, and it immediately expands throughout the inlet system. During this process, water is absorbed by the ascarite trap before a 2 mL gas sampling loop. After approximately 10 s of equilibration, the 6-port, 2-position sampling valve (Valco Instruments, Houston, TX, USA) is switched to isolate the sample gases within the gas sampling loop (see Figure 7B). The 4-port, 2-position sampling valve is then rotated to initiate He flow through the loop, pushing the sample gases onto the gas chromotograph column (Figure 7C). A 30 m $\times$ 0.53 mm o.d. molecular sieve 5 Å capillary column (Restek, Bellefonte, PA, USA) held at a constant temperature of 40 ˚C is used with a He head pressure of 23 psi to separate H_2 from the rest of the sample gases. The separated sample gases then enter the mass spectrometer, and the isotope ratio of the H_2 is determined and compared to the isotope ratio of the laboratory H_2 standard. The total time of the sample analysis is approximately 400 s.

A. Sample loading position

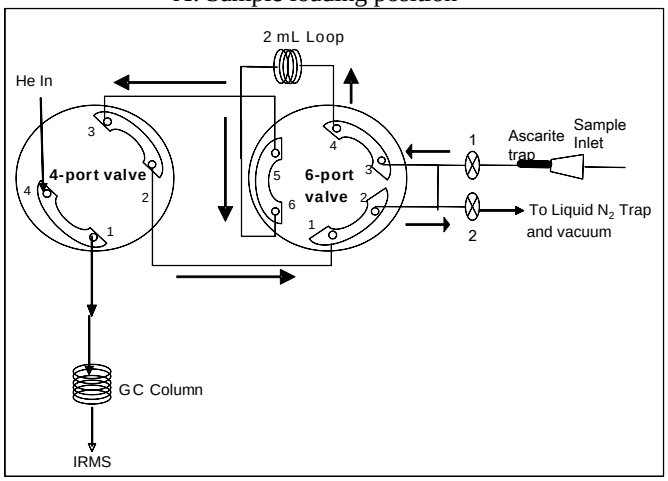

B. Sample holding position

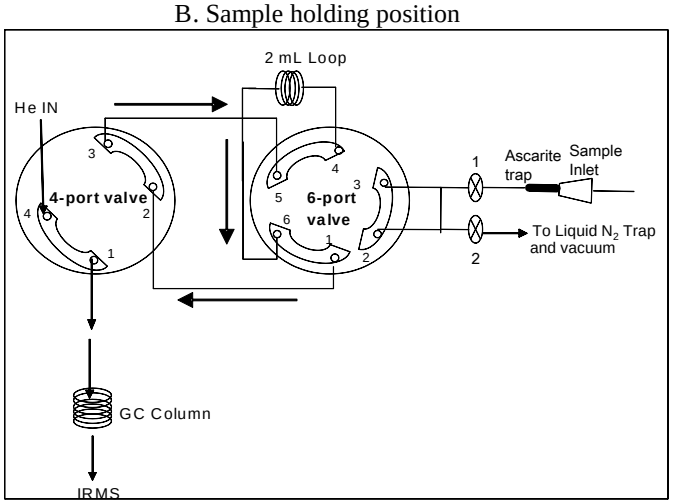

C. Sample injection position

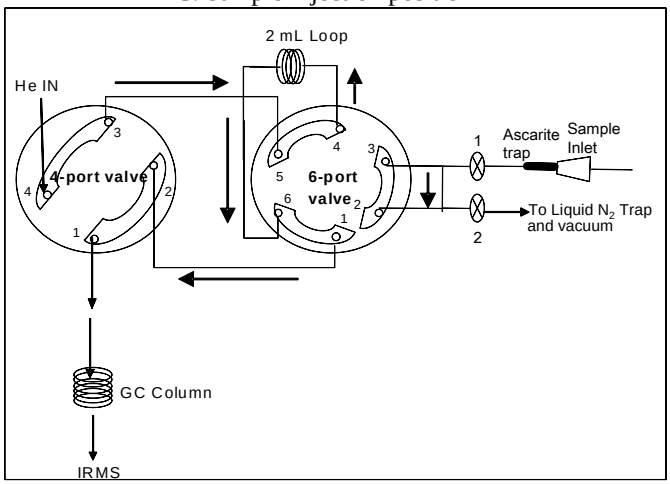

Figure 7: Schematic representation of the GC-IRMS system designed for the stable isotopic analysis of gaseous H_2. Arrows indicating directions of flow. See text for a detailed description.

Precision, accuracy and sensitivity of the instrument. The precision of our newly designed system was evaluated by daily measurement of the Oztech standard (1 L gas cylinder standard purchased from Oztech, Waltham, MA, USA) injected into the inlet system (Table 2). The precision was generally found to be better than ± 3‰. The accuracy was confirmed by comparing our calculated ^{2}H values of the working lab standards with the values determined by an independent laboratory (USGS, Denver, CO, USA) using a Thermo-Finnigan 252 mass spectrometer (Waltham, MA, USA) (Table 2). The difference between the average values reported by the USGS (n = 9 for standard A, n = 6 for standard B) and in our laboratory is less than 1.5‰. Furthermore, our tests demonstrated that samples containing as little as 0.63 μmoles of H_2 (Figure 8) yielded $\delta^{2}H$ values in agreement with the known isotope value of the tank standard (-424.3 ± 1.6‰). By central limit theorem, the mean and variance of δ values (measured via injections of different amount of H_2) was used to fit the y variables (δ values) to a normal distribution, and the 95% confidence interval region was determined.[30] The lower detection limit was determined as the injected H_2 amount that fell within the confidence intervals. Only 0.6 μmol of H_2 are needed to achieve a precision of 3‰ or better.

Table 2: $\delta^{2}H$ values of H_2 obtained for the Oztech H_2 reference gas.

Date	**Sample description[a]**	**No. of samples**	**$\delta^{2}H$ (‰)**
2010/5/3	syringe H_2 injection	4	-65.2 ± 3.6

Table 2 (cont'd)

2010/5/17	syringe H_2 injection	3	-62.7 ± 2.2
2010/5/18	syringe H_2 injection	4	-62.7 ± 0.4
mean ± SD			**-63.5 ± 2.0**
Oztec[b] mean ± SD			**-62.7 ± 0.5**
			D = 0.8

[a]The Oztech standard H_2 gas cylinder was used every day for adjustment of the MSU tank standard data.

[b]δ^2H values provided by the Oztech Trading Company in the Southern Methodist University Stable Isotope Laboratory.

Table 3: δ^2H values of MSU internal laboratory standards measured over three days as a function of the amount of H_2 injected.

Date	Sample	Tank A	Tank B
	0.42μmol H_2		
2010-5-3	Syringe standard[a]	-412.1	-339.6
2010-5-3	Bottle standard[b]	-416.8	-330.7

Table 3 (cont'd)

2010-5-17	Syringe standard	-424.1	-333.6
2010-5-17	Bottle standard	-423.6	-332.3
2010-5-18	Syringe standard	-423.6	-332.7
2010-5-18	Bottle standard	-419.1	-330.7
	mean ± SD	**-419.9 ± 4.8**	**-333.3 ± 3.3**
	0.83 μmol H_2		
2010-5-3	Syringe standard	-419.0	-336.3
2010-5-3	Bottle standard	-413.8	-328.7
2010-5-17	Syringe standard	-422.4	-329.1
2010-5-17	Bottle standard	-423.6	-332.3
2010-5-18	Syringe standard	-423.6	-331.7
2010-5-18	Bottle standard	-422.1	-328.2
	mean ± SD	**-420.8 ± 3.8**	**-331.0 ± 3.1**
	1.66 μmol H_2		
2010-5-3	Syringe standard	-420.3	-333.9
2010-5-3	Bottle standard	-426.2	-335.5

Table 3 (cont'd)

2010-5-18	Syringe standard	-423.6	-332.4
	mean ± SD	**-423.3 ± 2.9**	**-333.9 ± 1.6**
	2.50 μmol H_2		
2010-5-3	Syringe standard	-424.4	-333.4
2010-5-3	Bottle standard	-422.5	-331.0
2010-5-18	Syringe standard	-424.4	-332.6
	mean ± SD	**-423.8 ± 1.1**	**-332.3 ± 1.2**
	All MSU data mean ± SD	**-421.4 ± 3.9**	**-332.5 ± 2.8**
	USGS[c] mean ± SD	**-424.3 ± 1.6**	**-330.0 ± 1.8**
		Δ = 2.9	**Δ = 2.5**

[a]Syringe standards were H_2 gas standards introduced as pure gas samples into the gas chromatograph-isotope ratio mass spectrometer using a gas-tight syringe.

[b]Bottle standards were prepared by adding H_2 into a 13 mL serum bottle filled with Ar at atmospheric pressure; 1 mL of the H_2/Ar mixed gas was then injected using a gas-tight syringe.

[c]Samples of MSU tank standards were sent to the USGS laboratory for an independent analysis. A total of 9 analyses were conducted at the USGS over three days.

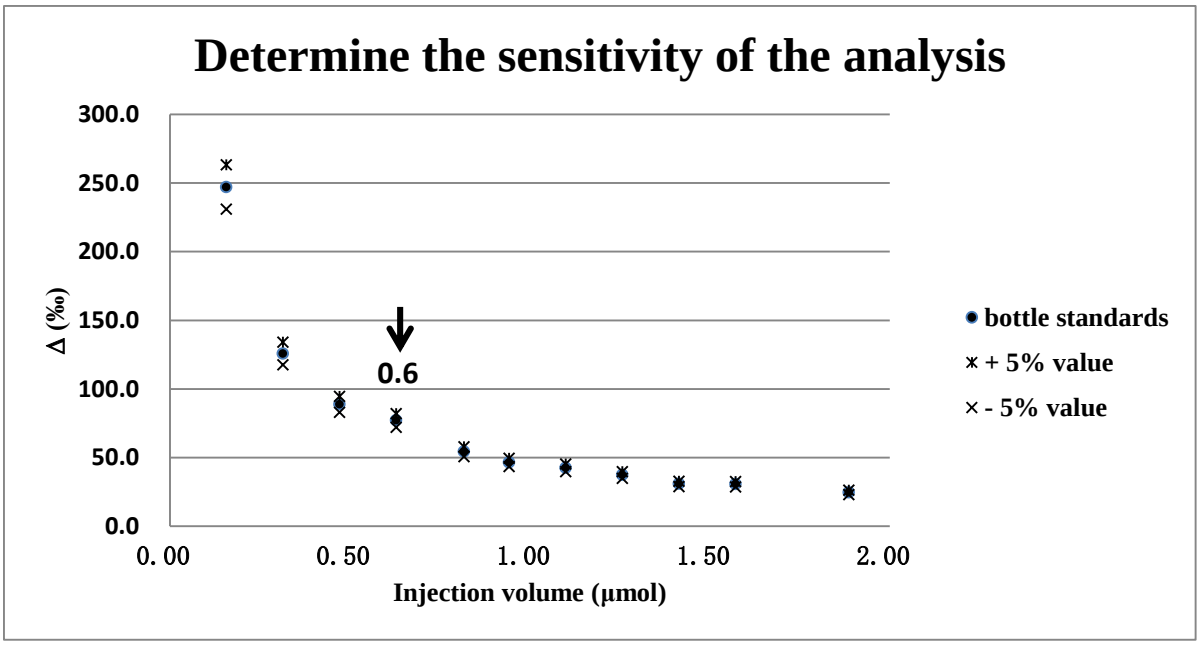

Figure 8: Determination of the detection limit for δ^2H by the GC-IRMS system. In the figure, the upper and lower boundary of the 95% confidence interval region of the Δ values are shown. Only 0.6 µmol of H2 is needed to achieve a precision of 3‰ or better; below this level the precision becomes unacceptable.

Measurement of δ^2H_2O

The δ^2H of H_2O (δ^2H_{H2O}) of the reactant solution was determined using a Los Gatos Research (Mountain View, CA, USA) Liquid Water Isotope Analyzer. The average value of δ^2H_{H2O} was -63.7 ± 1.5‰ (n = 10).

Data Analysis

Correction of δ^2H. To correct the raw isotope ratio value, a 1 L stainless steel cylinder containing pure H_2 with a known $^2H/^1H$ ratio (-62.7‰ versus VSMOW (Vienna Standard Mean

Ocean Water)) was acquired from Oztech Trading Corporation (Dallas, TX, USA). This reference gas and two other laboratory working standards (-424.3‰ and -333.0‰ versus VSMOW as determined by the USGS using a dual-inlet isotope ratio mass spectrometer) were used on a daily basis to calibrate the system. The software, MassLynx (Elementar Americas Inc., Mt. Laurel, NJ, USA), performs an internal correction for baseline drift and the contribution of H_3^+ to the mass 3 detector.

Standardization and notation. All results are reported with respect to VSMOW, whose absolute ratio of $^2H/^1H$ is 155.76 (±0.05) $\times 10^{-6}$. The relative ratio of a sample with respect to VSMOW is commonly given by the relationship:

$$\delta^2H = (R_{sample}/R_{VSMOW} - 1) \times 1000\ (‰)$$

where $R = {}^2H/{}^1H$.

RESULTS AND DISCUSSION

In this manuscript, we present a GC-IRMS method to measure isotopic fractionation during hydrogenase-catalyzed H_2 production. The headspace gas from a series of reactions was measured to determine the fractionation factor of [NiFe]-hydrogenase from *D. fructosovorans.* Like all catalysts, [NiFe]-hydrogenases can catalyze both the forward and the reverse reaction, as well as a H_2-H_2O exchange reaction. All of these reactions can occur even when the H_2 partial pressure is low.[27,28] Thus, the isotope ratio of the H_2 in the headspace may be influenced by reactions other than the evolution reaction. To limit the influence of the competing reactions, an excess amount of a strong reductant (80 mM $Na_2S_2O_4$) was used in the experiments to maintain a large thermodynamic driving force for H_2 production and to saturate the enzyme to ensure

maximal velocity. In addition, the enzyme concentration was adjusted such that the concentration of H_2 in the headspace never rose above 5%, and the reactions were performed for a relatively short period of time (≤ 5 h), further limiting H_2 uptake and H_2-H_2O exchange. Importantly, time course experiments were performed for each data set, and our results demonstrate that the $^2H_{H2}$ value remained constant (Table 3). Because the rates of the competing reactions increase as H_2 accumulates in the headspace, the observed isotope ratio of the headspace H_2 would most likely change over time if either of the competing reactions were influencing the observed δ^2H_{H2}.[3] The fact that the isotope ratio remained constant is consistent with isotope fractionation from an infinitely large reservoir of water, and it provides a strong indication that the competing reactions are not significant under our reaction condition.

Table 4: Isotope ratio of H_2 produced by *Desulfovibrio fructosovorans* hydrogenase.

Name	Time (h)	Ht (nA)	δ^2H (‰)	Fractionation factor (a)[a]
		2009-7-21		
Df Sample A[b]	1	4.03	-728.5	0.275
	2	5.36	-735.1	0.283
	3	6.31	-735.6	0.284

[3] Both the H_2-consumption and the nonproductive exchange reactions are first order with respect to $[H_2]$. These two reactions will perturb the observed δ^2H_{H2} value except in the unlikely event that the combined fractionation of the competing reactions exactly matches the fractionation of H_2 production.

Table 4 (cont'd)

Df Sample B	1	3.80	-730.4	0.275
	2	4.88	-731.8	0.275
	3	6.90	-736.6	0.286
		2009-8-6		
Df Sample C	1	3.58	-762.7	0.254
	2	5.14	-757.6	0.264
	3	6.00	-759.3	0.262
Df Sample D	1	3.46	-763.1	0.254
	2	5.08	-757.4	0.264
	3	5.67	-751.7	0.254
		2010-11-23		
Df Sample E	1	3.30	-722.0	0.295
	2	4.22	-733.6	0.280
	3	6.12	-743.9	0.274
		2010-12-1		
Df Sample F	1	5.70	-737.3	0.280

Table 4 (cont'd)

	2	6.37	-735.8	0.274
	3	7.11	-737.8	0.281
	4	7.85	-744.7	0.272
mean ± SD			**-742.4 ± 12.6**	**0.273 ± 0.006**

[a]The fractionation factor is defined as R_{H2}/R_{H2O}, taking into account the H_2 dissolved in the solution.

[b]Df refers to *D. fructosovorans* [NiFe]-hydrogenase. A to F indicate six different reaction preparations.

Calculations for determining the fractionation factor for H_2 evolution

The fractionation factor for H_2 evolution is defined as

$$\alpha_{H2evolution} = R_{H2(T)}/R_{H2O} \quad (1)$$

where $R_{H2(T)}$ and R_{H2O} is the ratio of deuterium to hydrogen in the total H_2 product and in the reactant (i.e. water), respectively. Thus, to calculate the fractionation factor of the [NiFe]-hydrogenase, we must first know the isotope ratio of the H_2 produced. Because H_2 can dissolve and fractionate between the gas and liquid phases, however, the fractionation factor determined using only the headspace H_2 must be corrected to account for this partitioning.

This partitioning can be described using the mass balance equation[31]

$$R_{H2(T)} = X_{H2(gas)}R_{H2(gas)} + X_{H2(sol)}R_{H2(sol)} \quad (2)$$

where $R_{H2(T)}$, $R_{H2(gas)}$, and $R_{H2(sol)}$ are the isotope ratios of the total H_2 produced, the H_2 in the headspace, and the H_2 in the solution, and $X_{H2(gas)}$ and $X_{H2(sol)}$ represent the molar fraction of H_2 in the headspace and in the solution, respectively. $R_{H2(sol)}$, however, is related to $R_{H2(gas)}$ by the fractionation factor $\alpha_{H2equal}$ ($\alpha_{H2equal} = R_{H2(gas)}/R_{H2(sol)} = 1.067$),[32] and equation 2 therefore becomes:

$$R_{H2(T)} = X_{H2(gas)}R_{H2(gas)} + X_{H2(sol)}R_{H2(gas)}/\alpha_{H2equal} \quad (3)$$

This equation describing a two-component mixture simplifies to:

$$R_{H2(T)} = X_{H2(gas)}R_{H2(gas)} + (1 - X_{H2(gas)})R_{H2(gas)}/\alpha_{H2equall} \quad (4)$$

Because the temperature and pressure remain essential constant during the course of the reaction, the molar fraction of H_2 in the gas phase ($X_{H2(gas)}$) can be approximated as

$$X_{H2(gas)} = V_{H2(gas)}/(V_{H2(gas)}+V_{H2(sol)}) \quad (5)$$

where $V_{H2(gas)}$ and $V_{H2(sol)}$ represent the volume of the H_2 in headspace and in solution, respectively. The amount of H_2 dissolved in solution can be calculated using the following equation

$$V_{H2(sol)} = V_{solution} * \lambda \quad (6)$$

where λ is the Ostwald coefficient (20.426×10^{-3} at 25 ℃ and 1 atm), $V_{solution}$ is the volume of the reaction solution (50 mL), and $V_{H2(sol)}$ is the volume of H_2 dissolved in the solution.[33] Thus, using the known constants and measurements from these experiments, $R_{H2(T)}$ can be quantified.

The fractionation factor of the hydrogenase-catalyzed H_2 evolution ($\alpha_{H2evolution}$) reaction can therefore be readily calculated using equation 1.

The fractionation factor for the production of H_2 catalyzed the [NiFe]-hydrogenase from *D. fructosovran* was calculated multiple times, and the results are shown in Table 3. As noted above, these values do not vary over time. The average value of the fractionation factor is 0.27 ± 0.01, indicating that protons react significantly faster than deuterium ions during H_2 formation. Interestingly, our calculated fractionation factor of 0.27 is in general agreement with the net fraction factor calculated for two cyanobacterial cultures ($\alpha = 0.43$).[34] This net fractionation factor, however, is the result of multiple H_2 fractionation steps in the cell, and the percentage of H_2 formed by hydrogenase versus nitrogenase in these cultures is not known. Thus, any direct comparisons between our fractionation factor determined using purified enzymes and the net fractionation factor calculated for cyanobacterial cultures must be made with caution.

Potential Applications

The findings presented here illustrate the potential for this method to provide precise and robust fractionation factors for H_2 evolving enzymes. These values can, in turn, expand our knowledge and understanding of microbial H_2 metabolism. In one potential application, knowledge of the fractionation factors can be used to ascertain the source of H_2. Because fractionation factors are multiplicative, with the fractionation factor ($\alpha_{H2evolution}$) being a product of the α values for each step in the reaction pathway, the observed fractionation factor is specific to the reaction coordinate profile. While [NiFe]- and [FeFe]-hydrogenases obviously have dissimilar active sites, even hydrogenases within the same class are expected to have dissimilar $\alpha_{H2evolution}$ values due to slight differences in H-bonding and hydrogen ion transport. Therefore, despite the fact

that all hydrogenases produce H_2 from protons and electrons, hydrogenase enzymes will nonetheless have distinct values for α_{total}. These differences in the fractionation factors will be manifested in the isotope ratio of the H_2 produced, thus providing each enzyme with its own unique signature. In an organism that contains two hydrogenases (either naturally or through genetic engineering), the relative activity of each hydrogenase can therefore be determined by measuring the isotope ratio of H_2.

In a second application, the fractionation factors can be used to test for proton channeling. Although it is well established that the addition of organic substrates can increase H_2 production in some organisms,[35-37] the precise mechanism by which this occurs is not entirely clear. Do the organic substrates merely provide an additional source of electrons to the general cellular pool, or are the two processes more directly coupled? For example, in *Shewanella oneidensis* the addition of certain organic substrates increases H_2 production even when electron acceptors are present,[15] suggesting that some channeling of electrons and protons may be occurring. A comparison of the *in vitro* and *in vivo* hydrogenase fractionation factors can be used to test this phenomenon. If channeling is occurring, the source of protons will not be the bulk intracellular water, and this will result in different apparent *in vivo* and *in vitro* hydrogenase fractionation factors.

Finally, knowledge of the fractionation factors can also aid in environmental reconstruction. Many organisms consume H_2 as an energy supply, and H_2 is consequently a source of cellular hydrogen atoms for lipid biosynthesis in these organisms.[19] The fractionation factor of H_2 uptake is therefore needed to interpret fully the isotope ratios of sedimentary lipids during geochemical reconstruction.

The instrument design described here is compatible with a wide variety of applications. Because pre-treatment of the sample is not required,[38] the design is well suited for high throughput measurement of enzymatic reactions. Furthermore, it is possible to configure the system such that a sample can be loaded directly from the side arm of a culture bottle or assay vial into the evacuated sample loop, thereby avoiding the potential for fractionation or leakage caused by syringe injections.[39]

CONCLUSIONS

The fractionation factors determined for hydrogenases can greatly aid in our understanding of H_2 metabolism. The method described in this paper is both fast and accurate, and it provides a rigorous strategy for quantifying the fractionation factor for H_2 evolution ($\alpha_{H2evolution}$). As a proof of concept, we determined $_{H2evolution}$ for the [NiFe]-hydrogenase from *D. fructosovorans*. The large discrimination observed in this reaction ($\alpha_{H2evolution} = 0.27$) indicates that hydrogen ions react much faster than deuterium ions during H_2 evolution. This fractionation factor can be used as a signature for the *D. fructosovorans* [NiFe]-hydrogenase and aid in the analysis of H_2 metabolizing pathways. Significantly, because this method is completely generic, it can be applied to a variety of other enzymes involved in H_2 metabolism.

Acknowledgements

We thank James J. Moran from Pacific Northwest National Lab (PNNL) for helpful discussions. Pacific Northwest National Laboratory is operated by Battelle Memorial Institute for the U.S. Department of Energy under Contract No. DE-AC05-76RL01830. Financial support was provided by the U.S. Department of Energy (DOE), Office of Biological and Environmental

Research (BER), as part of BER's Genomic Science Program (GSP). Support from NSF (#1053432) is also gratefully acknowledged.

BIBLIOGRAPHY

BIBLIOGRAPHY

[1]. U.S. Energy Information Administration. International energy outlook 2011. **2011**. Publication number: DOE/EIA-0484(2011)

[2]. K. Srirangan, M. E. Pyne, C. P. Chou. Biochemical and genetic engineering strategies to enhance hydrogen production in photosynthetic algae and cyanobacteria. *Bioresource Technol.* **2011**, *102*, 8589.

[3]. M. Balat. Potential importance of hydrogen as a future solution to environmental and transportation problems. *Int. J. Hydrogen Energy* **2008**, *33*, 4013.

[4]. J. B. McKinlay, C. S. Harwood. Photobiological production of hydrogen gas as a biofuel. *Curr.* Opin. *Biotech.* **2010**, *21*, 244.

[5]. M. L. Ghirardi, M. C. Posewitz, P. -C. Maness, A. Dubini, J. Yu, M. Seibert. Hydrogenases and hydrogen photoproduction in oxygenic photosynthetic organisms. *Annu. Rev. Plant Biol.* **2007**, *58*, 71.

[6]. D. C. Ducat, G. Sachdeva, P. A. Silver. Rewiring hydrogenase-dependent redox circuits in cyanobacteria. *P. Natl. Acad. Sci. USA* **2011**, *108*, 1.

[7]. T. Maeda, V. Sanchez-Torres, T. K. Wood, T.K. Enhanced hydrogen production from glucose by metabolically engineered *Escherichia coli*. *Appl.Microbiol. Biot.* **2007**, *77*, 879.

[8]. R. R. Adhikari, J. Kallmeyer. Detection and quantification of microbial activity in the subsurface. Chemie *der Erde* **2010**, *70*, 135.

[9]. D. W. Emerich, T. Ruiz-Argueso, S. A. Russell, H. J. Evans. Investigation of the hydrogen oxidation system in *Rhizobium japonicum* 122 DES nodule bacteroids. *Plant Physiol.* **1980**, *66*, 1061.

[10]. K. E. S. Tolvanen, M. T. Karp. Molecular methods for characterizing mixed microbial communities in hydrogen-fermenting systems. *Int. J. Hydrogen Energ.* **2011**, *36*, 5280.

[11]. M. Abo-Hashesh, R. Wang, P. C. Hallenbeck. Metabolic engineering in dark fermentative hydrogen production; theory and practice. *Bioresour. Technol.* **2011**, *In Press***.**

[12]. M. Y. Darensbourg. Hydrogenase active sites: A new paradigm for natural product-inspired synthesis based on organometallic chemistry. *Comment. Inorg. Chem.* **2010**, *31*, 144.

[13]. P. M. Vignais, B. Billoud, J. Meyer. Classification and phylogeny of hydrogenases. *FEMS Microbiol.* Rev. **2001**, *25*, 455.

[14]. P. M. Vignais, B. Billoud. Occurrence, classification, and biological function of hydrogenases: An overview. *Chem. Rev.* **2007**, *107*, 4206.

[15]. G. Meshulam-Simon, S. Behrens, A. D. Choo, A. M. Spormann. Hydrogen metabolism in *Shewanella oneidensis* MR-1. *Appl. Environ. Microb.* **2007**, *73*, 1153.

[16]. D. L. Valentine, A. Chidthaisong, A. Rice, W. S. Reeburgh, S. C. Tyler. Carbon and hydrogen isotope fractionation by moderately thermophilic methanogens. *Geochim. Cosmochim. Acta* **2004**, *68*, 1571.

[17]. A. L. Sessions, L. L. Jahnke, A. Schimmelmann, J. M. Hayes. Hydrogen isotope fractionation in lipids of the methane-oxidizing bacterium *Methylococcus capsulatus*. *Geochim.* Cosmochim. *Acta* **2002**, *66*, 3955.

[18]. L. -H. Lin, G. F. Slater, B. Sherwood Lollar, G. Lacrampe-Couloume, T. C. Onstott. The yield and isotopic composition of radiolytic H_2, a potential energy source for the deep subsurface biosphere. *Geochim. Cosmochim. Acta* **2005**, *69*, 893.

[19]. B. J. Campbell, C. Li, A. L. Sessions, D. L. Valentine. Hydrogen isotopic fractionation in lipid biosynthesis by H_2-consuming *Desulfobacterium autotrophicum*. *Geochim. Cosmochim. Acta* **2009**, *73*, 2744.

[20]. A. L. Sessions, T. W. Burgoyne, A. Schimmelmann, J. M. Hayes. Fractionation of hydrogen isotopes in lipid biosynthesis. *Org. Geochem.* **1999**, *30*, 1193.

[21]. D. L. Valentine, A. L. Sessions, S. C. Tyler, A. Chidthaisong. Hydrogen isotope fractionation during H_2/CO_2 acetogenesis: hydrogen utilization efficiency and the origin of lipid-bound hydrogen. *Geobiology* **2004**, *2*, 179.

[22]. S. E. Lamle, K. A. Vincent, L. M. Halliwell, S. P. J. Albracht, F. A. Armstrong. Hydrogenase on an electrode: a remarkable heterogeneous catalyst. *Dalton Trans.* **2003**, 4152

[23]. C. S. Romanek, C. L. Zhang, Y. Li, J. Horita, H. Vali, D. R. Cole, T. J. Phelps. Carbon and hydrogen isotope fractionations associated with dissimilatory iron-reducing bacteria. *Chem. Geo.* **2003**, *195*, 5.

[24]. H. W. Kreuzer-Martin, M. J. Lott, J. R. Ehleringer, E. L. Hegg. Metabolic processes account for the majority of the intracellular water in log-phase *Escherichia coli* cells as revealed by hydrogen isotopes. *Biochemistry* **2006**, *45*, 13622.

[25]. H. Tatsumi, K. Takagi, M. Fujita, K. Kano, T. Ikeda. Electrochemical study of reversible hydrogenase reaction of *Desulfovibrio vulgaris* cells with methyl viologen as an electron carrier. *Anal. Chem.* **1999**, 1753.

[26]. D. L. Erbes, R. H. Burris. The kinetics of methyl viologen oxidation and reduction by the hydrogenase from *Clostridium pasteurianum*. *Biochim. Biophys. Acta, Enzymology* **1978**, *525*, 45.

[27]. G. N. Smith, R. O. Marshall. Fixation of molecular tritium by bacterial suspensions. *Arch. Biochem. Biophys.* **1952**, *39*, 395.

[28]. J. A. Cracknell, K. A. Vincent, M. Ludwig, O. Lenz, B. Friedrich, F. A. Armstrong. Enzymatic oxidation of H_2 in atmospheric O_2: The electrochemistry of energy generation from trace H_2 by aerobic microorganisms. *J. Am. Chem. Soc.* **2008**, *130*, 424.

[29]. L. De Gilles, P. De Pascale, Z. Dermoun, M. Rousset, M., A. Vermegljo. Reduction of technetium(VII) by *Desulfovibrio fructosovorans* is mediated by the nickel-iron hydrogenase. *Appl. Environ. Microbiol.* **2001**, *67*, 4583.

[30]. I. Bárány, V. Vu. Central limit theorems for Gaussian polytopes. *Ann. Probab.* **2007**, *35*, 1593.

[31]. A. L. Sessions, J. M. Hayes, J.M. Calculation of hydrogen isotopic fractionations in biogeochemical systems. *Geochim. Cosmochim. Acta* **2005**, *69*, 593 (2005).

[32]. J. Muccitelli, W. -Y. Wen. Solubilities of hydrogen and deuterium gases in water and their isotope fractionation factor. *J. Solution Chem.* 1978, **7**, 257.

[33]. R. Battino. The Ostwald coefficient of gas solubility. *Fluid Phase Equilib.* **1984**, ***15***, 231.

[34]. Y. -H. Luo, L. Steinberg, S. Suda, S. Kumazawa, A. Mitsui. Extremely low D/H ratios of photoproduced hydrogen by cyanobacteria. *Plant Cell Physiol.* **1991**, *32*, 897.

[35]. E. S. Bamberger, D. King, D. L. Erbes, M. Gibbs. H_2 and CO_2 evolution by anaerobically adapted *Chlamydomonas reinhardtii* F-60. *Plant Physiol.* **1982**, *69*, 1268.

[36]. M. Gibbs, R. P. Gfeller, C. Chen. Fermentative metabolism of *Chlamydomonas reinhardii*. III. Photoassimilation of acetate. *Plant Physiol.* **1986**, *82*, 160.

[37]. L. Cournac, G. Guedeney, G. Peltier, P. M. Vignais. Sustained photoevolution of molecular hydrogen in a mutant of *Synechocystis sp.* strain PCC 6803 deficient in the type I NADPH-dehydrogenase complex. *J. Bacteriol.* **2004**, *186*, 1737.

[38]. A. L. Sessions. Isotope-ratio detection for gas chromatography. *J. Sep. Sci.* **2006**, *29*, 1946.

[39]. B. J. Roberts, M. E. Russ, N. E. Ostrom. Rapid and precise determination of the $\delta^{18}O$ of dissolved and gaseous dioxygen via gas chromatography-isotope ratio mass spectrometry. *Environ. Sci. Technol.* **2000**, *34*, 2337.

CHAPTER 3

ISOTOPIC FRACTIONATION ASSOCIATED WITH [NiFe]- AND [FeFe]-HYDROGENASES

Hasand Gandhi helped with the gas chromatography-isotope ratio mass spectrometry analyses. Adam J. Cornish provided constructs for four enzyme samples. Liang Shi and John Peters kindly provided purified [NiFe]-hydrogenases from *Desulfivibrio fructosovorans* and *Thiocapsa roseopersicina*, respectively. James J. Moran and Helen W. Kreuzer helped with the analyses and discussion. Nathaniel Ostrom and Eric Hegg helped analyze data and directed the research.

ABSTRACT

RATIONALE: Hydrogenases catalyze the reversible formation of H_2 from electrons and protons with high efficiency. Understanding the relationships between H_2 production, H_2 uptake, and H_2-H_2O exchange can provide insight into the metabolism of microbial communities in which H_2 is an essential component in energy cycling.

METHODS: In this manuscript, we used stable H isotopes (^1H and ^2H) to probe the isotope effects associated with three [FeFe]-hydrogenases and three [NiFe]-hydrogenases.

RESULTS: All six hydrogenases displayed fractionation factors for H_2 formation that were significantly less than 1, producing H_2 that was severely depleted in ^2H relative to the substrate, water. Consistent with differences in their active site structure, the fractionation factors for each class appear to cluster, with the three [NiFe]-hydrogenases (α = 0.27-0.40) generally having smaller values than the three [FeFe]-hydrogenases (α = 0.41-0.55). We also obtained isotopic fractionation factors associated with H_2 uptake and H_2-H_2O exchange under conditions similar to those utilized for H_2 production, providing us with a more complete picture of the three reactions catalyzed by hydrogenases.

CONCLUSIONS: The fractionation factors determined in our studies can be used as signatures for different hydrogenases to probe their activity under different growth conditions and to ascertain which hydrogenases are most responsible for H_2 production and/or uptake in complex microbial communities.

Key Words

[FeFe]-hydrogenase; [NiFe]-hydrogenase; fractionation factor; kinetic isotope effect (KIE); hydrogen isotopes; isotope ratio mass spectrometry (IRMS)

INTRODUCTION

Microbial H_2 production is of great interest to chemists, biologists, and biogeochemists. Because H_2 has the highest gravimetric energy density (-242 kJ mol^{-1})[1] of any fuel and can be produced from renewable sources both chemically and biochemically, it is often considered as a potential alternative energy source. In addition, H_2 is a key metabolite produced and/or consumed by many bacteria and algae. In natural ecosystems H_2 is often transferred between different microbial communities during syntrophic growth,[2-5] and the flux of H_2 through these systems can therefore provide important information about the interactions of these microbial communities.

Two of the most important classes of enzymes involved in microbial H_2 production and consumption are [FeFe]- and [NiFe]-hydrogeneases.[6, 7] These enzymes do not share any evolutionary relationships, and as their names imply, they differ significantly in their active site structures, with [FeFe]-hydrogenases containing a diiron center and [NiFe]-hydrogenases harboring a NiFe heterodinuclear center (Figure 9).[8, 9] In [FeFe]-hydrogenases, only the distal iron atom changes oxidation state in the observed intermediates of the catalytic cycle,[10] and the nitrogen atom of the unusual bridging dithiomethylamine ligand is proposed to play an integral role in proton transfer.[6, 11] Conversely, in [NiFe]-hydrogenases all of the redox chemistry happens at the Ni atom, and one of the cysteine ligands is proposed to participate in the acid-base chemistry.[6, 12] In addition, [FeFe]-hydrogenases tend to be more active in H_2 generation than [NiFe]-hydrogenases, with an *in vitro* rate for the [FeFe]-hydrogenases of up to 8.2 mmol

H_2 min^{-1} $mg\ protein^{-1}$ (~ 10^4 molecules of H_2 per second per molecule of enzyme).[13] Thus, despite the fact that both [FeFe]- and [NiFe]-hydrogenases catalyze the reversible reduction of protons to H_2, they utilize different reaction mechanisms.[8]

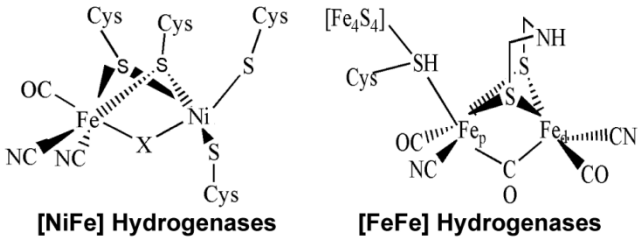

Figure 9: Structures of the active sites in [NiFe]- and [FeFe]-hydrogenases (modified from Lubitz et al.[6]).

Hydrogenases are capable of catalyzing the three following reactions: (1) H_2 production ($2H^+ + 2e^- \rightarrow H_2$),[7] (2) H_2 consumption via the heterolytic cleavage of H_2 ($H_2 \rightarrow H^+ + H^- \rightarrow 2H^+ + 2e^-$),[14] and (3) H_2-H_2O exchange.[15] In the exchange reaction, H_2 binds to the active site and is heterolytically cleaved to a proton and a metal-bound hydride as in the H_2 consumption reaction,[16] but then the proton exchanges with the surrounding water before recombining with the metal-bound hydride to regenerate H_2. Depending on the physiological conditions, more than one of these reactions may be occurring in the cell simultaneously. Due to these complexities, it is therefore advantageous when studying microbial H_2 production to isolate and analyze both H_2 consumption and H_2-H_2O exchange as well.

Hydrogen isotopes are uniquely suited to be a powerful and non-invasive tool for investigating microbial H_2 metabolism. Not only is the movement of hydrogen ions an essential component of most of the key steps of the reaction pathway, but the isotope effects tend to be large due to the substantial relative difference in mass between ^1H and ^2H. Consequently, hydrogen isotopes have been widely utilized over the years to interrogate hydrogenase function and mechanism. For example, experiments studying H_2-H_2O exchange have used hydrogen isotopes as a tracer to track the proton-hydride recombination process[17, 18] and as a mechanistic probe to confirm that H_2 is split by hydrogenases via heterolysis.[19]

The different active site structures and reaction mechanisms of [NiFe]- and [FeFe]-hydrogenases will inevitably lead to distinct reaction profiles. Not only might this result in unique isotopic preferences for these two classes of enzymes, we propose that even enzymes within the same class can have different isotopic preferences due to slight differences in substrate binding, proton transfer, hydrogen bonding, etc. that result in slight perturbations in the reaction profile. Thus, in theory each hydrogenase can have its own unique isotopic signature for both H_2 production and consumption. These isotopic signatures can be measured via isotope ratio mass spectrometry (IRMS)[§] and expressed as fractionation factors (α), i.e. $\alpha = R_{product}/R_{substrate}$, where $R_{product}$ and $R_{substrate}$ are the isotope ratio of the product and substrate, respectively. If these isotopic signatures can be precisely measured, then it may be possible to identify the source of hydrogenase activity in a complex community.[20]

[§] Abbreviations: CpFeFe, *Clostridium pasteurianum* [FeFe]-hydrogenase; CrFeFe, *Chlamydomonas reinhardtii* [FeFe]-hydrogenase; DfNiFe, *Desulfovibrio fructosovorans* [NiFe]-hydrogenase; GC-IRMS, gas chromatography-isotope ratio mass spectrometry; IRMS, isotope ratio mass spectrometry; KIE, kinetic isotope effect; SoFeFe, *Shewanella oneidensis* [FeFe]-hydrogenase; SoNiFe, *Shewanella oneidensis* [NiFe]-hydrogenase; TrNiFe, *Thiocapsa roseopersicina* [NiFe]-hydrogenase; VSMOW, Vienna Standard Mean Ocean Water.

In this manuscript we report fractionation factors associated with H_2 production, H_2 uptake, and H_2-H_2O exchange for 6 different hydrogenases under similar conditions. To our knowledge, this is the first manuscript that compares a variety of fractionation factors among different hydrogenases as well as different hydrogenase reactions.

EXPERIMENTAL

Enzyme preparation.

The [FeFe]-hydrogenase from *Clostridium pasteurianum* (CpFeFe), the [FeFe]-hydrogenase CrHydA1 from *Chlamydomonas reinhardtii* (CrFeFe), and both the [FeFe]- and [NiFe]-hydrogenases from *Shewanella oneidensis* MR-1 (SoFeFe and SoNiFe, respectively) were cloned into a modified pAC-BAD vector, overexpressed in *S. oneidensis* MR-1, and purified via Ni-NTA (Ni-nitrilotriacetic acid, Qiagen, Valencia, CA) affinity chromatography as described by Cornish et al.[21] Briefly, the coding sequence of the hydrogenases were amplified by PCR and inserted into the NcoI/SacI sites of the plasmid pAC-BAD which contains a kanamycin resistance marker and an L-arabinose inducible promoter. The resulting plasmids were transformed into a *S. oneidensis* strain lacking the native [FeFe]- and [NiFe]-hydrogenases (*ΔhydA/ΔhyaB*) but retaining the native maturation proteins required to assemble active hydrogenase. Following expression and purification,[21] the active hydrogenase fractions were pooled, concentrated, and stored in Tris buffer (100 mM Tris-HCl, pH 8.0, 200 mM NaCl, 10 mM sodium dithionite) with 10% (vol/vol) glycerol at -20 ℃. Sodium dodecyl sulfate-polyacrylamide gel electrophoresis of the purified hydrogenases showed that approximately 80%

of the total protein in the lane was present in a single band corresponding to the hydrogenase. The *Desulfivibrio fructosovorans* hydrogenase (DfNiFe), kindly provided to us by Liang Shi (Pacific Northwest National Lab, Richland, WA), was purified from the native organism as described previously.[22] The [NiFe]-hydrogenase from *Thiocapsa roseopersicina* (TrNiFe) was provided by John Peters (Montana State University, Bozeman, MT).[23, 24]

H_2 evolution assay.

H_2 evolution activity assays were performed using the procedure published in Yang et al.[25] Briefly, sodium dithionite (100 mM final concentration) and methyl viologen (20 mM final concentration) were dissolved in 100 mM Tris buffer (pH 8.0) in an anaerobic Coy chamber (filled with 2-4% H_2 balanced with N_2), sealed in a 125 mL serum vial (Wheaton Science Products, Millville, NJ, USA), and then degassed on a Schlenk line to remove excess H_2. Following the anaerobic addition of 100 μL of the appropriate hydrogenase (~ 0.4 mg/mL) using a gas-tight syringe, the concentration and isotope ratio of H_2 in the headspace were monitored and analyzed via continuous flow gas chromatography-isotope ratio mass spectrometry (GC-IRMS)[25] over the course of 3-4 h. The amount of H_2 in the headspace was quantified from the peak height (ion beam intensity at $m/z = 2$) using a standard curve, and the changes of the isotope ratios over time were fit to a Rayleigh equation to obtain the fractionation factors. Because hydrogenases can catalyze both H_2 uptake and H_2-H_2O exchange in addition to H_2 formation, the concentration of H_2 in the headspace was monitored and maintained below 5%. In addition, excess reductant was used to drive the reaction towards H_2 evolution and mitigate the effects of the competing reactions.

The raw data (Table 5) was subjected to a one-sided t test to determine the outliers[26] in which the mean values of 6 samples for CrFeFe, and mean values of 8 samples for CpFeFe were used. Two observations were ruled as outliers based on one-tailed 5% significance levels. In addition, the data for H_2-H_2O exchange (Figure 10) were also checked for outliers based on 5% confidence level by using a one-sided t test. In total, our analyses include data from 5 biological replicates for CrFeFe, 7 biological replicates for CpFeFe, 4 biological replicates for both SoFeFe and SoNiFe, 6 biological replicates for DfNiFe, and 2 biological replicates for TrNiFe.

Table 5: δ^2H data for production of H_2 by different hydrogenases.

Name	Time (h)	H_2[a] (μmol/mL)	δ^2H (‰)	Average
CrFeFe hydrogenase				
9/30/2010				
Cr Sample 1	1	1.65	-546.0	
	3	2.36	-584.3	-565.1
10/1/2010				
Cr Sample 2	1	2.09	-603.5	
	2	2.59	-614.7	
	3	2.95	-621.1	-613.1
11/22/2010				
Cr Sample 3	1	1.56	-543.2	

Table 5 (cont'd)

	3	1.74	-563.5	-553.4
Cr Sample 4	1	1.18	-567.7	
	2	1.12	-570.6	
	3	1.42	-523.7	
	4	1.20	-578.1	
	5	1.12	-579.6	-563.9
11/23/2010				
Cr Sample 5	1	1.89	-548.9	-548.9
mean ± SD				**-568.9 ± 25.7**
CpFeFe hydrogenase				
6/9/2011				
Cp Sample 1	2	1.55	-450.4	
	3	2.93	-505.5	
	4	1.21	-540.1	-498.7
8/4/2011				
Cp Sample 2	1	1.72	-498.4	
	2	3.16	-514.2	-506.3
Cp Sample 3	1	2.14	-492.9	
	2	2.50	-495.1	-494.0
8/5/2011				
Cp Sample 4	1	1.41	-465.6	

Table 5 (cont'd)

	2	1.86	-471.0	-468.3
Cp Sample 5	1	0.89	-349.6	
	2	1.03	-445.8	-397.7
Cp Sample 6	1	0.60	-427.1	
	2	1.40	-461.3	
	3	2.03	-472.1	-453.5
2/6/2012				
Cp Sample 7	1	0.16	-518.7	
	2	0.16	-519.0	
	3	0.30	-520.9	-519.5
mean ± SD				**-476.9 ± 41.5**
SoFeFe hydrogenase				
9/30/2010				
SoFe Sample 1[b]	1	0.35	-632.4	
	2	0.41	-639.9	
	3	0.45	-639.1	-637.1
8/5/2011				
SoFe Sample 2	1	2.62	-645.5	-645.5
11/7/2012				
SoFe Sample 3	1	0.55	-588.67	
	2	0.56	-590.26	

Table 5 (cont'd)

	3	0.68	-601.28	-593.40
SoFe Sample 4	1	0.55	-590.64	
	2	0.57	-594.52	-592.58
mean ± SD				**-617.2 ± 28.1**
SoNiFe hydrogenase				
8/5/2011				
SoNi Sample 1	3	0.78	-633.3	-633.3
SoNi Sample 2	3	0.81	-630.7	-630.7
11/7/2012				
SoNi Sample 3	1	0.32	-617.57	
	2	0.34	-620.19	
	3	0.39	-629.13	-622.30
SoNi Sample 4	1	0.32	-621.32	
	2	0.34	-618.91	-620.11
mean ± SD				**-626.6 ± 6.39**
DfNiFe hydrogenase				
7/21/2009				
Df Sample 1	1	0.63	-728.5	
	2	0.84	-735.1	
	3	1.00	-735.6	-733.1
Df Sample 2	1	0.59	-730.4	

Table 5 (cont'd)

	2	0.76	-731.8	
	3	1.09	-736.6	-732.9
8/6/2009				
Df Sample 3	1	0.55	-762.7	
	2	0.81	-757.6	
	3	0.95	-759.3	-759.9
Df Sample 4	1	0.53	-763.1	
	2	0.80	-757.4	
	3	0.89	-751.7	-757.4
11/23/2010				
Df Sample 5	1	0.51	-722	
	2	0.66	-733.6	
	3	0.96	-743.9	-733.2
12/1/2010				
Df Sample 6	1	0.90	-737.3	
	2	1.01	-735.8	
	3	1.13	-737.8	
	4	1.25	-744.7	-738.9
mean ± SD				**-742.6 ± 12.7**
TrNiFe hydrogenase				
9/9/2009				

Table 5 (cont'd)

TrNiFe Sample 1	1	0.22	-723.69	
	2	0.25	-725.46	
	3	0.28	-724.32	
	4	0.31	-723.05	-724.13
TrNiFe Sample 2	1	0.12	-725.13	
	2	0.14	-726.37	
	3	0.16	-726.56	
	4	0.18	-726.86	-726.23
mean ± SD				**-725.18 ± 1.05**

[a]The H_2 concentrations were calculated by comparing the peak heights of the samples generated via GC-IRMS to those of the standards with known amounts of H_2. Concentrations have not been corrected for sampling loss (~1% per injection).

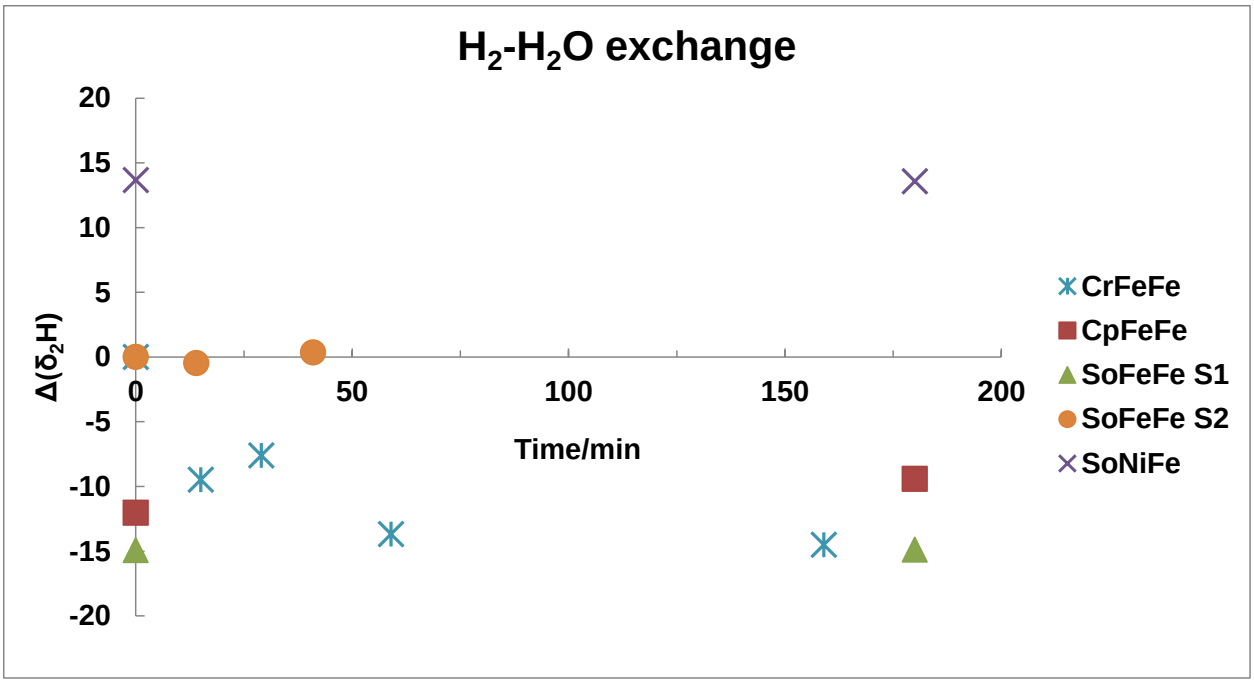

Figure 10: δ^2H measurements of H_2-H_2O exchange reactions catalyzed by different hydrogenases over the course of 180 min.

H_2 uptake assay.

A hydrogen uptake assay was performed similarly to the H_2 formation assay except that H_2 and the oxidant benzyl viologen were present instead of a reductant. The redox potential of benzyl viologen is approximately -0.370 V vs the standard hydrogen electrode,[27] providing the driving force for H_2 oxidation. Briefly, 50 mL of uptake buffer (100 mM Tris-HCl, pH 8.0, 200 mM NaCl, 10 mM benzyl viologen, 5% glycerol) were sealed in a 125 mL serum vial in an anaerobic Coy chamber with approximately 5% H_2 in the headspace (the maximum concentration of H_2 present in the headspace during H_2 evolution experiments). To initiate the reaction, a 1 mL syringe was used to inject 100 µL of purified enzyme (~ 0.4 mg/mL), and the reaction vial was

then inverted and shaken at room temperature. The reaction was allowed to proceed for 3-4 h, and 1 mL of the headspace was analyzed every ~60 min. The amount and isotope ratio of the H_2 that remained after the various time points were analyzed via GC-IRMS as described above for the H_2 evolution assay.

H_2-H_2O exchange assay.

A 1 mL syringe was used to inject 100 µL of purified enzyme (~ 0.4 mg/mL) into a 125 mL serum vial containing approximately 5% H_2 in the headspace (to simulate the maximum H_2 present in the headspace during the H_2 evolution experiments) and 50 mL of reaction buffer (100 mM Tris-HCl, pH 8.0, 200 mM NaCl, 5% glycerol). The mixture also contained one enzyme equivalent of the oxidant benzyl viologen to poise the enzyme for H_2 binding and exchange. The reaction vial was then mixed, inverted, and incubated at room temperature while shaking. The isotope ratio of the H_2 was measured via GC-IRMS for up to 50 h, and the amount of H_2 remaining in the headspace was quantified from the peak height (ion beam intensity at m/z 2) using a standard curve.

Standardization and notation.

All results are reported with respect to VSMOW (Vienna Standard Mean Ocean Water), whose absolute ratio of $^2H/^1H$ is $155.76\ (\pm 0.05) \times 10^{-6}$.[28] The relative ratio of a sample with respect to VSMOW is commonly given by the relationship:

$$\delta^2H = (R_{sample}/R_{VSMOW} - 1) \times 1000\ (‰)$$

where $R = {}^2H/{}^1H$.

The preference that any given reaction has for one isotope over another is defined as α:

$$\alpha = R_{product}/R_{reactant,}$$

where $R_{product}$ and $R_{reactant}$ are isotope ratios of the product and reactant, respectively. For H_2 production $\alpha = R_{H2}/R_{H2O}$, while for H_2 uptake $\alpha = R_{H2O}/R_{H2}$. Under our experimental conditions the water was in vast excess in these reactions, and R_{H2O} was therefore essentially constant during the course of our reactions.

The kinetic isotope effect (KIE) is a related term that describes the difference in rate between the two isotopes:

$$KIE = k_{light}/k_{heavy}$$

where k_{light} and k_{heavy} are the rate constants for the light (^1H) and heavy (^2H) isotopes, respectively.[29] In this formalism, the fractionation factor (α) and the KIE are the inverse of one another:

$$\alpha = R_{product}/R_{reactant} = (k_{light}/k_{heavy})^{-1} = KIE^{-1}$$

RESULTS

Isotopic fractionation associated with H_2 evolution

Figure 11 and Table 6 report the isotope ratios of H_2 produced by six different hydrogenases as well as the corresponding KIEs and fractionation factors. Because the water (δ^2H = -60‰) in these experiments can be considered an infinite reservoir, R_{H2} is directly proportional to α, and

the isotope ratio of the H_2 produced can therefore be used to characterize the fractionation patterns by different hydrogenases. From the figure, it can be seen that CrFeFe and CpFeFe produced H_2 with the δ^2H values of approximately -570‰ and -480‰, respectively. Conversely, DfNiFe and TrNiFe both generated H_2 with considerably more negative δ^2H values of roughly -745‰ and -725‰, respectively. Interestingly, the two purified hydrogenases from *S. oneidensis* produced H_2 with isotope ratios that were between these two extremes, and within error indistinguishable from each other ($p = 0.55$), with SoFeFe generating H_2 with a δ^2H value of approximately -615‰ and SoNiFe yielding H_2 with an isotope ratio of roughly -625‰.

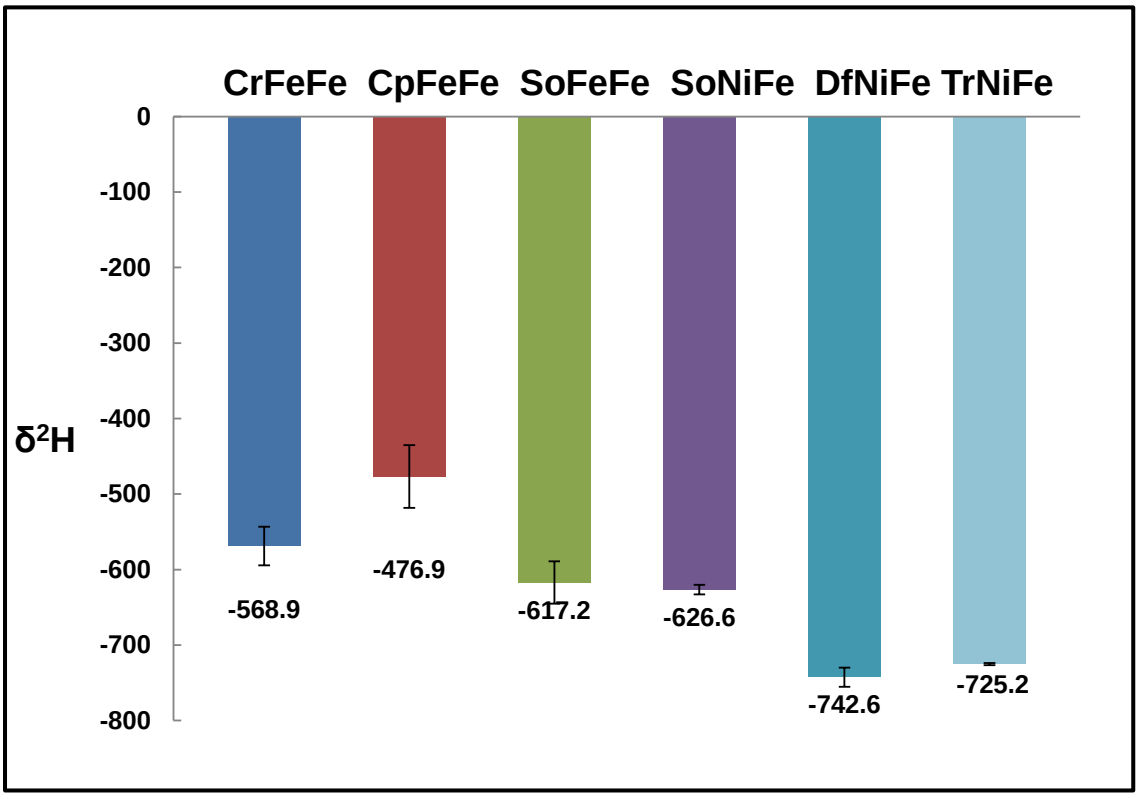

Figure 11: Isotope ratio of H_2 produced by different hydrogenases. For each enzyme, at least 3 samples were analyzed to calculate the average and standard deviation values.

Table 6: Fractionation factors (α) and kinetic isotope effect (KIE) values calculated for H_2 production catalyzed by different [NiFe]- and [FeFe]-hydrogenases. Values are expressed as the mean ± SD (standard deviation).

	CrFeFe	CpFeFe	SoFeFe	SoNiFe	DfNiFe	TrNiFe
δ^2H ± SD	-568.9 ± 25.7	-479.6 ± 41.5	-617.2 ± 28.1	-626.6 ± 6.4	-742.6 ± 12.7	-725.2 ± 1.4
α ± SD	0.46 ± 0.03	0.55 ± 0.04	0.41 ± 0.03	0.40 ± 0.01	0.27 ± 0.01	0.293 ± 0.001
KIE ± SD	2.18 ± 0.14	1.80 ± 0.13	2.46 ± 0.18	2.51 ± 0.04	3.65 ± 0.18	3.41 ± 0.02

To ensure that the results obtained were not significantly altered by the competing pathways (i.e H_2 consumption or H_2-H_2O exchange), experimental conditions were set such that excess reductant was used to drive the reaction toward H_2 production and the headspace H_2 concentration was kept below 5% to minimize the back reaction. In addition, analyses were carried out to determine if there was a correlation between the rate of the reaction and the extent of H_2 production. The rationale was that H_2 consumption (which would alter the apparent H_2 production rate) is strongly dependent on the partial pressure of H_2. Therefore, if H_2 consumption is occurring to a significant extent in our reaction, the apparent H_2 production rate should slow in a predictable manner over time. Figure 12, however, indicated that there was no obvious correlation between H_2 production rate and the extent of reaction, suggesting that H_2

consumption is not significant under our reaction conditions. Nevertheless, the variations observed in the isotope ratio of H_2 produced by some of the hydrogenases, particularly CrFeFe and CpFeFe (the two hydrogenases that were the most active in H_2 production) suggested that competing reactions might be occurring despite our best efforts to minimize them.

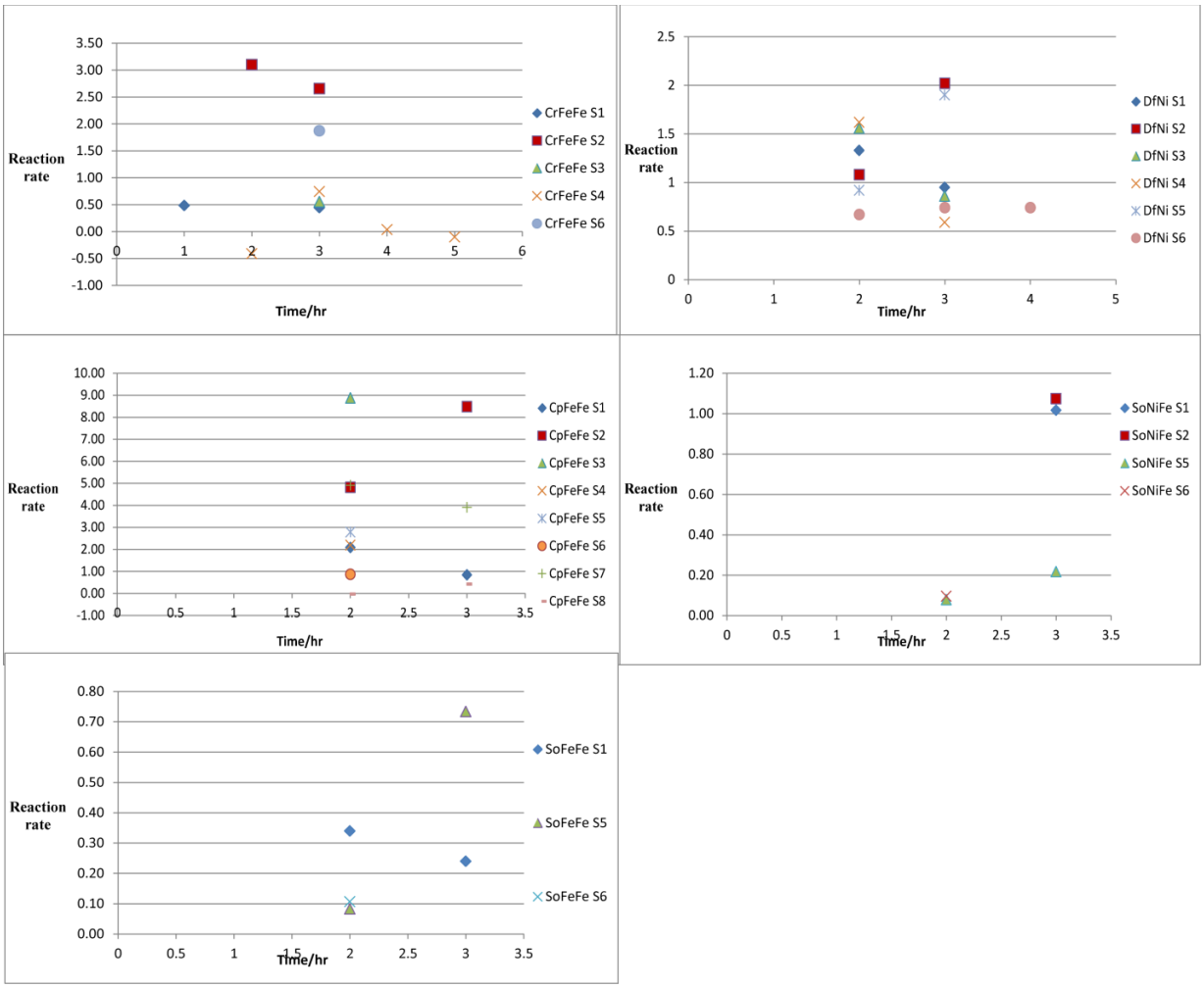

Figure 12: Measured H_2 production rate over the course of the analyses. No obvious correlation was observed between the apparent rate of H_2 production and the extent of the reaction.

To assess whether competing reactions were significantly impacting the α and KIE values calculated for H_2 production, we analyzed the δ^2H of the H_2 produced by each enzyme over time (Figure 13, Table 5). Because water is an infinitely large substrate reservoir, a constant δ^2H value for H_2 production should be observed in the absence of competing reactions. If, however, either H_2 uptake or H_2-H_2O exchange (which have distinct fractionation factors) where occurring to a large extent under our H_2 production reaction conditions, then the rates of these competing reactions would increase over time as the concentration of H_2 in the headspace increased. This would, in turn, alter the isotope ratio of the headspace H_2 in a time-dependent manner that reflected the increased importance of the isotope effects associated with the secondary reaction(s). For most of the hydrogenases used in this study, no consistent trend in δ^2H with reaction time was observed (Figure 13), suggesting that these competing reactions were not a significant factor under our experimental conditions.

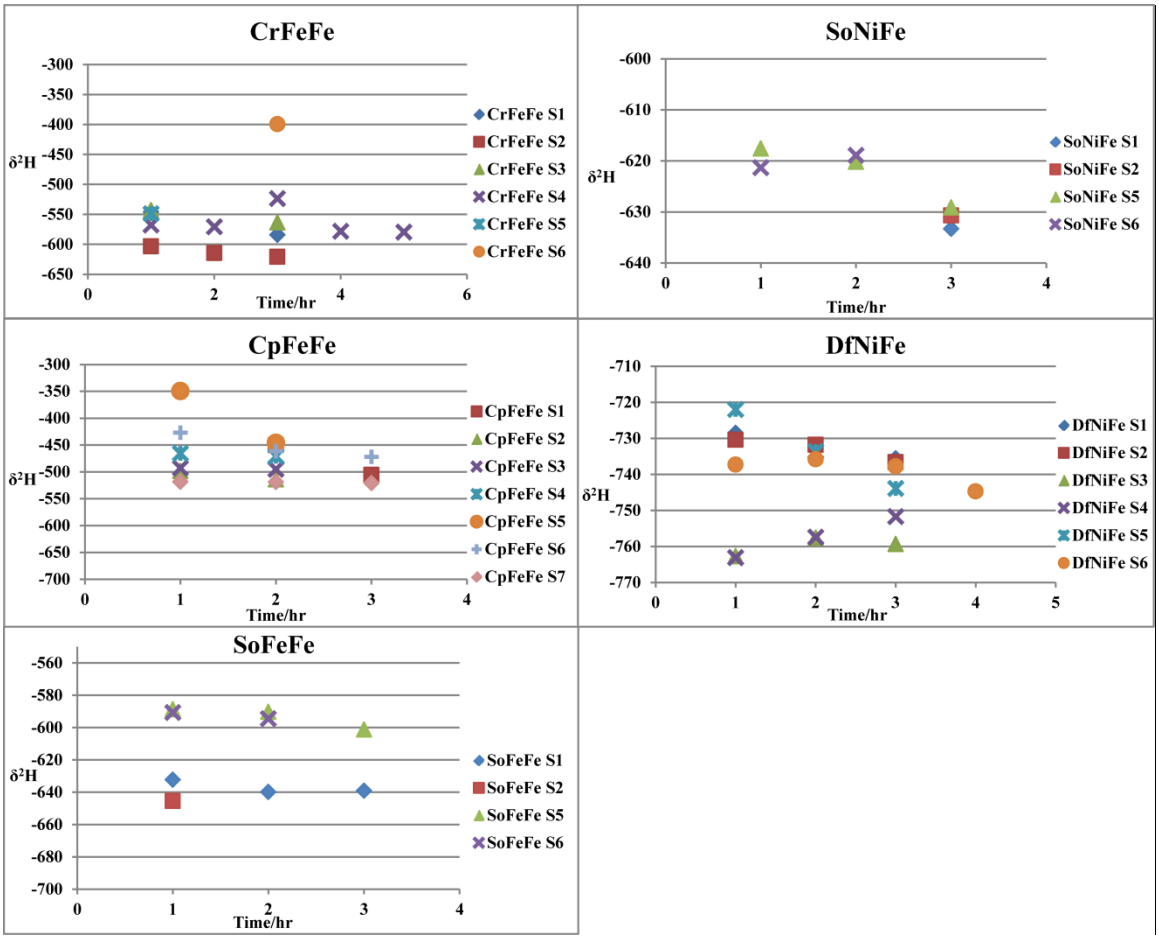

Figure 13: Relationship between reaction rate and δ^2H of the H_2 produced in H_2 evolution reaction tested. In different graphs, different symbol represents different samples tested.

In the case of CpFeFe, however, the H_2 produced became more depleted in ^2H over time in approximately half of the experiments (Table 5, Figure 13). This decreasing trend in δ^2H in the CpFeFe reaction could be explained if H_2-H_2O exchange drove the accumulated H_2 toward a value reflecting isotopic equilibrium (δ^2H = -755‰ when equilibrated with Michigan tap water of δ^2H = -60‰; see Supplementary Information for calculation) between H_2 and H_2O.[30] Alternatively, H_2 uptake may have been occurring, in which case our data indicates this reaction

would have a preference for ^{2}H (i.e. an inverse KIE). To address these issues, we performed experiments to measure independently both H_2 uptake and H_2-H_2O exchange for each of the hydrogenases.

Isotopic fractionation associated with H_2 consumption

To quantify the isotope effect associated with enzymatic H_2 consumption, H_2 with a precisely defined isotope ratio was incubated with each of the hydrogenases in the presence of a strong oxidant, benzyl viologen. The reaction conditions mimicked those used in the H_2 production assay, including maintenance of the headspace H_2 concentration below 5%, with the exception that an electron acceptor was used instead of an electron donor. Both the amount and the isotope ratio of H_2 remaining in the headspace at each time point were used to fit the Rayleigh equation[31, 32] to calculate the fractionation factors associated with each enzyme (Figure 14).

$$\delta_{H_{2,T=t}} = -\frac{f*\ln f}{1-f} \times \varepsilon + \delta_{H_{2,T=0}} \quad (1)$$

$$\alpha = \varepsilon/1000 + 1 \quad (2)$$

where $\delta_{H_{2,T=t}}$ is the isotope ratio of H_2 at different time points, *f* is the fraction of H_2 remaining in the headspace, ε is the enrichment factor related to the reaction, and α is the fractionation factor related to the uptake reaction.

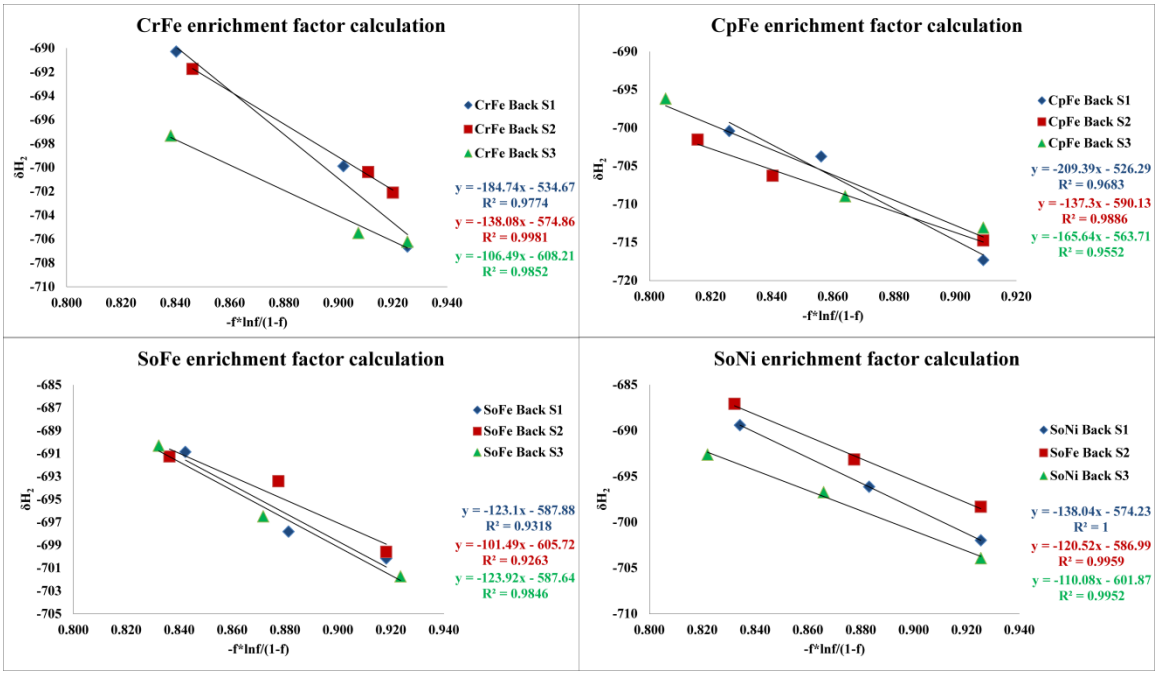

Figure 14: Relationships between isotope ratio of headspace H_2 (δH_2) and the fraction of H_2 consumed (*f*) for 4 different hydrogenases tested. According to the Rayleigh equation, the slope of the line is the enrichment factor (ε).

As shown in Table 7, the fractionation factors calculated for H_2 consumption associated with each of the four different hydrogenases tested are very similar to each other. This seemingly surprising result can be easily explained if H_2 diffusion from the headspace into solution is the rate-limiting step in the reaction, thereby masking the true fractionation factor for H_2 consumption associated with each hydrogenase.

Table 7: Fractionation factors (α) and enrichment factors (ε) measured for H_2 consumption (i.e. oxidation) catalyzed by different [NiFe]- and [FeFe]-hydrogenases.

Samples were monitored for approximately 3 hours as described in the Experimental section. Values are expressed as the mean ± SD (standard deviation).

	CrFeFe	CpFeFe	SoFeFe	SoNiFe
ε	-143.10 ± 39.36	-170.78 ± 36.32	-116.17 ± 12.72	-122.88 ± 14.13
α	0.86 ± 0.04	0.83 ± 0.04	0.88 ± 0.01	0.88 ± 0.01
KIE ± SD	1.17 ± 0.05	1.21 ± 0.05	1.13 ± 0.02	1.14 ± 0.02

Isotopic fractionation associated with H_2-H_2O exchange reaction

The H_2-H_2O exchange isotopic fractionation factor was quantified to assess whether this reaction might be contributing to the isotopic variations observed in the H_2 production experiments. Thus, H_2-H_2O exchange reactions were established using experimental conditions similar to the H_2 production reactions only without the addition of reductant. Furthermore, the isotopic compositions of the H_2 and H_2O were chosen such that they were very distinct (δ^2H-$H_2 \approx$ -430‰, δ^2H-H_2O = -60‰) and δ^2H-H_2 was far away from the equilibrium isotope value (δ^2H-H_2 at equilibrium is calculated to be -755‰ at 25°C[30]). Although minor variations at initial time points in δ^2H of H_2 were evident (perhaps due to a small degree of isotope fractionation during

introduction of the H_2 gas into the headspace), the isotopic ratio headspace H_2 did not vary substantially during 3 h measurements (Figure 10), suggesting that H_2-H_2O exchange is not occurring to a great extent under our reaction conditions.

DISCUSSION

Three important observations can be made from the H_2 production results presented in Figure 11 and Table 6. First, when producing H_2, all of the hydrogenases have fractionation factors much less than one and therefore produce H_2 that is severely depleted in ^2H relatively to H_2O. This indicates that, as expected, protons (^1H) react to form H_2 faster than deuterons (^2H) react, consistent with deuterons forming stronger and less labile hydrogen bonds.

The second important observation is that the data seem to partition into two separate clusters (Figure 15, $p = 0.01$), with the [FeFe]-hydrogenases generally having smaller α values and producing H_2 that is typically more enriched in ^2H relative to the H_2 produced by the [NiFe]-hydrogenases. (It should be noted that while the SoFeFe and SoNiFe enzymes appear to follow these general trends, the H_2 produced from these two enzymes is indistinguishable based on the t-test ($p = 0.55$), making any definitive distinction of H_2 production from these two enzymes tenuous.) To our knowledge, this is the first report of fractionation factors for purified [FeFe]-hydrogenases ($\alpha = 0.41 – 0.55$). However, our calculated fractionation factors for the [NiFe]-hydrogenases ($\alpha = 0.27 – 0.40$) agree well with other published results in which fractionation factors of 0.3-0.5 can be calculated.[18, 33, 34] Together, these observations are consistent with our hypothesis that [FeFe]- and [NiFe]-hydrogenases generally produce isotopically distinct H_2 due to differences in their active site structures.

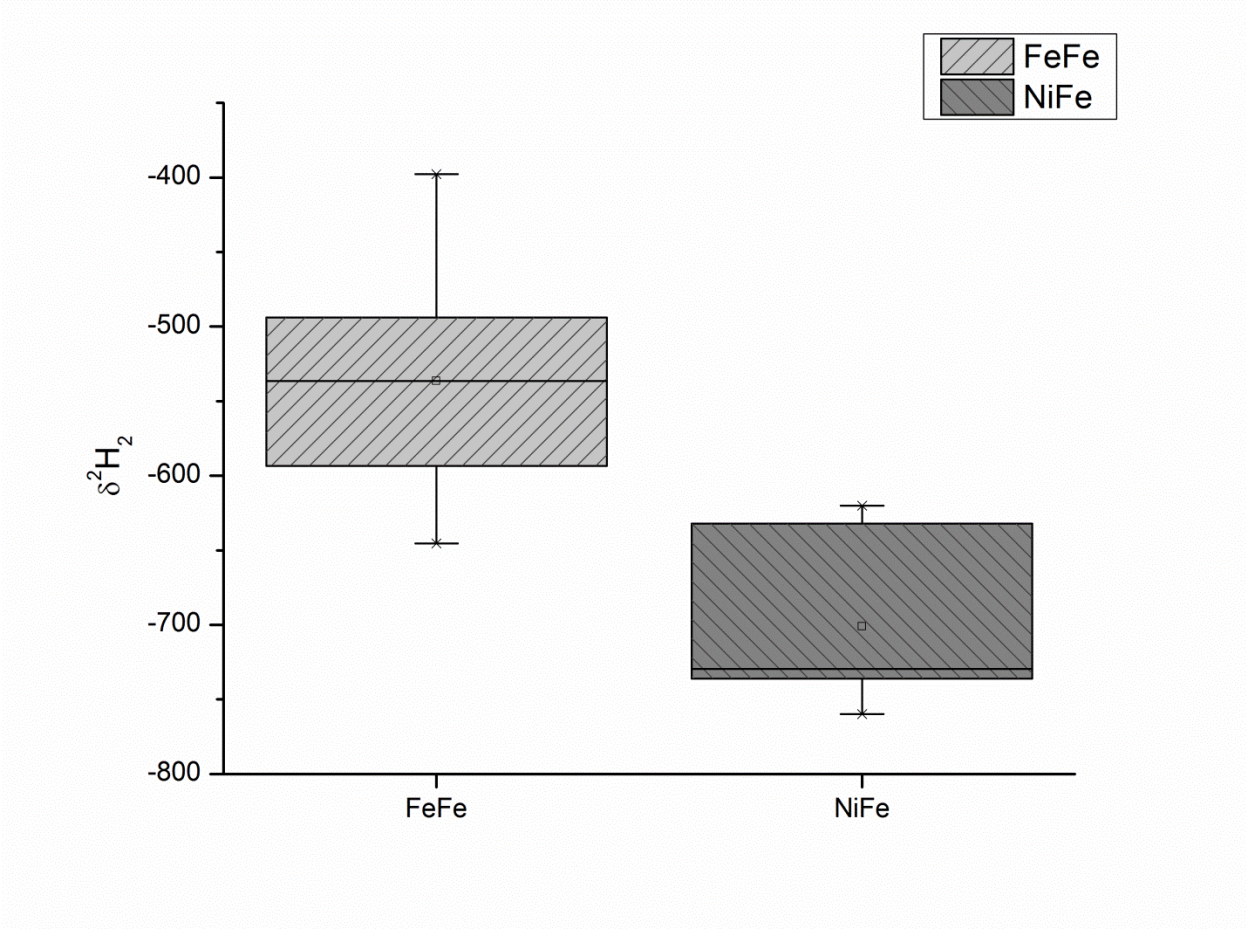

Figure 15: Box plot analysis comparing δ^2H of the H_2 produced by [FeFe]-hydrogenases versus [NiFe]-hydrogenases. The H_2 produced by the [FeFe]-hydrogenases is statistically different from the H_2 produced by the [NiFe]-hydrogenases ($p = 0.01$). The shaded area in the box plot represents the 25-75 percentile for that data set, the line represents the median, the dot indicates the average, and the error bars represent highest/lowest values observed.

Third, even within the same class, different hydrogenases can possess different fractionation factors and produce H_2 with different isotope ratios. In fact, the variation within an enzyme class can be larger than the variation between classes. This result was unexpected

because the amino acids involved in the proton transport pathway are predicted to be conserved within each class.[21, 35] The relatively large variation of α within a class could result from differences in the extent to which the true isotope effect is masked by other processes such as product release (i.e. the release of H_2 after enzyme catalysis), proton transfer, or the extent to which each proton transfer step is reversible under our reaction conditions (i.e. the commitment to catalysis). Consistent with this idea, Hexter et al. noted that different hydrogenases within the same class can have substantially different activation enthalpies,[36] which could affect the reversibility of individual steps. Our current data do not allow us to discriminate between these different possibilities.

One question that remains to be resolved is why the isotope ratio of the H_2 produced by some of the CpFeFe samples became further depleted in ^2H over time. This phenomenon could be explained if H_2 uptake (for which the rate relative to production would increase over time as the concentration of H_2 in the headspace increased) were occurring to a significant extent and if ^1H-^2H were oxidized faster than $^1H_2$ (i.e. if there were an inverse KIE). The data in Table 7, however, indicates that CpFeFe exhibits a normal KIE during H_2 oxidation, indicating a preference for the lighter isotope. This finding is consistent with previous studies of metal-hydrogen binding studies in various M (η^2-H_2) complexes which display normal equilibrium isotope effects of 1.217 to 1.685.[37] In addition, because both of the M-H_2 interactions ($\sigma_{H2} \rightarrow d_M$ and $d_M \rightarrow \sigma^*_{H2}$)[38, 39] will inevitably lead to a weakening of the H-H bond in the transition state, a normal KIE can also be anticipated for H_2 binding and splitting. Thus, H_2 uptake cannot explain the results obtained for CpFeFe.

In theory, H_2-H_2O exchange could also explain the depletion of δ^2H in the accumulated H_2 observed over time during the CpFeFe H_2 production assay. This reaction is well documented in a number of different hydrogenases,[17, 18, 40, 41] and ultimately leads to an δ^2H value for H_2 in equilibrium with the water in our experiments ($\delta^2H \approx -60‰$[42]) of -755‰[30]. If CpFeFe is very efficient at catalyzing this exchange reaction, it could explain the trends we observe in approximately half of the CpFeFe H_2 production reactions. Figure 10, however, indicates that no significant H_2-H_2O exchange is occurring during any of our experiments, all of which utilize relatively low concentrations of natural abundance H_2 for short periods of time. Thus, neither H_2 uptake/oxidation nor H_2-H_2O exchange can account for the depletion of δ^2H in the accumulated H_2 produced by CpFeFe, and further experiments will be needed to explain this observation.

The kinetic isotope effects that we have systematically measured in purified [FeFe]- and [NiFe]-hydrogenases can provide key insights into microbial H_2 metabolism. For example, the relative difference between the H_2 produced by the *S. oneidensis* [FeFe]- and [NiFe]-hydrogenases is about 10‰, which agrees quite well with *in vivo* studies.[20] Interestingly, the initial δ^2H values of H_2 measured in vivo by Kreuzer et al. (-735‰ and -743‰ for [FeFe]- and [NiFe]-hydrogenases, respectively) [20] differ from these current *in vitro* studies by approximately 55‰ even after correcting for the isotope ratio of the water used in the two studies.[42, 43] Isotopic gradients between intracellular and extracellular water are known to exist in certain circumstances,[44-46]which could alter the isotope ratio of H_2 produced *in vivo* relative to what would be expected based on the growth medium water. However, both the [FeFe]- and [NiFe]-hydrogenase in *S. oneidensis* are located in the periplasm, and it is not clear whether a sufficient isotopic gradient is maintained across the outer membrane to account for the observed difference

in δ^2H of H_2 between the in vivo and in vitro experiments. Nevertheless, the nearly identical relative differences in δ^2H between *S. oneidensis* [FeFe]- and [NiFe]-hydrogenases observed in the two studies is intriguing.

Kreuzer et al.[20] used a combination of *in vivo* transcription data and hydrogen isotope ratios to ascertain when the [FeFe]- and [NiFe]-hydrogenases in wild-type *S. oneidensis* were expressed and active. Transcription did not always correlate with activity, highlighting the importance of developing techniques to measure enzyme activity directly when analyzing H_2 production in complex biological communities. The variation in fractionation factors and kinetic isotope effects we observe for [FeFe]- and [NiFe]-hydrogenases indicate that the δ^2H of the H_2 produced can be one important tool.

In conclusion, we determined the fractionation factors and the kinetic isotope effects for both H_2 production and H_2 uptake for three purified [FeFe]-hydrogenases and three purified [NiFe]-hydrogenases. The large normal isotope effects observed for H_2 production for all six hydrogenases indicates that, as expected, protons react faster than deuterons to form H_2. In addition, the calculated fractionation factors seem to cluster, with the [FeFe]-hydrogenases generally having larger fractionation factors than [NiFe]-hydrogenases, consistent with our hypothesis that variations in the active site will contribute to different isotopic preferences. Interestingly, differences within the same class can be just as large or larger than the differences between classes, indicating that other factors are also affecting the reaction coordinates and the isotopic preferences. Importantly, the isotopic fractionation factors reported here provide a basis for distinguishing which enzymes are active in a complex microbial community where H_2 is used as an energy carrier between different species.

Acknowledgements

Financial support was provided by the U.S. Department of Energy (DOE), Office of Biological and Environmental Research (BER), as part of BER's Genomic Science Program (GSP). Pacific Northwest National Laboratory is operated by Battelle Memorial Institute for the U.S. Department of Energy under Contract No. DE-AC05-&6RL01830. Support from NSF (#1053432) is also gratefully acknowledged.

APPENDIX

Calculation of δH_2 after equilibration with H_2O

The fractionation factor for the H_2-H_2O exchange is defined as

$\alpha = R_{H2O}/R_{H2}$

where R_{H2O} and R_{H2} are the isotope ratios for the H_2O and H_2, respectively.

The isotope ratio of H_2O (R_{H2O}) can be calculated using the known δ value of Michigan tap water, where

$\delta H_2O = -60‰$

$R_{H2O} = (\delta H_2O/1000 + 1)*R_{H2O(standard)}$

The $R_{H2O(standard)}$ is known to be $155.76*10^{-6}$ for the H isotope, and R_{H2O} is calculated to be $1.46*10^{-6}$.

According to Horibe et al.[31], the equilibrium fractionation factor (α) for the H_2-H_2O exchange is defined as

$\alpha = 1.0473 + 201036/T^2 + 2.060*10^9/T^4 + 0.180*10^{15}/T^6$

where T is the temperature in Kelvin.

At 25 °C, the α value is calculated to be 3.83. Therefore:

$R_{H2} = R_{H2O}/\alpha = 1.46*10^{-6}/3.83 = 3.81*10^{-5}$

This R value gives rise to a δH_2 value following equilibration with Michigan tap water to be -755‰.

BIBLIOGRAPHY

BIBLIOGRAPHY

[1] M. Trincado, D. Banerjee, H. Grutzmacher. Molecular catalysts for hydrogen production from alcohols. *Energy Environ. Sci.* **2014**, *7*, 2464.

[2] C.B. Walker, Z. He, Z.K. Yang, J.A. Ringbauer, Q. He, J. Zhou, G. Voordouw, J.D. Wall, A.P. Arkin, T.C. Hazen, S. Stolyar, D.A. Stahl. The electron transfer system of syntrophically grown *Desulfovibrio vulgaris*. *J. Bacteriol.* **2009**, *191*, 5793.

[3] C.M. Plugge, J.C.M. Scholten, D.E. Culley, L. Nie, F.J. Brockman, W. Zhang. Global transcriptomics analysis of the *Desulfovibrio vulgaris* change from syntrophic growth with *Methanosarcina barkeri* to sulfidogenic metabolism. *Microbiology* **2010**, *156*, 2746.

[4] X. Li, M.J. McInerney, D.A. Stahl, L.R. Krumholz. Metabolism of H_2 by *Desulfovibrio alaskensis* G20 during syntrophic growth on lactate. *Microbiology* **2011**, *157*, 2912.

[5] K.C. Wrighton, C.J. Castelle, M.J. Wilkins, L.A. Hug, I. Sharon, B.C. Thomas, K.M. Handley, S.W. Mullin, C.D. Nicora, A. Singh, M.S. Lipton, P.E. Long, K.H. Williams, J.F. Banfield. Metabolic interdependencies between phylogenetically novel fermenters and respiratory organisms in an unconfined aquifer. *ISME J* **2014**, *8*, 1452.

[6] W. Lubitz, H. Ogata, O. Rudiger, E. Reijerse. Hydrogenases. *Chem. Rev.* **2014**, *114*, 4081.

[7] P.M. Vignais, B. Billoud. Occurrence, classification, and biological function of hydrogenases: an overview. *Chem. Rev.* **2007**, *107*, 4206.

[8] M. Frey. Hydrogenases: hydrogen-activating enzymes. *Chembiochem* **2002**, *3*, 153.

[9] J.C. Fontecilla-Camps, P. Amara, C. Cavazza, Y. Nicolet, A. Volbeda. Structure–function relationships of anaerobic gas-processing metalloenzymes. *Nature* **2009**, *460*, 814.

[10] W. Lubitz, E. Reijerse, M. van Gastel. [NiFe] and [FeFe] hydrogenases studied by advanced magnetic resonance techniques. *Chem. Rev.* **2007**, *107*, 4331.

[11] A. Silakov, B. Wenk, E. Reijerse, W. Lubitz. ^{14}N HYSCORE investigation of the H-cluster of [FeFe] hydrogenase: evidence for a nitrogen in the dithiol bridge. *Phys. Chem. Chem. Phys.* **2009**, *11*, 6592.

[12] M.-E. Pandelia, H. Ogata, W. Lubitz. Intermediates in the catalytic cycle of [NiFe] hydrogenase: functional spectroscopy of the active site. *ChemPhysChem* **2010**, *11*, 1127.

[13] E.C. Hatchikian, N. Forget, V.M. Fernandez, R. Williams, R. Cammack. Further characterization of the [Fe]-hydrogenase from *Desulfovibrio desulfuricans* ATCC 7757. *Eur. J. Biochem.* **1992**, *209*, 357.

[14] A.I. Krasna. Hydrogenase: Properties and applications. *Enzyme Microb. Technol.* **1979**, *1*, 165.

[15] T. Yagi, Y. Higuchi. Studies on hydrogenase. *Proc. Jpn. Acad. Ser. B Phys. Biol. Sci.* **2013**, *89*, 16.

[16] A.L. De Lacey, V.M. Fernández, M. Rousset, R. Cammack. Activation and inactivation of hydrogenase function and the catalytic cycle: spectroelectrochemical studies. *Chem. Rev.* **2007**, *107*, 4304.

[17] A.R. Klein, G.C. Hartmann, R.K. Thauer. Hydrogen isotope effects in the reactions catalyzed by H_2-forming N^5,N^{10}-methylenetetrahydromethanopterin dehydrogenase from methanogenic Archaea. *Eur. J. Biochem.* **1995**, *233*, 372.

[18] N.A. Zorin, B. Dimon, J. Gagnon, J. Gaillard, P. Carrier, P.M. Vignais. Inhibition by iodoacetamide and acetylene of the H-D-exchange reaction catalyzed by *Thiocapsa roseopersicina* hydrogenase. *Eur. J. Biochem.* **1996**, *241*, 675.

[19] J.-S. Chen, L.E. Mortenson. Purification and properties of hydrogenase from *Clostridium pasteurianum* W5. *Biochim. Biophys. Acta* **1974**, *371*, 283.

[20] H.W. Kreuzer, E.A. Hill, J.J. Moran, R.A. Bartholomew, H. Yang, E.L. Hegg. Contributions of the [NiFe]- and [FeFe]-hydrogenase to H_2 production in *Shewanella oneidensis* MR-1 as revealed by isotope ratio analysis of evolved H_2. *FEMS Microbiol. Lett.* **2014**, *352*, 18.

[21] A.J. Cornish, K. Gärtner, H. Yang, J.W. Peters, E.L. Hegg. Mechanism of proton transfer in [FeFe]-hydrogenase from *Clostridium pasteurianum*. *J. Biol. Chem.* **2011**, *286*, 38341.

[22] L. Shi, S.M. Belchik, A.E. Plymale, S. Heald, A.C. Dohnalkova, K. Sybirna, H. Bottin, T.C. Squier, J.M. Zachara, J.K. Fredrickson. Purification and characterization of the [NiFe]-hydrogenase of *Shewanella oneidensis* MR-1. *Appl. Environ. Microb.* **2011**, *77*, 5584.

[23] O.A. Zadvornyy, M. Allen, S.K. Brumfield, Z. Varpness, E.S. Boyd, N.A. Zorin, L. Serebriakova, T. Douglas, J.W. Peters. Hydrogen enhances nickel tolerance in the purple sulfur bacterium *Thiocapsa roseopersicina*. *Environ. Sci. Technol.* **2009**, *44*, 834.

[24] O.A. Zadvomy, N.A. Zorin, I.N. Gogotov. Influence of metal ions on hydrogenase from the purple sulfur bacterium *Thiocapsa roseopersicina*. *Biochemistry (Moscow)* **2000**, *65*, 1287.

[25] H. Yang, H. Gandhi, L. Shi, H.W. Kreuzer, N.E. Ostrom, E.L. Hegg. Using gas chromatography/isotope ratio mass spectrometry to determine the fractionation factor for H_2 production by hydrogenases. *Rapid Commun. Mass Spectrom.* **2012**, *26*, 61.

[26] F.E. Grubbs. Procedures for detecting outlying observations in samples. *Technometrics* **1969**, *11*, 1.

[27] D. Wang, W.E. Crowe, R.M. Strongin, M. Sibrian-Vazquez. Exploring the pH dependence of viologen reduction by a-carbon radicals derived from Hcy and Cys. *Chem. Commun.* **2009**, 1876.

[28] J.R. De Laeter, J.K. Böhlke, P. De Bièvre, H. Hidaka, H.S. Peiser, K.J.R. Rosman, P.D.P. Taylor. Atomic weights of the elements: Review 2000. *Pure Appl. Chem.* **2003**, *75*, 683.

[29] M. Elsner, L. Zwank, D. Hunkeler, R.P. Schwarzenbach. A new concept linking observable stable isotope fractionation to transformation pathways of organic pollutants. *Environ. Sci. Technol.* **2005**, *39*, 6896.

[30] Y. Horibe, H. Craig. D/H fractionation in the system methane-hydrogen-water. *Geochim. Cosmochim. Acta* **1995**, *59*, 5209.

[31] K.M. Scott, X. Lu, C.M. Cavanaugh, J.S. Liu. Optimal methods for estimating kinetic isotope effects from different forms of the Rayleigh distillation equation. *Geochim. Cosmochim. Acta* **2004**, *68*, 433.

[32] A. Mariotti, A. Leclerc, J.C. Germon. Nitrogen isotope fractionation associated with the $NO_2^- \rightarrow N_2O$ step of denitrification in soils. *Can. J. Soil Sci.* **1982**, *62*, 227.

[33] Y.-H. Luo, L. Steinberg, S. Suda, S. Kumazawa, A. Mitsui. Extremely low D/H ratios of photoproduced hydrogen by cyanobacteria. *Plant Cell Physiol.* **1991**, *32*, 897.

[34] D.J. Arp, R.H. Burris. Isotope exchange and discrimination by the H_2-oxidizing hydrogenase from soybean root nodules. *Biochim. Biophys. Acta* **1982**, *700*, 7.

[35] I. Sumner, G.A. Voth. Proton transport pathways in [NiFe]-hydrogenase. *J. Phys. Chem. B* **2012**, *116*, 2917.

[36] S.V. Hexter, F. Grey, T. Happe, V. Climent, F.A. Armstrong. Electrocatalytic mechanism of reversible hydrogen cycling by enzymes and distinctions between the major classes of hydrogenases. *Proc. Natl. Acad. Sci. U.S.A.* **2012**, *109*, 11516.

[37] L. Torres, R. Gelabert, M. Moreno, J.M. Lluch. Nuclear dynamics discrete variable representation study of the equilibrium isotope effect on H_2 Binding in $M(\eta^2\text{-}H_2)L_n$ complexes: An effective theoretical way to account for anharmonicity. *J. Phys. Chem. A* **2000**, *104*, 7898.

[38] J. Kubas Gregory. Molecular hydrogen complexes: coordination of a .sigma. bond to transition metals. *Acc. Chem. Res.* **1988**, *21*, 120.

[39] P.J. Hay. Ab initio theoretical studies of a novel tungsten dihydrogen complex. *Chem. Phys. Lett.* **1984**, *103*, 466.

[40] P.M. Vignais. H/D exchange reactions and mechanistic aspects of the hydrogenases. *Coord. Chem. Rev.* **2005**, *249*, 1677.

[41] D.L. Valentine, A.L. Sessions, S.C. Tyler, A. Chidthaisong. Hydrogen isotope fractionation during H_2/CO_2 acetogenesis: hydrogen utilization efficiency and the origin of lipid-bound hydrogen. *Geobiology* **2004**, *2*, 179.

[42] G.J. Bowen, C.D. Kennedy, P.D. Henne, T. Zhang. Footprint of recycled water subsidies downwind of Lake Michigan. *Ecosphere* **2012**, *3*, art53.

[43] C. Kendall, T.B. Coplen. Distribution of oxygen-18 and deuterium in river waters across the United States. *Hydrol. Process.* **2001**, *15*, 1363.

[44] H.W. Kreuzer-Martin, M.J. Lott, J.R. Ehleringer, E.L. Hegg. Metabolic processes account for the majority of the intracellular water in log-phase *Escherichia coli* cells as revealed by hydrogen isotopes. *Biochemistry* **2006**, *45*, 13622.

[45] H.W. Kreuzer-Martin, J.R. Ehleringer, E.L. Hegg. Oxygen isotopes indicate most intracellular water in log-phase *Escherichia coli* is derived from metabolism. *Proc. Natl. Acad. Sci. USA* **2005**, *102*, 17337.

[46] H.W. Kreuzer, L. Quaroni, D.W. Podlesak, T. Zlateva, N. Bollinger, A. McAllister, M.J. Lott, E.L. Hegg. Detection of metabolic fluxes of O and H atoms into intracellular water in mammalian cells. *PLoS ONE* **2012**, *7*, e39685.

CHAPTER 4

ISOTOPIC FRACTIONATOIN BY A FUNGAL P450 NITRIC OXIDE REDUCTASEDURING THE PRODUCTION OF N_2O

This chapter is modified from the *Environmental Science & Technology* 48(18): 10707-10715 (2014) by Hui Yang, Hasand Gandhi, Nathaniel E. Ostrom, Eric L. Hegg

Hasand Gandhi performed isotope ratio analyses of the N_2O molecules. Nathaniel Ostrom and Eric Hegg helped analyze the data and directed the research.

Abstract

Nitrous oxide (N_2O) is a potent greenhouse gas with a 100-year global warming potential approximately 300 times that of CO_2. Because microbes account for over 75% of the N_2O released in the U.S., understanding the biochemical processes by which N_2O is produced is critical to our efforts to mitigate climate change. In the current study, we used gas chromatography-isotope ratio mass spectrometry (GC-IRMS) to measure the $\delta^{15}N$, $\delta^{18}O$, $\delta^{15}N^{\alpha}$, and $\delta^{15}N^{\beta}$ of N_2O generated by purified fungal nitric oxide reductase (P450nor) from *Histoplasma capsulatum*. The isotope values were used to calculate site preference (SP) values (difference in $\delta^{15}N$ between the central (α) and terminal (β) N atoms in N_2O), enrichment factors (ε), and kinetic isotope effects (KIEs). Both oxygen and N^{α} displayed normal isotope effects during enzymatic NO reduction with ε values of -25.7‰ (KIE = 1.0264) and -12.6‰ (KIE = 1.0127), respectively. However, bulk nitrogen (average $\delta^{15}N$ of N^{α} and N^{β}) and N^{β} exhibited inverse isotope effects with values of 14.0‰ (KIE = 0.9862) and 36.1‰ (KIE = 0.9651), respectively. The observed inverse isotope effect in $\delta^{15}N^{\beta}$ is consistent with reversible binding of the first NO in the P450nor reaction mechanism. In contrast to the constant SP observed during NO reduction in microbial cultures, the site preference measured for purified *H. capsulatum* P450nor was not constant, increasing from ~15‰ to ~29‰ during the course of the reaction. This indicates that SP for microbial cultures can vary depending on the growth conditions, which may complicate source tracing during microbial denitrification.

Keywords: enrichment factor, fungal NO reductase, isotopomer, kinetic isotope effect, nitrous oxide, P450nor, site preference

Introduction

The nitrogen cycle is a fundamental biogeochemical process that is crucial to all living organisms. Two especially important components of the nitrogen cycle are nitrification (a process in which ammonia is oxidized into nitrate), and denitrification (the reduction of nitrate and nitrite to N_2). Nitrous oxide (N_2O), a potent greenhouse gas that is also involved in ozone layer destruction, is produced both as an intermediate and as a side product during microbial nitrification and denitrification.[48] With the rise of agricultural activities and the associated use of fertilizers, N_2O levels have risen to approximately 325 ppb (19% higher than pre-industrial levels),[49] and they are currently increasing at a rate of 0.25% per year.[50] Because microbial denitrification is one of the major sources of biologically generated N_2O,[51] it is imperative that we obtain a better understanding of the specific enzymatic steps involved in N_2O generation during denitrification.

Quantifying the magnitude of isotopic discrimination at natural abundance levels during biochemical reactions provides a non-invasive and physiological way to probe biological N_2O production.[52] Evaluation of isotopic fractionation during denitrification, however, is generally based on net isotopic enrichment factors (ε), which approximate the change in isotopic composition between nitrate and N_2 in either microbial cultures[53] or controlled field settings.[54] Ultimately these studies describe the fractionation for the entire denitrification sequence (NO_3^- → N_2) or a series of steps rather than the fractionation occurring at an individual step (e.g. NO → N_2O). As a result, while the measured bulk N (the average of $\delta^{15}N$ at the central (N^{α}) and the terminal (N^{β}) positions) and O isotope values can be helpful, they are often inconclusive. For example, microbial denitrification generates N_2O depleted in ^{15}N relative to nitrate between -45‰ and -13‰, which is distinct from the range reported for N_2O production via nitrification of -111‰

to -45‰.[53a, 55] This difference in fractionation patterns has been used to classify N_2O production in soils as coming either from denitrification or nitrification. The observed fractionation, however, can theoretically be 0‰ if diffusion of inorganic N into cells is the rate limiting step and masks the true fractionation occurring at a specific enzymatic transformation.[56] Further, exchange of O between water and N_2O during its production is common and can alter the isotope signature of a specific production pathway.[57] Thus, the specific microbial source(s) of N_2O based on bulk $\delta^{15}N$ and $\delta^{18}O$ often cannot be quantified.

Site preference (SP), the difference between the $\delta^{15}N$ of the central and terminal N atom in the asymmetric N_2O molecule, has emerged as an additional tool by which N_2O biosynthesis can be characterized. The advantage of SP relative to bulk $\delta^{15}N$ and $\delta^{18}O$ values is that it is independent of the isotopic composition of the inorganic substrates,[58] and thus far no evidence of fractionation in SP during N_2O production has been reported.[56] Furthermore, while fractionation during N_2O reduction in $\delta^{15}N$ and $\delta^{18}O$ can be substantial, the effect of reduction on SP is generally quite small.[59] On this basis, the difference in SP observed in pure culture[60] and purified enzyme experiments[61] between bacterial denitrification (including nitrifier-denitrification, i.e. the reduction of nitrite to N_2O under O_2-limiting conditions by nitrifiers) of -10‰ to 0‰ and nitrification (as a byproduct during hydroxylamine oxidation) of 33‰ to 37‰ has been used to estimate the relative production of N_2O from these two pathways.[60a] Likewise, the SP for N_2O production via fungal denitrification was measured to be approximately 37‰.[55c] Nonetheless, considerable variation in the SP values for specific processes exists, and this variation is best explained by differences in isotope fractionation associated with specific steps in the nitrification and denitrification pathways. In particular, the NO reduction step is especially

important in controlling SP because this is the step where two NO atoms are assembled to create the N_2O molecule.[62]

Bacteria and fungi are the two major producers of N_2O in the soil. N_2O produced by bacteria, however, is not necessarily an end product because it can be subsequently consumed by the bacterial nitrous oxide reductase (i.e. N_2O can either be an end product or an intermediate in bacterial systems). Conversely, most fungal organisms do not contain nitrous oxide reductase and therefore produce N_2O only as an end product.[63] Based on the low SP values observed in N_2O evolving from soils, bacterial denitrification is proposed to dominate N_2O production in many environments.[58b, 64] However, there is a growing recognition of the importance of fungal denitrification in producing N_2O in some ecosystems, notably plantation forests and some grassland soils.[65]

In this manuscript, we report the isotopic fractionation that occurs during the reduction of NO to N_2O by purified fungal P450 nitric oxide reductase (P450nor) from *Histoplasma capsulatum*. By working with P450nor directly, we avoid the issue of compounding fractionation factors associated with multiple steps that is characteristic of microbial cultures, and we report the fractionation factors specific to NO reduction. Our findings provide insight into the application of stable isotopes to reveal microbial production pathways as well as the reaction mechanism by which N_2O is assembled by the P450nor enzyme. Importantly, the amino acid sequence of *H. capsulatum* P450nor is highly similar (approximately 60% identity) to other sequenced fungal P450nors (Figure 16), and it is therefore likely that our results will be generally applicable to this entire class of enzyme.

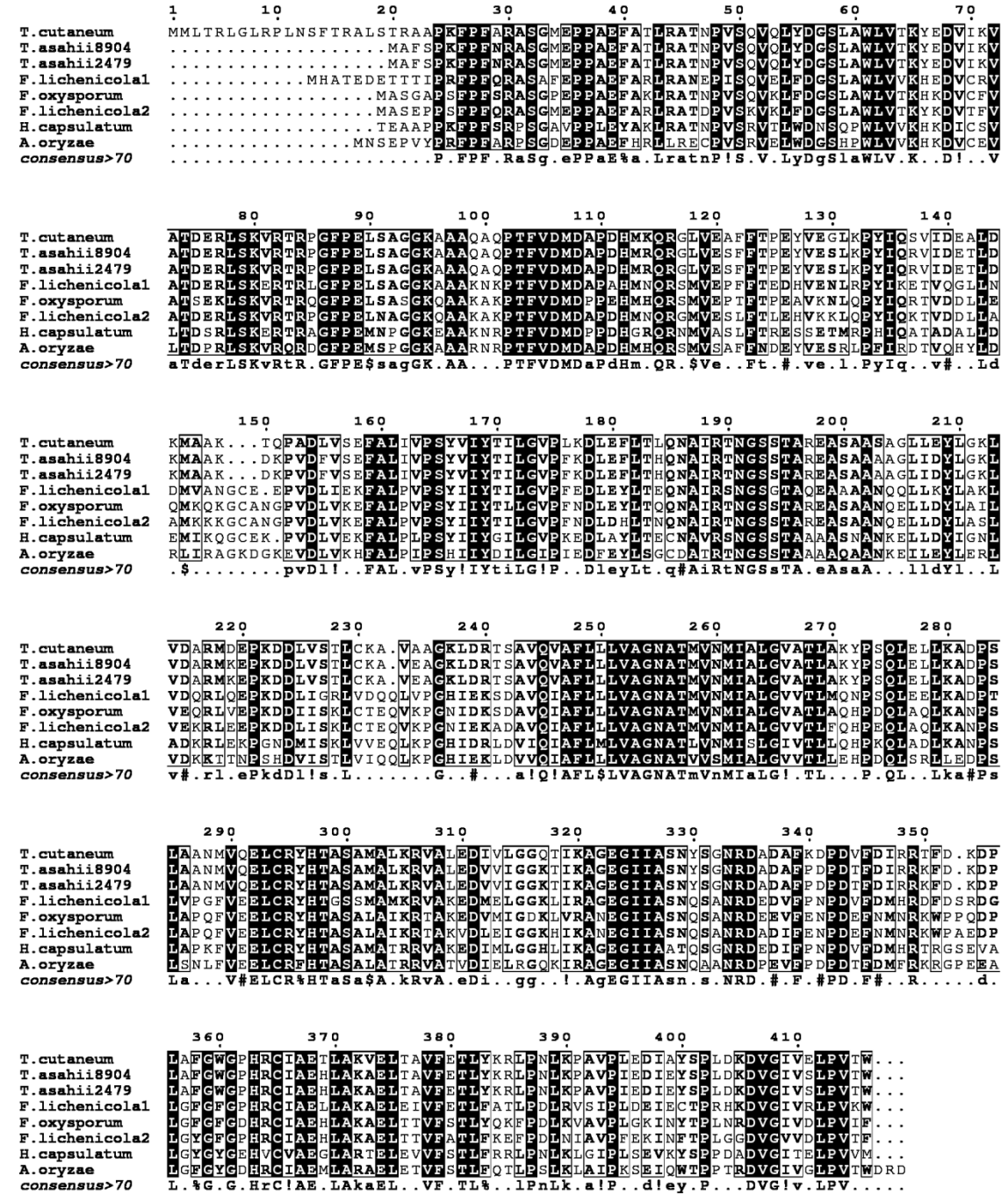

Figure 16: Multiple sequence alignment of P450nor(s) from *Trichosporon cutaneum* (*T. cutaneum*), *Trichosporon asahii* var. asahii CBS 8904 (*T. asahii*8904), *Trichosporon asahii* var. asahii CBS 2479 (*T. asahii*2479), *Fusarium lichenicola* (*F. lichenicola*1 and *F. lichenicola*2), *Fusarium oxysporum* (*F. oxysporum*), *Histoplasma capsulatum* (*H. capsulatum*), *Aspergillus oryzae* (*A. oryzae*). All sequences were obtained from NCBI (www.ncbi.nlm.nih.gov/) except for *H. capsulatum* P450nor (47-450) which

Figure 16 (cont'd)

was obtained from Chao et al. (*Arch. Biochem. Biophys.* **2008,** *480*, 132-137). The multiple sequence alignment was performed using Clustal Omega (www.ebi.ac.uk/Tools/msa/clustalo/) and ESPript 3 (espript.ibcp.fr/ESPript/ESPript/).

Methods

Expression and purification of P450nor. The P450nor gene (*NOR1*) from *Histoplasma capsulatum* was expressed as a C-terminal 6x-His-tagged protein on a pCW/Nor1p vector kindly provided by Prof. M. A. Marletta (Scripps Research Institute).[66] The plasmid was transformed into *Escherichia coli* JM109 and a single colony was used to inoculate a 100 mL starter culture supplemented with 100 μg/mL ampicillin, and the culture was shaken overnight at 37 °C. The following morning, a 2 L flask with 1 L of Luria-Bertani (LB) medium was inoculated with the overnight culture to an OD_{600nm} of 0.1 and shaken at 37 ℃. After an OD_{600nm} of 0.6 was reached, isopropyl- -D-1-thiogalactopyranoside (IPTG) was added to a final concentration of 1 mM and the culture was shaken overnight at 25 ℃. P450nor was isolated as described by Chao *et al*.[66] and purified using 1 mL of Ni-NTA Agarose resin (QIAGEN, Valencia, CA) in a 5 mL polypropylene column.

P450nor activity assay. *H. capsulatum* P450nor reduces NO to N_2O according to the following reaction:[66]

$$2NO + NADH + H^+ \rightarrow N_2O + NAD^+ + H_2O$$

All activity assays were performed under anaerobic conditions. Triplicate samples were mixed in 250 mL sterilized serum vials (Wheaton Glass, Milville, NJ) sealed with butyl rubber septa (Geo-Microbial Technologies, Ochelata, OK). NO gas (99.5% purity, Airgas) was purified overnight by exposure to preconditioned (heated under vacuum at 300 ℃) molecular sieves (5 Å) to reduce the N_xO_y background to less than 1%. Purified NO (1 mL) was injected using a gas-tight syringe (Hamilton) into a 250 mL glass serum vial (Wheaton Glass) containing 20 mL of anaerobic buffer (20 mM Hepes (pH 7.5), 1 mM DTT, 1mM NADH (β-nicotinamide adenine dinucleotide), and 5% glycerol). The reaction was initiated by injecting 100 μL of purified P450nor, and the progress was monitored by removing 3 mL of headspace gas and injecting it onto a Shimadzu Greenhouse Gas Analyzer gas chromatograph (model GC-2014, Shimadzu Scientific Instruments, Columbia, MD) equipped with an electron capture detector (ECD) and a Hayesep N separation column (GC oven temperature = 100 ℃, ECD detector temperature = 350 ℃, N_2 carrier gas at a flow rate of 25 mL/min and 5% CH_4/95% Ar make-up gas (Airgas) at a flow rate of 2.5 mL/min). Samples were incubated on their side with shaking at room temperature for 60 min, and a headspace sample was taken every 5 min. To maintain the headspace at atmospheric pressure in the reaction vials, 3 mL of ultra-high-purity (UHP) N_2 was injected into the vial prior to removal of each 3 mL sample using a 5 mL gas tight glass syringe (Hamilton). Concentration data were recorded and analyzed by Shimadzu's GCSolutions software. A commercial 1 ppm standard (Scott Specialty Gases, Plumsteadville, PA), laboratory air, and standards prepared from UHP N_2O and UHP N_2 tanks (Airgas) were used for the calibration and calculation of the headspace concentrations of N_2O.

IRMS measurements. Isotope ratio data for N_2O was obtained using a Trace Gas sample introduction system (Elementar Americas, Inc., Mount Laurel, NJ) interfaced to an

Isoprime isotope ratio mass spectrometer (IRMS) (Elementar Americas, Inc.). The ion source settings in the mass spectrometer were optimized to provide precisions better than 0.5, 0.5, 0.7, 0.7, and 1.2‰ for $\delta^{15}N$, $\delta^{18}O$, $\delta^{15}N^{\alpha}$, $\delta^{15}N^{\beta}$ and SP, respectively, for sample quantities between 6 and 20 nmol. The Trace Gas system uses He as the carrier gas, and CO_2 and H_2O are removed from the sample gas by passage through Carbosorb and magnesium perchlorate traps (Costech Analytical Technologies Inc, Valencia, CA), respectively. The N_2O in the sample gas was purified and concentrated via cryo-focusing followed by chromagraphic separation on a Poroplot Q column (Agilent, Foster City, CA). Based on controlled fragmentation studies, the relative abundance of the $^{14}N^{15}N^{16}O$ (α) and $^{15}N^{14}N^{16}O$ (β) isotopomers was measured using the N_2O^+ and NO^+ ions in a single run as described by Sutka *et al.* (2006). Final values of $\delta^{15}N^{\alpha}$-N_2O and $\delta^{15}N^{\beta}$-N_2O were obtained following mass overlap correction as presented in Toyoda and Yoshida.[67] The concentration of N_2O was determined using the area under the mass 44 N_2O peak. The $\delta^{15}N$, $\delta^{15}N^{\alpha}$, and $\delta^{18}O$ values of our laboratory pure N_2O standard are 1.6‰, 14.9‰, and 41.7‰, respectively.

Isotope value notations. The relative abundance of ^{15}N and ^{18}O in N_2O molecules is expressed in δ notations:

$$\delta = [(R_{sample}/R_{standard}) - 1] \times 1000$$

where:

R_{sample} = $^{15}N/^{14}N$ or $^{18}O/^{16}O$ for the N_2O in the samples

$R_{standard}$ = $^{15}N/^{14}N$ or $^{18}O/^{16}O$ for the N_2O in the standards.

The N and O standards are atmospheric N_2 and VSMOW,[37] respectively.

Site preference is defined as the difference between the isotope values of N^{α} and N^{β} in N_2O, as described in the following equation:

Site preference (SP) = $\delta^{15}N^{\alpha}$ - $\delta^{15}N^{\beta}$

where:

$$\delta^{15}N^{\alpha} = \left[\left({}^{15}R^{\alpha}_{sample} / {}^{15}R^{\alpha}_{standard}\right) - 1\right] \times 1000$$

$$\delta^{15}N^{\beta} = \left[\left({}^{15}R^{\beta}_{sample} / {}^{15}R^{\beta}_{standard}\right) - 1\right] \times 1000$$

and where ^{15}R and ^{15}R are defined as:

^{15}R = [$^{14}N^{15}N^{16}O$/$^{14}N^{14}N^{16}O$]

^{15}R = [$^{15}N^{14}N^{16}O$/$^{14}N^{14}N^{16}O$]

All results are expressed as the mean ± standard deviation (SD).

Calculations for determining enrichment factors (ε) and kinetic isotope effects (KIE)

Microbial denitrification proceeds by the progressive reduction of NO_3^- to NO_2^- to NO to N_2O and finally to N_2. Each step in this sequence, including diffusion of substrates into and out of cells, can be expected to discriminate against one isotope over the other depending on the specific reaction sequence. This, in turn, will give rise to different isotope fractionation patterns depending on the types of organism and the specific reaction pathway. Here we follow the convention of Mariotti *et al.*[68] by defining the magnitude of isotopic fractionation during a single unidirectional reaction as the fractionation factor, α,

$\alpha = k_2/k_1$ (1)

where k_1 and k_2 are the reaction rates for the light and heavy isotopically substituted compounds, respectively (although some authors use the inverse of this ratio). As defined by Mariotti *et al.*,[68] α is therefore equal to the inverse of the standard kinetic isotope effect (KIE).[38]

$$\alpha = (k_1/k_2)^{-1} = (KIE)^{-1} \quad (2)$$

We further define an isotopic enrichment factor, ε,

$$\varepsilon = (\alpha - 1)*1000 \quad (3)$$

that can be quantified by the following expression of the Rayleigh isotope fractionation model:

$$\delta^{15}N_p = \delta^{15}N_{so} - \varepsilon_{p/s}[(f\ln f)/(1-f)] \quad (4)$$

where *f* is defined as the fraction of NO remaining (determined as the ratio of the calculated NO concentration using measured N_2O concentration at any point in time divided by the initial NO concentration), $\varepsilon_{p/s}$ is the isotopic enrichment factor for any substrate (s) converted to a product (p), and $\delta^{15}N_{so}$ refers to the isotopic composition of the substrate prior to initiation of the reaction.[69] This expression can be plotted such that a linear regression fit to the data yields the enrichment factor (ε) as the slope from which the fractionation factor (α) can be calculated (Figures 17-20). The kinetic isotope effect values (KIEs) were then calculated using the fractionation factor values according to Equation (2). Due to the complexity of the x-axis (-[(*f*ln*f*)/(1-*f*)]), however, Rayleigh fractionation plots are not intuitive with respect to the time course of the reaction. Therefore, in this manuscript we present simplified graphs that depict the actual change of the isotope values vs. the percentage of substrate converted (1-*f*). While these graphs were not used to calculate either enrichment factors or kinetic isotope effects, they offer a

better perspective of the dynamics of the different isotopologues as a function of the reaction time course.

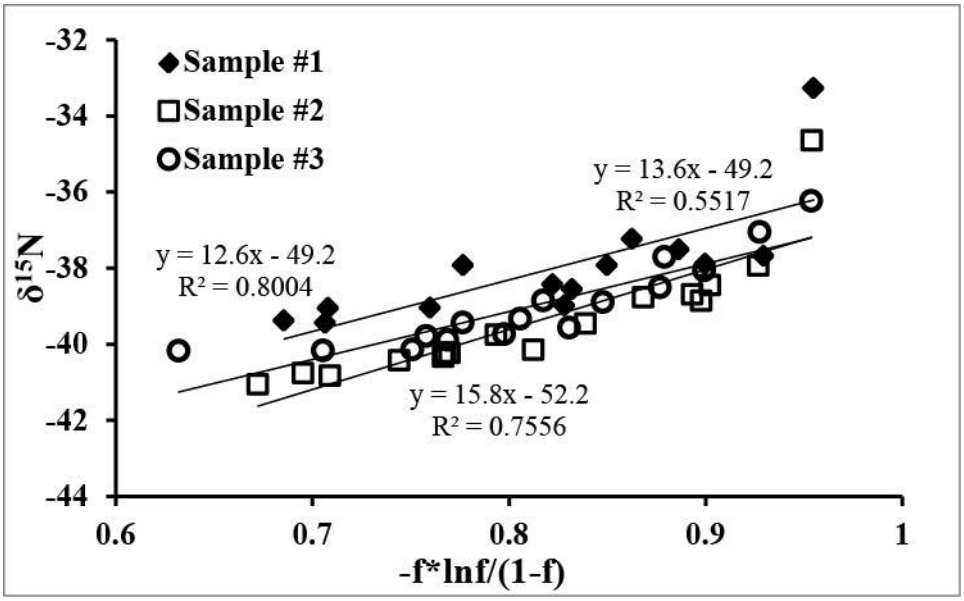

Figure 17: Best fit line of the Rayleigh equation to bulk $\delta^{15}N$ in N_2O produced by P450nor. The enrichment factors (ε) were calculated using the slopes of the lines for each of the three biological replicates.

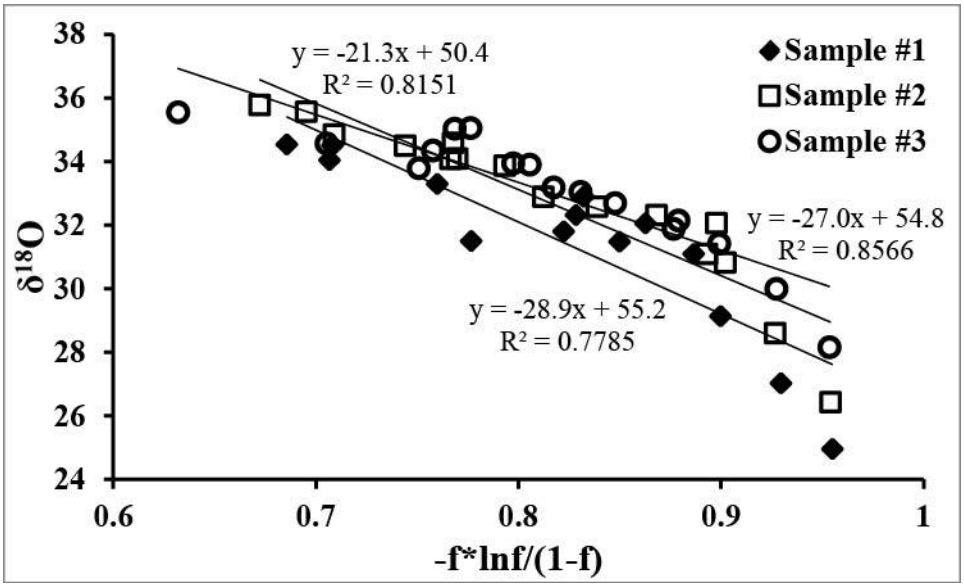

Figure 18: Best fit line of the Rayleigh equation to $\delta^{18}O$ in N_2O produced by P450nor. The enrichment factors (ε) were calculated using the slopes of the lines for each of the three biological replicates.

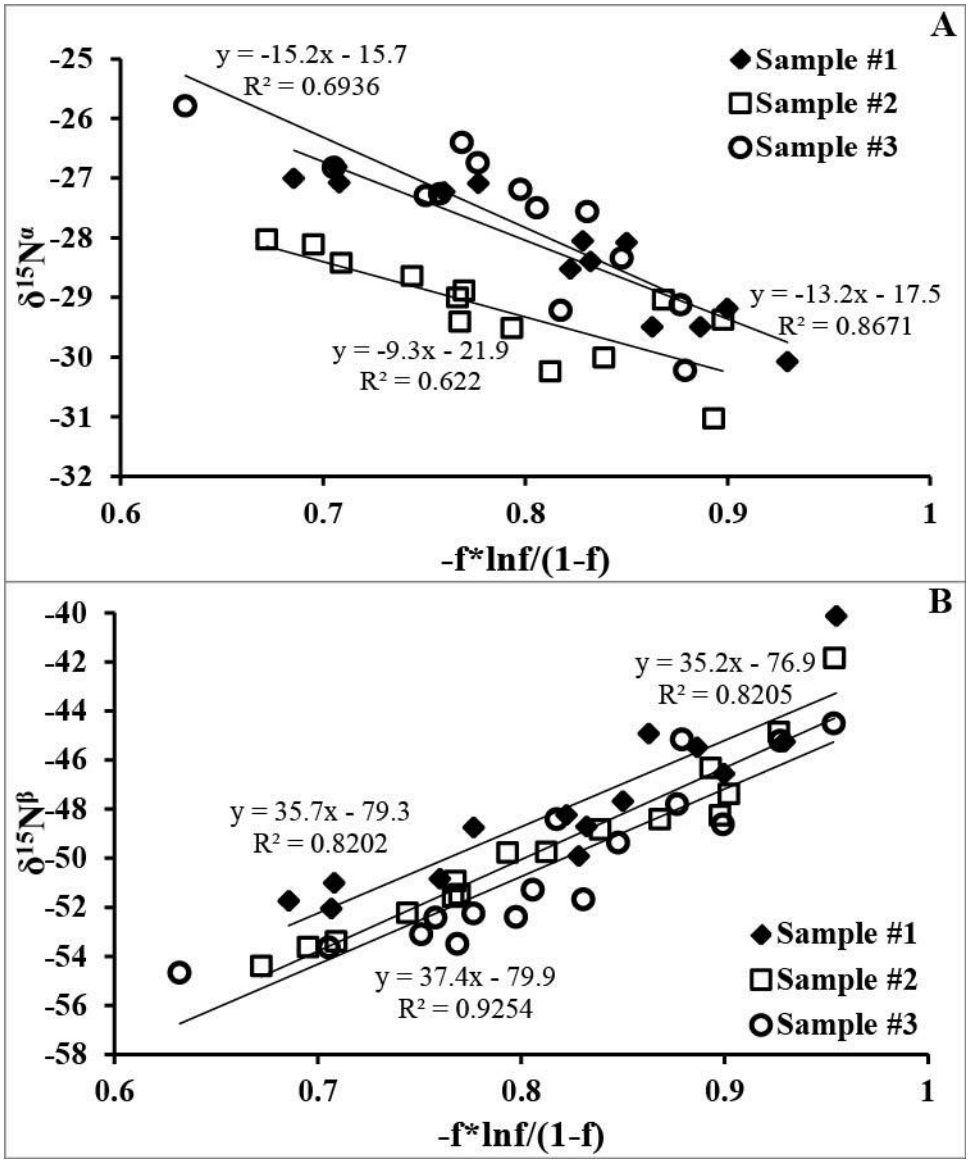

Figure 19: The enrichment factors (ε) were calculated using the slopes of the lines for each of the three biological replicates. (A) Best fit line of the Rayleigh equation to $\delta^{15}N^{\alpha}$ in N_2O produced by purified P450nor. (B) Best fit line of the Rayleigh equation to $\delta^{15}N^{\beta}$ in N_2O produced by purified P450nor.

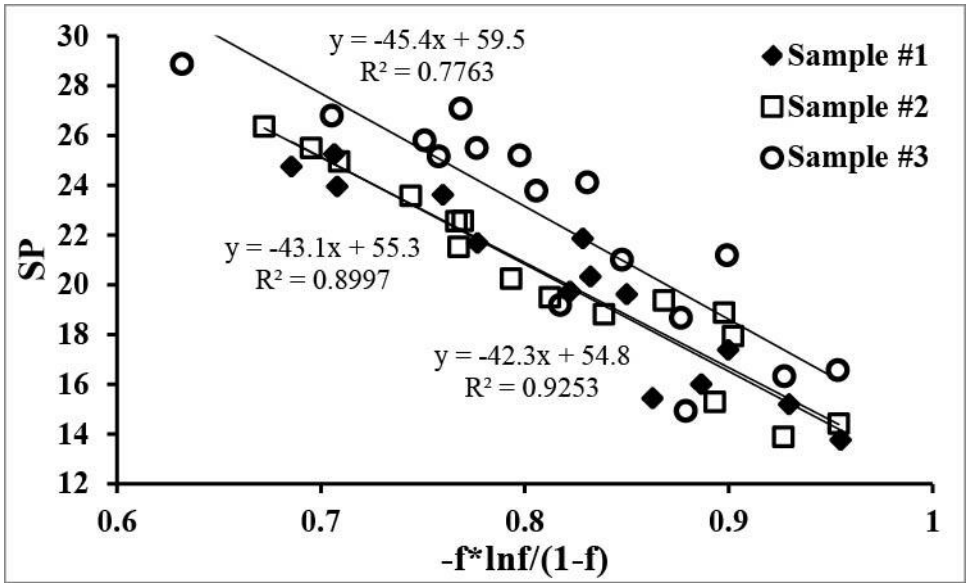

Figure 20: Best fit line of the Rayleigh equation to site preference (SP) values. The enrichment factors were calculated using the slopes of the lines as outlined in Equation 4 for each of the three biological replicates.

Results

$\delta^{15}N$ and $\delta^{18}O$ analyses for N_2O produced by *H. capsulatum* P450nor

Prior to analysis of the isotopic fractionation by P450nor from *H. capsulatum*, activity assays were performed to ensure that the different P450nor preparations yielded consistent enzyme activity. The reduction of NO to N_2O was monitored by analyzing the headspace gas via GC-ECD in three separate enzyme preparations. As shown in Figure 21, all three samples showed continuous N_2O production and identical production profiles over approximately 60 min, highlighting the robustness and reproducibility of the reaction conditions. Thus, these same

reaction conditions were employed during the analysis of N_2O via isotope ratio mass spectrometry.

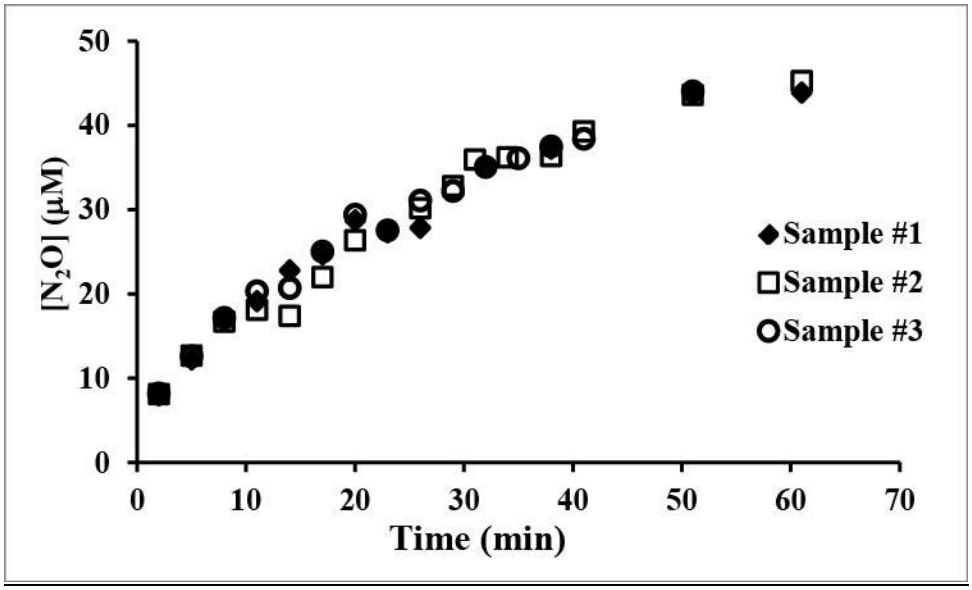

Figure 21: N_2O production by *H. capsulatum* P450nor over the course of 60 min.

The isotope ratio values were measured for different isotopologues of N_2O ($\delta^{15}N$, $\delta^{15}N^{\alpha}$, $\delta^{15}N^{\beta}$ and $\delta^{18}O$). As shown in Figure 22A, when half of the NO was consumed there was a depletion of ~6‰ in $\delta^{15}N$ in the accumulated N_2O relative to the initial N_2O measured. This is in contrast to what is expected in a normal isotope effect in which the molecules containing the light isotopes are preferentially converted first, resulting in enrichment in the heavy isotope of the residual substrate. As the relative abundance of heavy isotopes in the substrate pool slowly increases over time, there is a concomitant progressive enrichment in the heavy isotopes in the product. Thus, the depletion of $\delta^{15}N$ in the accumulated N_2O over time indicates that ^{15}NO

molecules were converted to N_2O preferentially over ^{14}NO molecules by P450nor. Consistent with this observation, the calculated bulk N enrichment factor values ($\varepsilon^{15}N$) and kinetic isotope effect (^{15}N-KIE) values (Table 8) for N_2O production revealed an inverse isotope effect, with an $\varepsilon^{15}N$ of 14.0‰ (± 1.6‰) and a ^{15}N-KIE of 0.9862 (± 0.0016). Conversely, the N_2O became enriched in ^{18}O during the course of the reaction (Figure 22B). This gives rise to a normal isotope effect and an ^{18}O enrichment factor ($\varepsilon^{18}O$) of -25.7‰ (± 4.0‰) and a kinetic isotope effect (^{18}O-KIE) of 1.0264 (± 0.0041).

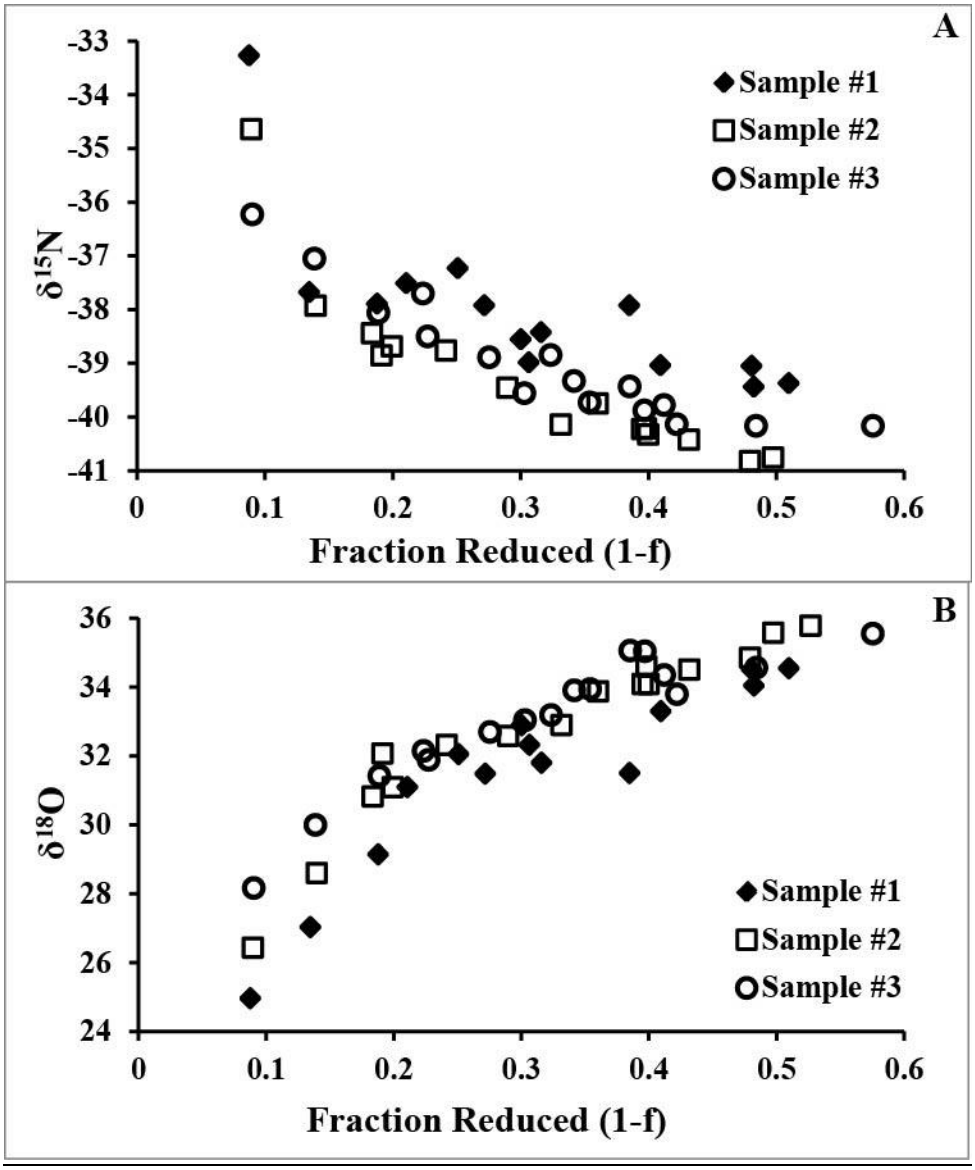

Figure 22: $\delta^{15}N$ and $\delta^{18}O$ of N_2O produced by P450nor as a function of the fraction of NO reduced (1-*f*). (A) $\delta^{15}N$ of N_2O plotted against the fraction of NO reduced for three samples. (B) $\delta^{18}O$ of N_2O plotted against the fraction of NO reduced for three samples.

Table 8: Enrichment factors (ε) and kinetic isotope effects (KIEs) for individual biological replicates of *H. capsulatum* P450nor. The ε values were determined based on Equation 4 by linear regression. The KIE values were calculated based on Equations 2 and 3 using the corresponding ε values. Mass averaged values and standard deviations are shown for all values.

	Sample #1	**Sample #2**	**Sample #3**	**Average ± SD**
$\varepsilon^{15}N$ (‰)	13.6	15.8	12.6	14.0 ± 1.6
^{15}N-KIE	0.9866	0.9844	0.9876	0.9862 ± 0.0016
$\varepsilon^{15}N^{\alpha}$ (‰)	-13.2	-9.3	-15.2	-12.6 ± 3.0
$^{15}N^{\alpha}$-KIE	1.0134	1.0094	1.0154	1.0127 ± 0.0030
$\varepsilon^{15}N^{\beta}$(‰)	35.2	37.4	35.7	36.1 ± 1.2
$^{15}N^{\beta}$-KIE	0.9660	0.9639	0.9655	0.9651 ± 0.0011
$\varepsilon^{18}O$ (‰)	-28.9	-27.0	-21.3	-25.7 ± 4.0
^{18}O-KIE	1.0298	1.0277	1.0218	1.0264 ± 0.0041
εSP (‰)	-43.1	-42.3	-45.4	-43.6 ±1.6
SP-KIE	1.0450	1.0442	1.0476	1.0456 ±0.0018

Two important control experiments were performed to ensure that the ε and KIE values calculated represented the enzymatic conversion of NO to N_2O by P450nor. In the first experiment, a mixture of N_2O, NAD^+, and P450nor were incubated under conditions that simulated the end point of our reactions to evaluate if the back reaction was occurring. After 70 minutes, there was no detectable enzyme-mediated consumption of N_2O (Figure 23). In the second experiment, equal concentrations of NO and N_2O were incubated either in the presence of $NADH/NAD^+$ or in the presence of enzyme without $NADH/NAD^+$. In both cases, any change in

the isotope ratio of the N_2O over time was not greater than the analytical precision of the instrument, demonstrating that all of the enzymatic components need to be present for the interconversion between NO and N_2O (Figure 24). Together, these control experiments establish that our observed isotope effects cannot be explained by either N_2O consumption or non-enzymatic exchange reactions, and that our calculated fractionation factors must therefore represent inherent properties of NO reduction by P450nor.

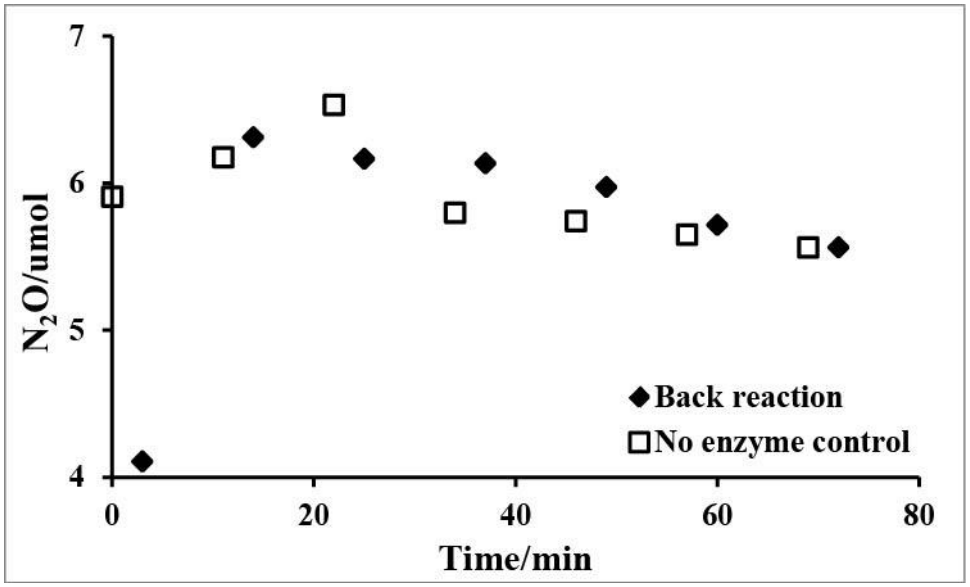

Figure 23: Quantification of N_2O in the headspace in both the presence and absence of P450nor. The conditions were chosen to test if the back reaction (i.e. N_2O oxidation) was occurring, and the conditions therefore mimicked those anticipated at the end of the N_2O production assay except that no NO was present. The back reaction contained 6.1 mM NADH, 0.7 mM NAD^+, and 0.02 mg/mL *H. capsulatum* P450nor. The 'No enzyme control' experiment was the same as the "Back reaction" except that there was no P450nor present. There is no significant difference in the data between the "Back reaction" and the "No enzyme control."

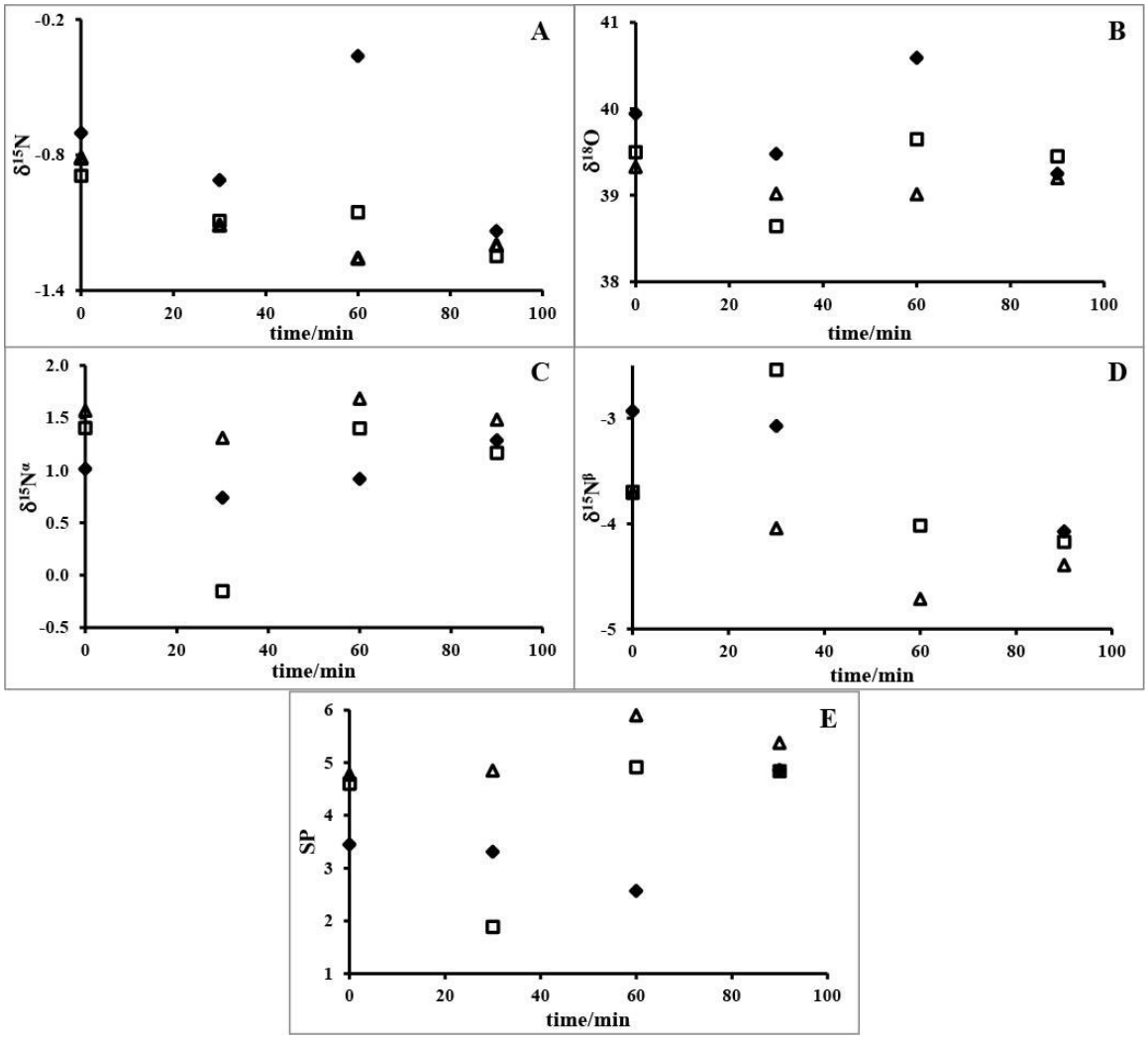

Figure 24: Characterization of the N_2O isotope values to test for the presence of NO-N_2O exchange. In sample #1 (◆) and #2 (□), equal amounts (10 μmol in 225 mL of headspace) of N_2O and NO were incubated with 1.35 mM NAD^+ and 1.35 mM NADH in the absence of P450nor for up to 90 min. In sample #3 (△), the same amounts of N_2O and NO were incubated with purified P450nor (0.02 mg/mL), but neither NAD^+ nor NADH was added. (A) $\delta^{15}N$ value of N_2O measured during the course of 90 minutes. (B) $\delta^{18}O$ value of N_2O measured for 90 minutes. (C) and (D) $\delta^{15}N^{\alpha}$ and $\delta^{15}N^{\beta}$ values of N_2O measured for 90 minutes (E) Site preference values of SP during the course of 90 minutes.

Site preference values for N_2O produced by *H. capsulatum* P450nor

To obtain a more detailed understanding of the isotopic preference during NO reduction to N_2O by P450nor, we calculated the fractionation for both N^{α} and N^{β}. In general, the isotope ratio of the N^{α} in N_2O exhibited a relatively modest change as the reaction progressed. While we have no clear explanation for the ~3‰ depletion observed between the 10% and 15% NO reduction points, there is a slight ~4‰ isotope enrichment trend for N^{α} from -30‰ to -26‰ between 15-55% NO reduction, indicating that there is a small preference for the light isotope of nitrogen to be incorporated into the α position. This second trend gives rise to a normal isotope effect for N^{α} with an ε of -12.6‰ (± 3.0‰) and a KIE value of 1.0127 (± 0.0030). Conversely, during this same time period the $\delta^{15}N^{\beta}$ values exhibited a depletion of ~10‰ relative to the N_2O initially produced (Figure 25B), indicating that ^{15}NO was preferentially incorporated into the β position of N_2O. Therefore, N^{β} showed a very clear inverse isotope effect with an ε of 36.1‰ (± 1.2‰) and a KIE value of 0.9651 (± 0.0011) (Table 8). Overall, these results indicate that during the course of the reaction, ^{15}N was strongly preferred over ^{14}N in the N^{β} position when N_2O was formed, while a weaker reverse pattern was observed in the N^{α} position. The bulk N fractionation factor is an average of the α- and β-$\delta^{15}N$ values and therefore the isotope effect for the bulk N is driven by the larger inverse isotope effect present in the β position.

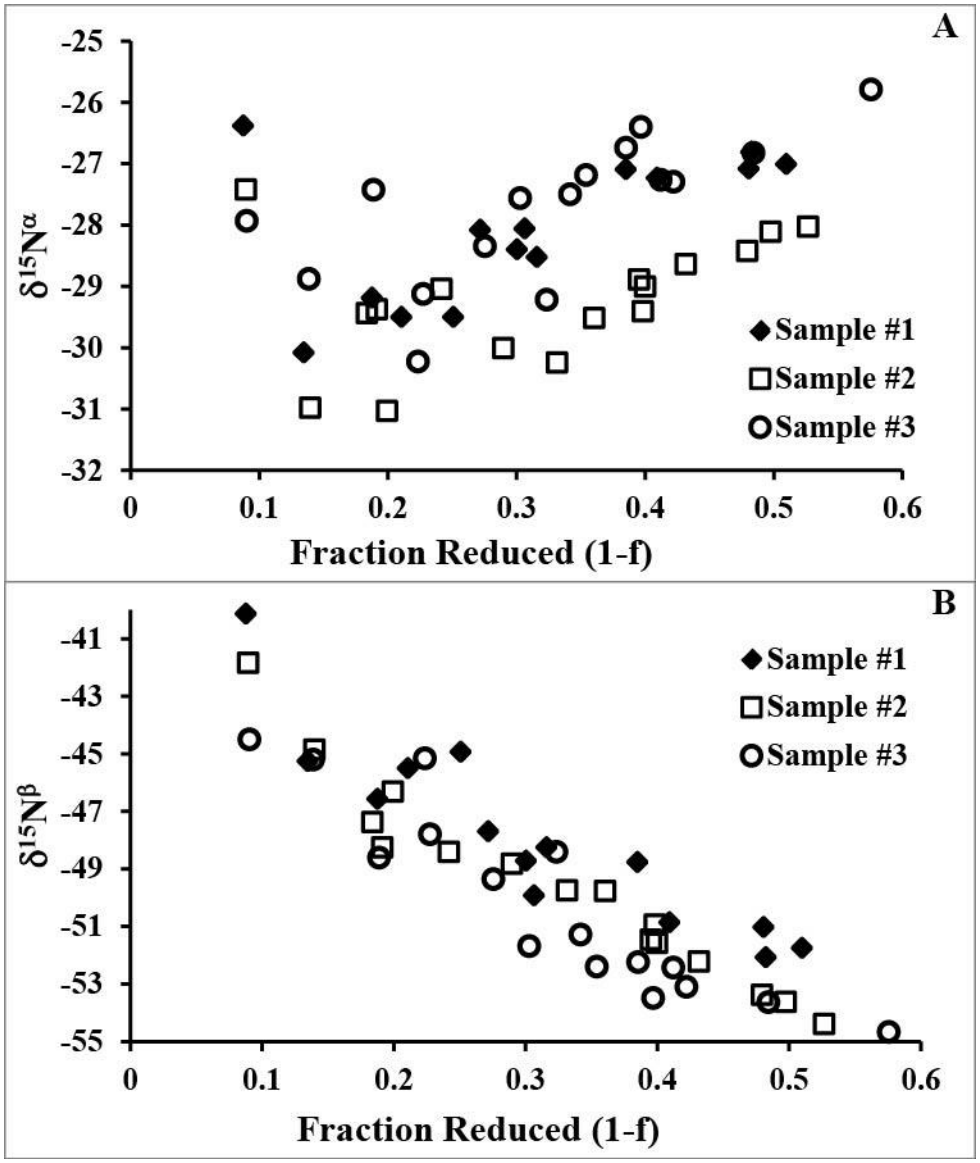

Figure 25: $\delta^{15}N^{\alpha}$ and $\delta^{15}N^{\beta}$ of N_2O produced by as a function of the fraction of NO reduced (1-*f*). (A) $\delta^{15}N^{\alpha}$ of N_2O plotted against the fraction of NO reduced for three samples. (B) $\delta^{15}N^{\beta}$ of N_2O plotted against the fraction of NO reduced for three samples.

The SP of N_2O increased from 15‰ at the beginning of the reaction to approximately 29‰ by the time half of the NO was reduced, giving rise to an enrichment in ^{15}N of 14‰ (Figure 26).

This is consistent with the slight increase in $\delta^{15}N^{\alpha}$ and stronger decrease in $\delta^{15}N^{\beta}$ during the course of the reaction. The enrichment factor (ε) and the kinetic isotope effect (SP-KIE) for the SP were calculated to be -43.6‰ (± 1.6‰) and 1.0456 (± 0.0018), respectively, indicating that during N_2O production SP has a normal isotope effect. In contrast, previous results using pure cultures revealed no change in SP over time,[55c] which highlights the importance of using purified enzymes to measure individual steps in the denitrification pathway.

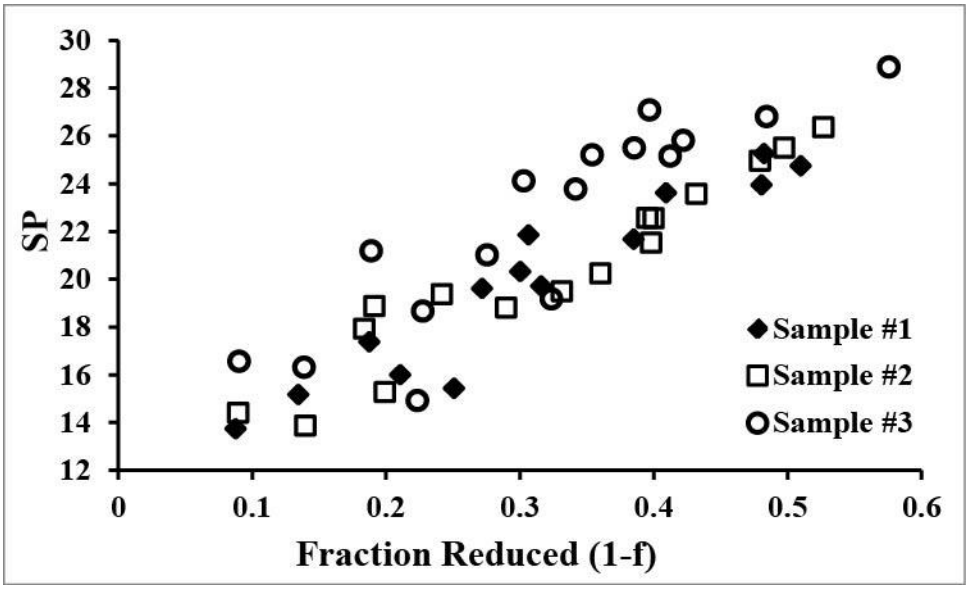

Figure 26: Site preference (SP) values of N_2O versus the fraction of NO reduced (1-*f*). Three independent biological replicates are shown.

Discussion

Fractionation during reduction of NO by P450nor

The typical behavior of a kinetic isotope effect in an enzymatic reaction is for the light isotope to be preferentially transferred to the initial product followed by progressive enrichment in the abundance of the heavy isotope as a function of time or with the extent of the reaction. Normal kinetic isotope fractionation is evident during NO reduction by P450nor for $\delta^{15}N^{\alpha}$, $\delta^{18}O$ and SP. By the Rayleigh fractionation model described in Equation 4, normal fractionation results in negative isotopic enrichment factors (Table 8). Inverse isotope effects, in which the product becomes preferentially depleted in the heavy isotope as a function of the extent of the reaction, are rarely observed in enzymatic reactions,[70] but they are evident in our data in $\delta^{15}N$ and $\delta^{15}N^{\beta}$ during NO reduction (Table 8). Similar to our findings is the observation of an inverse isotope effect associated with formation of the N-O bond during microbial nitrification,[70] although in our study the inverse isotope effect is associated with the binding of the first NO molecule (whose N atom ultimately becomes N^{β} in N_2O)[71] to the Fe active site. An inverse isotope effect is also evident in the bulk $\delta^{15}N$, however, as $\delta^{15}N$ is the average of the $\delta^{15}N$ of the N^{α} and N^{β} positions. The inverse isotope effect for $\delta^{15}N$ is caused by the greater isotopic enrichment factor for the N^{β} position that is greater and opposite in direction to that associated with the N^{α} position.

Two possible trivial explanations could account for an apparent inverse isotope effect during the reduction of NO to N_2O.[70a] The first, enzyme-level reversibility, results if the reverse reaction fractionates to a greater extent than the forward reaction and can only be significant if there is sufficient mass flux in the reverse direction to express the fractionation. We exposed N_2O to the identical conditions we used to catalyze NO reduction and observed no enzyme-catalyzed decrease in the abundance of N_2O with time (Figure 23). Consequently, we observed no indication of the reverse reaction under our experimental conditions. Secondly, isotopic

equilibrium between the substrate of the reaction and another species in the system prior to enzymatic reduction could also result in the appearance of inverse fractionation. For example, a pH dependent pre-equilibrium between H_2S and HS^- was used to explain an inverse fractionation during anaerobic sulfide oxidation.[72] The only other N species of relevance in our experiments is N_2O and we allowed NO and N_2O to equilibrate for 90 minutes and observed no changes in the isotopic composition of N_2O (Figure 24). Consequently, we conclude that isotopic equilibration is not a factor driving our experimental results.

Based on these results, we conclude that the inverse isotope effect observed for the β nitrogen atom must result from an inherent property of the enzyme reaction mechanism. Simply stated, the N atom must be more strongly bonded in the transition state than in the ground state of the reaction. This has been proposed to be the case for the inverse isotope effect observed in both $\delta^{15}N$ and $\delta^{18}O$ during the oxidation of nitrite to nitrate during microbial nitrification.[70] Conversely, if the N atom is more strongly bonded in the substrate than in the transition state, then a normal isotope effect is observed. This is the case for most N oxide reducing reactions (nitrate reduction, nitrite reduction and nitrous oxide reduction) during the denitrification process.[53b, 54a, 59] Our case is distinct, however, in that we observe an inverse isotope effect only for the β position and a normal isotope effect for both the α position and for the oxygen atom.

Implications for the reaction pathways of NO reduction by P450nor

Two scenarios have been proposed to explain the SP values in N_2O resulting from reduction of NO that involve either simultaneous or sequential binding of the two N atoms to the Fe centers of bacterial or fungal NOR.[58a, 62a] If the two N atoms bind simultaneously, then little isotopic preference is expected between the N^{α} and N^{β} positions and SP would be near 0‰. SP

values for N_2O production via bacterial denitrification range between approximately -10‰ and 0‰[58, 64] and are consistent with simultaneous binding. Although the precise catalytic mechanism of bacterial nitric oxide reductase remains uncertain, a reasonable hypothesis is that one NO binds to the non-heme iron while the other NO binds to the heme iron.[73] P450nor, however, contains only a single heme iron at the active site,[74] and studies have clearly indicated that each NO molecule binds separately to the enzyme prior to formation of the N=N bond.[75] Isotopic discrimination between the N atoms could occur in sequential binding if the first molecule of NO (whose nitrogen atom becomes N^{β} in N_2O)[71] binds with a strong preference for ^{14}N followed by the slower binding of the second NO molecule that experiences a smaller degree of isotopic segregation.[62a] However, this does not match the inverse kinetic isotope effect we observed for N^{β} (KIE = 0.9651). In addition, this would result in a positive SP value that trends toward zero over time, and our results indicate that SP becomes more positive over time. Therefore, we propose an alternative mechanism in which the initial binding of the first (β) NO molecule to the heme center of P450nor results in a more tightly bonded N atom in the transition state than the ground state, which leads to an inverse *kinetic* isotope effect (Figure 27). In addition, the N atom of this enzyme-NO complex has a higher bond order than the free NO molecule itself,[76] and it is known that this reaction step is freely reversible,[77] both of which give rise to an inverse *equilibrium* isotope effect. Thus, we propose that it is this combination of kinetic and equilibrium inverse isotope effects that gives rise to the trend of SP becoming more positive over time.

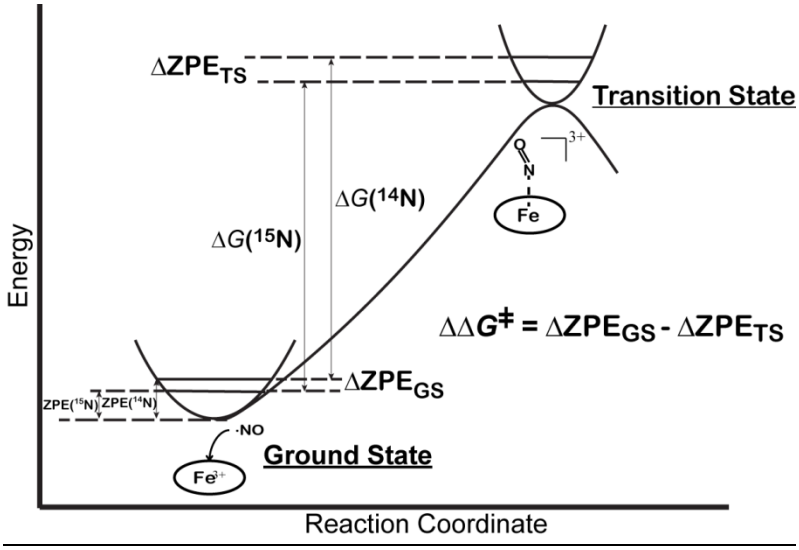

Figure 27: An energy diagram depicting the proposed binding of the first NO to the P450nor heme active site. The bond order increases from the ground state to the transition state[82] leading to a steeper energy well and a larger isotopic difference in zero-point energy (ZPE) in the transition state.[83] The magnitude and type (i.e. normal or inverse) of the isotope effect is determined by the relative difference in ΔZPEs in the ground state and the transition state.

The addition of the second NO molecule, whose N atom ultimately becomes N , involves the conversion of an Fe(IV)-$NHOH^-$ complex to a protonated Fe(III)-$N_2O_2H_2$ species.[71] It is likely that this is the rate-limiting step between the binding of the second NO molecule and release of N_2O. In contrast to the observations of an in $\delta^{18}O$ during oxidation of nitrite,[70b] we observe a normal isotope effect during production of N_2O via P450nor. This observation is consistent with the oxygen atom in N_2O being derived from the second NO molecule, whose nitrogen atom ultimately becomes N^{α}.

Implications for isotope source tracing of N_2O production

Our observations of inverse fractionation in $\delta^{15}N$ and $\delta^{15}N^{\beta}$ as well as normal fractionation in SP and $\delta^{18}O$ are in contrast with the isotope effects observed during N_2O production via nitrite reduction in two species of fungi that utilize the P450nor enzyme.[55c] No evidence of fractionation was found in $\delta^{18}O$ and SP during fungal denitrification using pure culture whereas substantial isotope effects were found in this study during NO reduction by purified P450nor. While an isotope effect during fungal denitrification in the N^{α} and N^{β} positions was not reported by Sutka *et al.*,[55c] two of the four cultures showed evidence of fractionation with values for $\delta^{15}N^{\beta}$ of -62.6 and -61.9‰ and apparent conflicting values for $\delta^{15}N^{\beta}$ of -34.3 and +32.6‰. Thus, while the data to evaluate $\delta^{15}N^{\beta}$ in Sutka *et al.*[55c] are limited, there is evidence of an inverse isotope effect of comparable magnitude to what we observe with the P450nor enzyme from *H. capsulatum*. Sutka *et al.*[55c] also observed markedly large variation in $\delta^{15}N$ of -74.7 to -6.6 ‰, which was attributed to the potential for diffusion of substrates into the cell to limit expression of the enzymatic fractionation during NO reduction in fungi.[78] Indeed, a correlation between $\delta^{15}N$ and the rate constant was observed which is consistent with diffusion control of both the reaction rate and the net isotopic fractionation. Consequently, the contrast in the direction and magnitude of fractionation factors for N_2O production between the entire fungal denitrification process and those of purified fungal P450nor may be the result of variable expression of the small fractionation imposed by diffusion of substrates into and out of cells. In other words, the large isotope effect associated with enzymatic reduction can only be expressed when diffusion does not limit the supply of NO to the enzyme. When diffusion is limiting, isotopic discrimination by the enzyme cannot be expressed as all available NO to the enzyme is reduced.[56] An additional isotope effect is undoubtedly imposed by the reduction of nitrite to NO

during fungal denitrification that was also not a factor in this current study because we used NO as the substrate. Because there is a tendency for the most rate limiting step in denitrification to control the expressed fractionation, the fractionation observed in fungal denitrification may largely have been controlled by diffusion, nitrite reduction to NO, and/or reduction of NO. Further, it is conceivable that the rate-limiting step changed during the course of the fungal culture reactions or that the fractionation of the individual steps ($NO_3^- \rightarrow NO_2^- \rightarrow NO \rightarrow N_2O$) partially cancel one another. Thus, compared to experiments utilizing microbial cultures, it is likely that our results more accurately describe the isotope effects associated specifically with NO reduction to N_2O catalyzed by the P450 enzyme.

Nonetheless, it is recognized that SP must be controlled by the NO reduction step given that it is during this process that two NO atoms are joined to produce the linear, asymmetric N_2O molecule.[62] Schmidt *et al.* (2004)[62b] proposed that SP would invariably experience fractionation given the unique pathway of formation for each N atom in N_2O by both P450nor and bacterial nitric oxide reductase, but no supporting data was provided. Our study clearly demonstrates that there is substantial fractionation in SP during N_2O formation from the P450nor enzyme. In other words, we found that the fractionation factors for $\delta^{15}N^{\alpha}$ and $\delta^{15}N^{\beta}$ are not equivalent, which is in contrast to what has been observed in microbial culture.[55c, 58] Curiously, no alteration was observed in SP during *in vivo* N_2O production in pure culture, while we observed a clear trend *in vitro* with purified P450nor. Because the two N atoms in N_2O combine during the NO reduction step, SP values should be independent of the steps preceding NO reduction, and one would therefore expect *in vivo* and *in vitro* studies to give similar results. Although the reduction of N_2O to N_2 is known to affect SP,[59] the species of fungi cultured in Sutka *et al.*[55c] lack the ability to reduce N_2O, and this can therefore not explain the different SP results.

Interestingly, the SP values obtained near the end of the P450nor experiment (with an extent of conversion of approximately 60%) was approximately 29‰ (Figure 26) which is similar to the SP value of 37‰ observed by Sutka *et al.*[55c] Extrapolation of our data to 100% conversion indicates that SP values during NO reduction by the fungal NOR enzyme could reach 55-60‰. It is puzzling that we observed a wide range of SP values over the course of NO reduction whereas in pure fungal cultures the SP values during nitrite reduction were nearly constant at 37‰. If the value of 37‰ is entered into the Rayleigh equation for SP (obtained by linear regression in Figure 25) we obtain an extent of conversion (1-*f*) within the fungal cultures of approximately 65%. This seems to imply that the rate of nitrite and NO reduction are the same (thereby maintaining a steady NO concentration in the cell), and that the magnitude of the P450nor NO binding constant (K_d) maintains (1-*f*) at 65%. Nonetheless, the observation of an inverse isotope effect in one culture of fungi in Sutka *et al.*[55c] indicates that nitrite and NO reduction do not work in harmony under all circumstances.

The observation of constant SP values in microbial cultures even as substrates are depleted[58b, 79] has led some to suggest that SP could be used as a conservative tracer of N_2O production, and in fact, this approach has been used in a number of studies.[60a, 80] Indeed, the predominance of low SP values for N_2O evolving from soils provides a strong indication that bacterial denitrification is the predominant microbial source of this gas in many terrestrial ecosystems.[48b, 60] Our results, however, clearly indicate that fractionation of SP during N_2O production by P450nor is not zero, and that SP values higher and lower than the proposed end member value of 37‰ can be expected during fungal denitrification. Therefore, extra caution should be taken when one tries to determine the sources of N_2O production under different field settings as various growth conditions (i.e. pH, moisture level, nutrient source, etc.) might perturb

the flux in the denitrification pathway, thereby altering the intracellular NO concentration and resulting in a change of the SP value. Nonetheless, the observation of constant SP in pure culture implies a steady NO concentration is maintained in the cell under many growth conditions.

In summary, isotopic fractionation patterns during NO reduction ($NO \rightarrow N_2O$) catalyzed by fungal P450nor were analyzed in detail. The O and N^{α} showed normal isotope effects while the bulk $\delta^{15}N$ and $\delta^{15}N^{\beta}$ exhibit inverse isotope effects. These data are consistent with the sequential binding and reduction reaction mechanism proposed for P450nor. The high sequence identity observed among fungal P450nors suggests that these isotopic fractionation patterns may be characteristic of this entire class of enzyme. Interestingly, the SP values showed isotopic enrichment during the course of the reaction, indicating that the SP value associated with a specific pathway may not remain constant in pure microbial culture or in the field.

Acknowledgement

The research was funded by the National Science Foundation (EAR-1053432). We would like to thank Kateri Salk (Michigan State University) for her help in setting up the GC-IRMS for the analysis of NO-N_2O exchange reaction and Nicolai Lehnert (University of Michigan) for helpful discussions.

BIBLIOGRAPHY

BIBLIOGRAPHY

1. Giauque, W. F.; Johnston, H. L., An isotope of oxygen, mass 18. *Nature (London, U. K.)* **1929,** *123* (Copyright (C) 2014 American Chemical Society (ACS). All Rights Reserved.), 318.

2. Birge, R. T.; Menzel, D. H., The Relative Abundance of the Oxygen Isotopes, and the Basis of the Atomic Weight System. *Physical Review* **1931,** *37* (12), 1669-1671.

3. Urey, H. C.; Murphy, G. M.; Duncan, J. A., A HYDROGEN DISCHARGE TUBE FOR THE CONTINUOUS ULTRAVIOLET SPECTRUM. *Review of Scientific Instruments* **1932,** *3* (9), 497-498.

4. Lewis, G. N.; Macdonald, R. T., Concentration of H2 Isotope. *The Journal of Chemical Physics* **1933,** *1* (6), 341-344.

5. (a) Cremer, E.; Polanyi, M., Test of "tunnel" theory of heterogeneous catalysis on hydrogenation of styrene. *Z. physik. Chem.* **1932,** *B19* (Copyright (C) 2014 American Chemical Society (ACS). All Rights Reserved.), 443-50; (b) Eyring, H., The Zero Point Energy and the Separation of Isotopes. *Proceedings of the National Academy of Sciences* **1933,** *19* (1), 78-81.

6. Bigeleisen, J., Chemistry of Isotopes. *Science* **1965,** *147* (3657), 463-471.

7. Czajka, D. M.; Finkel, A. J.; Fischer, C. S.; Katz, J. J., *Physiological effects of deuterium on dogs*. 1961; Vol. 201, p 357-362.

8. Coggan, A. R., Use of stable isotopes to study carbohydrate and fat metabolism at the whole-body level. *Proc Nutr Soc* **1999,** *58* (4), 953-61.

9. Gannes, L. Z.; del Rio, C. M. n.; Koch, P., Natural Abundance Variations in Stable Isotopes and their Potential Uses in Animal Physiological Ecology. *Comparative Biochemistry and Physiology Part A: Molecular & Integrative Physiology* **1998,** *119* (3), 725-737.

10. Bigeleisen, J.; Lee, M. W.; Mandel, F., Equilibrium Isotope Effects. *Annual Review of Physical Chemistry* **1973,** *24* (1), 407-440.

11. Cleland, W. W., Use of isotope effects to determine enzyme mechanisms. *Journal of Labelled Compounds and Radiopharmaceuticals* **2007,** *50* (11-12), 1006-1015.

12. Northrop, D. B., Steady-state analysis of kinetic isotope effects in enzymic reactions. *Biochemistry* **1975,** *14* (12), 2644-2651.

13. Elsner, M., Stable isotope fractionation to investigate natural transformation mechanisms of organic contaminants: principles, prospects and limitations. *J. Environ. Monit.* **2010,** *12* (Copyright (C) 2014 American Chemical Society (ACS). All Rights Reserved.), 2005-2031.

14. Casciotti, K. L.; Sigman, D. M.; Hastings, M. G.; Böhlke, J. K.; Hilkert, A., Measurement of the Oxygen Isotopic Composition of Nitrate in Seawater and Freshwater Using the Denitrifier Method. *Analytical Chemistry* **2002,** *74* (19), 4905-4912.

15. Kendall, C.; Caldwell, E. A., Chapter 2 - Fundamentals of Isotope Geochemistry. In *Isotope* Tracers *in Catchment Hydrology*, McDonnell, C. K. J., Ed. Elsevier: Amsterdam, 1998; pp 51-86.

16. De Luca, G.; de Philip, P.; Dermoun, Z.; Rousset, M.; Vermeglio, A., Reduction of technetium(VII) by *Desulfovibrio fructosovorans* is mediated by the nickel-iron hydrogenase. *Appl. Environ. Microbiol.* **2001,** *67* (10), 4583-7.

17. Trincado, M.; Banerjee, D.; Grutzmacher, H., Molecular catalysts for hydrogen production from alcohols. *Energy Environ. Sci.* **2014,** *7* (8), 2464-2503.

18. (a) Walker, C. B.; He, Z.; Yang, Z. K.; Ringbauer, J. A.; He, Q.; Zhou, J.; Voordouw, G.; Wall, J. D.; Arkin, A. P.; Hazen, T. C.; Stolyar, S.; Stahl, D. A., The Electron Transfer System of Syntrophically Grown Desulfovibrio vulgaris. *Journal of Bacteriology* **2009,** *191* (18), 5793-5801; (b) Plugge, C. M.; Scholten, J. C. M.; Culley, D. E.; Nie, L.; Brockman, F. J.; Zhang, W., Global transcriptomics analysis of the Desulfovibrio vulgaris change from syntrophic growth with Methanosarcina barkeri to sulfidogenic metabolism. *Microbiology* **2010,** *156* (9), 2746-2756; (c) Li, X.; McInerney, M. J.; Stahl, D. A.; Krumholz, L. R., Metabolism of H2 by Desulfovibrio alaskensis G20 during syntrophic growth on lactate. *Microbiology* **2011,** *157* (10), 2912-2921; (d) Wrighton, K. C.; Castelle, C. J.; Wilkins, M. J.; Hug, L. A.; Sharon, I.; Thomas, B. C.; Handley, K. M.; Mullin, S. W.; Nicora, C. D.; Singh, A.; Lipton, M. S.; Long, P. E.; Williams, K. H.; Banfield, J. F., Metabolic interdependencies between phylogenetically novel fermenters and respiratory organisms in an unconfined aquifer. *ISME J* **2014,** *8* (7), 1452-1463.

19. (a) Lubitz, W.; Ogata, H.; Rudiger, O.; Reijerse, E., Hydrogenases. *Chem Rev* **2014,** *114* (8), 4081-148; (b) Vignais, P. M.; Billoud, B., Occurrence, classification, and biological function of hydrogenases: an overview. *Chem Rev* **2007,** *107* (10), 4206-72.

20. (a) Frey, M., Hydrogenases: hydrogen-activating enzymes. *Chembiochem* **2002,** *3* (2-3), 153-60; (b) Fontecilla-Camps, J. C.; Amara, P.; Cavazza, C.; Nicolet, Y.; Volbeda, A., Structure–function relationships of anaerobic gas-processing metalloenzymes. *Nature* **2009,** *460* (7257), 814-822.

21. (a) Silakov, A.; Wenk, B.; Reijerse, E.; Lubitz, W., 14N HYSCORE investigation of the H-cluster of [FeFe] hydrogenase: evidence for a nitrogen in the dithiol bridge. *Physical Chemistry Chemical Physics* **2009,** *11* (31), 6592-6599; (b) Berggren, G.; Adamska, A.; Lambertz, C.; Simmons, T. R.; Esselborn, J.; Atta, M.; Gambarelli, S.; Mouesca, J. M.; Reijerse, E.; Lubitz, W.; Happe, T.; Artero, V.; Fontecave, M., Biomimetic assembly and activation of [FeFe]-hydrogenases. *Nature* **2013,** *499* (7456), 66-69.

22. Pandelia, M.-E.; Ogata, H.; Lubitz, W., Intermediates in the Catalytic Cycle of [NiFe] Hydrogenase: Functional Spectroscopy of the Active Site. *ChemPhysChem* **2010,** *11* (6), 1127-1140.

23. Hatchikian, E. C.; Forget, N.; Fernandez, V. M.; Williams, R.; Cammack, R., Further characterization of the [Fe]-hydrogenase from Desulfovibrio desulfuricans ATCC 7757. *Eur J Biochem* **1992,** *209* (1), 357-65.

24. Krasna, A. I., Hydrogenase: Properties and applications. *Enzyme and Microbial Technology* **1979,** *1* (3), 165-172.

25. Yagi, T.; Higuchi, Y., Studies on hydrogenase. *Proc Jpn Acad Ser B Phys Biol Sci* **2013,** *89* (1), 16-33.

26. De Lacey, A. L.; Fernández, V. M.; Rousset, M.; Cammack, R., Activation and Inactivation of Hydrogenase Function and the Catalytic Cycle: Spectroelectrochemical Studies. *Chemical Reviews* **2007,** *107* (10), 4304-4330.

27. (a) Klein, A. R.; Hartmann, G. C.; Thauer, R. K., Hydrogen isotope effects in the reactions catalyzed by H2-forming N5,N10-methylenetetrahydromethanopterin dehydrogenase from methanogenic Archaea. *Eur J Biochem* **1995,** *233* (1), 372-6; (b) Zorin, N. A.; Dimon, B.; Gagnon, J.; Gaillard, J.; Carrier, P.; Vignais, P. M., Inhibition by iodoacetamide and acetylene of the H-D-exchange reaction catalyzed by Thiocapsa roseopersicina hydrogenase. *Eur J Biochem* **1996,** *241* (2), 675-81.

28. Chen, J.-S.; Mortenson, L. E., Purification and properties of hydrogenase from Clostridium pasteurianum W5. *Biochimica et Biophysica Acta (BBA) - Protein Structure* **1974,** *371* (2), 283-298.

29. Kreuzer, H. W.; Hill, E. A.; Moran, J. J.; Bartholomew, R. A.; Yang, H.; Hegg, E. L., Contributions of the [NiFe]- and [FeFe]-hydrogenase to H2 production in Shewanella oneidensis MR-1 as revealed by isotope ratio analysis of evolved H(2). *FEMS Microbiol Lett* **2014,** *352* (1), 18-24.

30. Cornish, A. J.; Gartner, K.; Yang, H.; Peters, J. W.; Hegg, E. L., Mechanism of proton transfer in [FeFe]-hydrogenase from Clostridium pasteurianum. *J Biol Chem* **2011,** *286* (44), 38341-7.

31. Cornish, A. J.; Gärtner, K.; Yang, H.; Peters, J. W.; Hegg, E. L., Mechanism of Proton Transfer in [FeFe]-Hydrogenase from Clostridium pasteurianum. *Journal of Biological Chemistry* **2011,** *286* (44), 38341-38347.

32. Shi, L.; Belchik, S. M.; Plymale, A. E.; Heald, S.; Dohnalkova, A. C.; Sybirna, K.; Bottin, H.; Squier, T. C.; Zachara, J. M.; Fredrickson, J. K., Purification and Characterization of the [NiFe]-Hydrogenase of Shewanella oneidensis MR-1. *Applied and Environmental Microbiology* **2011,** *77* (16), 5584-5590.

33. Zadvornyy, O. A.; Allen, M.; Brumfield, S. K.; Varpness, Z.; Boyd, E. S.; Zorin, N. A.; Serebriakova, L.; Douglas, T.; Peters, J. W., Hydrogen Enhances Nickel Tolerance in the Purple Sulfur Bacterium Thiocapsa roseopersicina. *Environmental Science & Technology* **2009,** *44* (2), 834-840.

34. Yang, H.; Gandhi, H.; Shi, L.; Kreuzer, H. W.; Ostrom, N. E.; Hegg, E. L., Using gas chromatography/isotope ratio mass spectrometry to determine the fractionation factor for H2 production by hydrogenases. *Rapid Commun Mass Spectrom* **2012,** *26* (1), 61-8.

35. Grubbs, F. E., Procedures for detecting outlying observations in samples. *Technometrics* **1969,** *11* (1), 1-21.

36. Michaelis, L.; Hill, E. S., The viologen indicators. *J. Gen. Physiol.* **1933,** *16* (6), 859-873.

37. De Laeter, J. R.; Böhlke, J. K.; De Bièvre, P.; Hidaka, H.; Peiser, H. S.; Rosman, K. J. R.; Taylor, P. D. P., Atomic weights of the elements: Review 2000. *Pure Appl. Chem.* **2003,** *75* (6), 683-800.

38. Elsner, M.; Zwank, L.; Hunkeler, D.; Schwarzenbach, R. P., A new concept linking observable stable isotope fractionation to transformation pathways of organic pollutants. *Environ. Sci. Technol.* **2005,** *39* (18), 6896-6916.

39. (a) Luo, Y.-H.; Steinberg, L.; Suda, S.; Kumazawa, S.; Mitsui, A., Extremely Low D/H Ratios of Photoproduced Hydrogen by Cyanobacteria. *Plant and Cell Physiology* **1991,** *32* (6), 897-900; (b) Arp, D.

J.; Burris, R. H., Isotope exchange and discrimination by the H2-oxidizing hydrogenase from soybean root nodules. *Biochimica et Biophysica Acta (BBA) - Protein Structure and Molecular Enzymology* **1982,** *700* (1), 7-15.

40. Sumner, I.; Voth, G. A., Proton Transport Pathways in [NiFe]-Hydrogenase. *The Journal of Physical Chemistry B* **2012,** *116* (9), 2917-2926.

41. Hexter, S. V.; Grey, F.; Happe, T.; Climent, V.; Armstrong, F. A., Electrocatalytic mechanism of reversible hydrogen cycling by enzymes and distinctions between the major classes of hydrogenases. *Proc Natl Acad Sci U S A* **2012,** *109* (29), 11516-21.

42. Torres, L.; Gelabert, R.; Moreno, M.; Lluch, J. M., Nuclear Dynamics Discrete Variable Representation Study of the Equilibrium Isotope Effect on H2 Binding in M(η2-H2)Ln Complexes: An Effective Theoretical Way To Account for Anharmonicity. *The Journal of Physical Chemistry A* **2000,** *104* (33), 7898-7905.

43. (a) Kubas Gregory, J., Molecular hydrogen complexes: coordination of a .sigma. bond to transition metals. *Accounts of Chemical Research* **1988,** *21* (3), 120-128; (b) Hay, P. J., Ab initio theoretical studies of a novel tungsten dihydrogen complex. *Chemical Physics Letters* **1984,** *103* (6), 466-469.

44. Vignais, P. M., H/D exchange reactions and mechanistic aspects of the hydrogenases. *Coordination* Chemistry *Reviews* **2005,** *249* (15-16), 1677-1690.

45. (a) Horibe, Y.; Craig, H., DH fractionation in the system methane-hydrogen-water. *Geochimica et Cosmochimica Acta* **1995,** *59* (24), 5209-5217; (b) Valentine, D. L.; Sessions, A. L.; Tyler, S. C.; Chidthaisong, A., Hydrogen isotope fractionation during H2/CO2 acetogenesis: hydrogen utilization efficiency and the origin of lipid-bound hydrogen. *Geobiology* **2004,** *2* (3), 179-188.

46. Bowen, G. J.; Kennedy, C. D.; Henne, P. D.; Zhang, T., Footprint of recycled water subsidies downwind of Lake Michigan. *Ecosphere* **2012,** *3* (6), art53.

47. (a) Kreuzer-Martin, H. W.; Lott, M. J.; Ehleringer, J. R.; Hegg, E. L., Metabolic Processes Account for the Majority of the Intracellular Water in Log-Phase Escherichia coli Cells As Revealed by Hydrogen Isotopes†. *Biochemistry* **2006,** *45* (45), 13622-13630; (b) Kreuzer-Martin, H. W.; Ehleringer, J. R.; Hegg, E. L., Oxygen isotopes indicate most intracellular water in log-phase Escherichia coli is derived from metabolism. *Proceedings of the National Academy of Sciences of the United States of America* **2005,** *102* (48), 17337-17341.

48. (a) Ravishankara, A. R.; Daniel, J. S.; Portmann, R. W., Nitrous oxide (N_2O): The dominant ozone-depleting substance emitted in the 21st century. *Science* **2009,** *326* (5949), 123-125; (b) Stein, L. Y., Surveying N_2O-producing pathways in bacteria. In *Methods in Enzymol.*, Academic Press: 2011; Vol. 486, pp 131-152.

49. (a) Climate change indicators in the United States: atmospheric concentrations of greenhouse gases. U.S. Environmental Protection Agency: http://www.epa.gov/climatechange/science/indicators/ghg/ghg-concentrations.html, 2013; (b) Montzka, S. A.; Dlugokencky, E. J.; Butler, J. H., Non-CO_2 greenhouse gases and climate change. *Nature* **2011,** *476* (7358), 43-50.

50. Ruser, R.; Flessa, H.; Schilling, R.; Beese, F.; Munch, J., Effect of crop-specific field management and N fertilization on N_2O emissions from a fine-loamy soil. *Nutr. Cycling Agroecosyst.* **2001,** *59* (2), 177-191.

51. Galloway, J. N.; Cowling, E. B., Reactive nitrogen and the world: 200 years of change. *Ambio* **2002,** *31* (2), 64-71.

52. Baggs, E. M., A review of stable isotope techniques for N_2O source partitioning in soils: Recent progress, remaining challenges and future considerations. *Rapid Commun. Mass Spectrom.* **2008,** *22* (11), 1664-1672.

53. (a) Barford, C. C.; Montoya, J. P.; Altabet, M. A.; Mitchell, R., Steady-state nitrogen isotope effects of N_2 and N_2O production in *Paracoccus denitrificans*. *Appl. Environ. Microbiol.* **1999,** *65* (3), 989-994; (b) Bryan, B. A.; Shearer, G.; Skeeters, J. L.; Kohl, D. H., Variable expression of the nitrogen isotope effect associated with denitrification of nitrite. *J. Biol. Chem.* **1983,** *258* (14), 8613-8617.

54. (a) Mariotti, A.; Landreau, A.; Simon, B., ^{15}N isotope biogeochemistry and natural denitrification process in groundwater: Application to the chalk aquifer of Northern France. *Geochim. Cosmochim. Acta* **1988,** *52* (7), 1869-1878; (b) Ostrom, N. E.; Hedin, L. O.; von Fischer, J. C.; Robertson, G. P., Nitrogen transformations and NO_3^- removal at a soil-stream interface: A stable isotope approach. *Ecol Appl* **2002,** *12* (4), 1027-1043.

55. (a) Naohiro, Y., ^{15}N-depleted N_2O as a product of nitrification. *Nature* **1988,** *335* (6190), 528-529; (b) Perez, T.; Garcia-Montiel, D.; Trumbore, S.; Tyler, S.; de, C. P.; Moreira, M.; Piccolo, M.; Cerri, C., Nitrous oxide nitrification and denitrification ^{15}N enrichment factors from Amazon forest soils. *Ecol Appl* **2006,** *16* (6), 2153-2167; (c) Sutka, R. L.; Adams, G. C.; Ostrom, N. E.; Ostrom, P. H., Isotopologue fractionation during N_2O production by fungal denitrification. *Rapid Commun. Mass Spectrom.* **2008,** *22* (24), 3989-3996.

56. Ostrom, N.; Ostrom, P., The isotopomers of nitrous oxide: Analytical considerations and application to resolution of microbial production pathways. In *Handbook of Environmental Isotope* Geochemistry, Baskaran, M., Ed. Springer: Berlin/Heidelberg: 2012; pp 453-476.

57. (a) Kool, D. M.; Wrage, N.; Oenema, O.; Dolfing, J.; Van Groenigen, J. W., Oxygen exchange between (de)nitrification intermediates and H_2O and its implications for source determination of NO_3^- and N_2O: a review. *Rapid Commun.Mass Spectrom.* **2007,** *21* (22), 3569-3578; (b) Kool, D. M.; Müller, C.; Wrage, N.; Oenema, O.; Van Groenigen, J. W., Oxygen exchange between nitrogen oxides and H_2O can occur during nitrifier pathways. *Soil Biol. Biochem.* **2009,** *41* (8), 1632-1641; (c) Kool, D. M.; Wrage, N.; Oenema, O.; Harris, D.; Van Groenigen, J. W., The ^{18}O signature of biogenic nitrous oxide is determined by O exchange with water. *Rapid Commun. Mass Spectrom.* **2009,** *23* (1), 104-108.

58. (a) Toyoda, S.; Mutobe, H.; Yamagishi, H.; Yoshida, N.; Tanji, Y., Fractionation of N_2O isotopomers during production by denitrifier. *Soil Biol. Biochem.* **2005,** *37* (8), 1535-1545; (b) Sutka, R. L.; Ostrom, N. E.; Ostrom, P. H.; Breznak, J. A.; Gandhi, H.; Pitt, A. J.; Li, F., Distinguishing nitrous oxide production from nitrification and denitrification on the basis of isotopomer abundances. *Appl. Environ. Microbiol.* **2006,** *72* (1), 638-644.

59. (a) Ostrom, N. E.; Pitt, A.; Sutka, R.; Ostrom, P. H.; Grandy, A. S.; Huizinga, K. M.; Robertson, G. P., Isotopologue effects during N_2O reduction in soils and in pure cultures of denitrifiers. *J.* Geophys. *Res.:Biogeosci.* **2007,** *112* (G2), G02005; (b) Jinuntuya-Nortman, M.; Sutka, R. L.; Ostrom, P. H.;

Gandhi, H.; Ostrom, N. E., Isotopologue fractionation during microbial reduction of N_2O within soil mesocosms as a function of water-filled pore space. *Soil Biol. Biochem.* **2008,** *40* (9), 2273-2280.

60. (a) Opdyke, M. R.; Ostrom, N. E.; Ostrom, P. H., Evidence for the predominance of denitrification as a source of N_2O in temperate agricultural soils based on isotopologue measurements. *Global Biogeochem. Cycles* **2009,** *23* (4), GB4018; (b) Ostrom, N. E.; Sutka, R.; Ostrom, P. H.; Grandy, A. S.; Huizinga, K. M.; Gandhi, H.; von Fischer, J. C.; Robertson, G. P., Isotopologue data reveal bacterial denitrification as the primary source of N_2O during a high flux event following cultivation of a native temperate grassland. *Soil Biol. Biochem.* **2010,** *42* (3), 499-506.

61. Yamazaki, T.; Hozuki, T.; Arai, K.; Toyoda, S.; Koba, K.; Fujiwara, T.; Yoshida, N., Isotopomeric characterization of nitrous oxide produced by reaction of enzymes extracted from nitrifying and denitrifying bacteria. *Biogeosciences* **2014,** *11* (10), 2679-2689.

62. (a) Stein, L. Y.; Yung, Y. L., Production, isotopic composition, and atmospheric fate of biologically produced nitrous oxide. *Annu. Rev. Earth Planet. Sci.* **2003,** *31* (1), 329-356; (b) Schmidt, H.-L.; Werner, R. A.; Yoshida, N.; Well, R., Is the isotopic composition of nitrous oxide an indicator for its origin from nitrification or denitrification? A theoretical approach from referred data and microbiological and enzyme kinetic aspects. *Rapid Commun. Mass Spectrom.* **2004,** *18* (18), 2036-2040.

63. Shoun, H.; Kim, D.; Uchiyama, H.; Sugiyama, J., Denitrification by fungi. *FEMS Microbiol. Lett.* **1992,** *94* (3), 277-281.

64. Frame, C. H.; Casciotti, K. L., Biogeochemical controls and isotopic signatures of nitrous oxide production by a marine ammonia-oxidizing bacterium. *Biogeosciences* **2010,** *7* (9), 2695-2709.

65. (a) Laughlin, R. J.; Stevens, R. J., Evidence for fungal dominance of denitrification and codenitrification in a grassland soil. *Soil Sci. Soc. Am. J.* **2002,** *66* (5), 1540-1548; (b) Spokas, K.; Wang, D.; Venterea, R.; Sadowsky, M., Mechanisms of N_2O production following chloropicrin fumigation. *Appl. Soil Ecol.* **2006,** *31* (1–2), 101-109; (c) Chen, H.; Mothapo, N. V.; Shi, W., The significant contribution of fungi to soil N_2O production across diverse ecosystems. *Appl. Soil Ecol.* **2014,** *73* (0), 70-77.

66. Chao, L. Y.; Rine, J.; Marletta, M. A., Spectroscopic and kinetic studies of Nor1, a cytochrome P450 nitric oxide reductase from the fungal pathogen *Histoplasma capsulatum*. *Arch.* Biochem. *Biophys.* **2008,** *480* (2), 132-137.

67. Toyoda, S.; Yoshida, N., Determination of nitrogen isotopomers of nitrous oxide on a modified isotope ratio mass spectrometer. *Anal. Chem.* **1999,** *71* (20), 4711-4718.

68. Mariotti, A.; Germon, J. C.; Hubert, P.; Kaiser, P.; Letolle, R.; Tardieux, A.; Tardieux, P., Experimental determination of nitrogen kinetic isotope fractionation: Some principles; illustration for the denitrification and nitrification processes. *Plant Soil* **1981,** *62* (3), 413-430.

69. Mariotti, A.; Leclerc, A.; Germon, J. C., Nitrogen isotope fractionation associated with the NO_2^- → N_2O step of denitrification in soils. *Can. J. Soil Sci.* **1982,** *62* (2), 227-241.

70. (a) Casciotti, K. L., Inverse kinetic isotope fractionation during bacterial nitrite oxidation. *Geochim. Cosmochim. Acta* **2009,** *73* (7), 2061-2076; (b) Casciotti, K. L.; McIlvin, M.; Buchwald, C., Oxygen isotopic exchange and fractionation during bacterial ammonia oxidation. *Limnol Oceanogr* **2010,** *55* (4), 1805-1805.

71. Lehnert, N.; Praneeth, V. K. K.; Paulat, F., Electronic structure of iron(II)–porphyrin nitroxyl complexes: Molecular mechanism of fungal nitric oxide reductase (P450nor). *J. Comput. Chem.* **2006,** *27* (12), 1338-1351.

72. Fry, B.; Gest, H.; Hayes, J. M., Isotope effects associated with the anaerobic oxidation of sulfide by the purple photosynthetic bacterium, *Chromatium vinosum*. *FEMS Microbiol. Lett.* **1984,** *22* (3), 283-287.

73. Kumita, H.; Matsuura, K.; Hino, T.; Takahashi, S.; Hori, H.; Fukumori, Y.; Morishima, I.; Shiro, Y., NO reduction by nitric-oxide reductase from denitrifying bacterium *Pseudomonas aeruginosa*: Characterization of reaction intermediates that appear in the single turnover cycle. *J. Biol. Chem.* **2004,** *279* (53), 55247-55254.

74. Daiber, A.; Shoun, H.; Ullrich, V., Nitric oxide reductase (P450nor) from Fusarium oxysporum. *J. Inorg. Biochem.* **2005,** *99* (1), 185-193.

75. Shiro, Y.; Fujii, M.; Iizuka, T.; Adachi, S.-i.; Tsukamoto, K.; Nakahara, K.; Shoun, H., Spectroscopic and kinetic studies on reaction of cytochrome P450nor with nitric oxide. *J. Biol. Chem.* **1995,** *270* (4), 1617-1623.

76. Obayashi, E.; Takahashi, S.; Shiro, Y., Electronic structure of reaction intermediate of cytochrome P450nor in its nitric oxide reduction. *J. Am. Chem. Soc.* **1998,** *120* (49), 12964-12965.

77. Franke, A.; Hessenauer-Ilicheva, N.; Meyer, D.; Stochel, G.; Woggon, W.-D.; van Eldik, R., Thermodynamic and kinetic studies on the binding of nitric oxide to a new enzyme mimic of cytochrome P450. *J. Am. Chem. Soc.* **2006,** *128* (41), 13611-13624.

78. Smemo, K.; Ostrom, N.; Opdyke, M.; Ostrom, P.; Bohm, S.; Robertson, G. P., Improving process-based estimates of N_2O emissions from soil using temporally extensive chamber techniques and stable isotopes. *Nutr. Cycl. Agroecosys.* **2011,** *91* (2), 145-154.

79. Well, R.; Flessa, H.; Jaradat, F.; Toyoda, S.; Yoshida, N., Measurement of isotopomer signatures of N_2O in groundwater. *J. Geophys. Res.: Biogeosci.* **2005,** *110* (G2), G02006.

80. Yamagishi, H.; Westley, M. B.; Popp, B. N.; Toyoda, S.; Yoshida, N.; Watanabe, S.; Koba, K.; Yamanaka, Y., Role of nitrification and denitrification on the nitrous oxide cycle in the Eastern Tropical North Pacific and Gulf of California. *J. Geophys. Res.: Biogeosci.* **2007,** *112* (G2), G02015.

81. Johnson, M. S.; Feilberg, K. L.; von Hessberg, P.; Nielsen, O. J., Isotopic processes in atmospheric chemistry. *Chem. Soc. Rev.* **2002,** *31* (6), 313-323.

82. Linder, D. P.; Rodgers, K. R.; Banister, J.; Wyllie, G. R. A.; Ellison, M. K.; Scheidt, W. R., Five-Coordinate FeIIINO and FeIICO Porphyrinates: Where Are the Electrons and Why Does It Matter? *J. Am. Chem. Soc.* **2004,** *126* (43), 14136-14148.

83. Huskey, W. P., *Enzyme Mechanism from Isotope Effects*. CRC Press: Boca Raton, FL, 1991.

CHAPTER 5

CONCLUSIONS AND FUTURE DIRECTIONS

In this thesis I demonstrated that by using stable isotopes and purified hydrogenase enzymes, the isotope fractionation factors can be measured and determined with the help of isotope ratio mass spectrometry (Chapter 2). Hydrogenases are enzymes that catalyze the reversible formation of H_2, which can be used as a clean and renewable energy. H isotopes have the potential to be a powerful tool in quantifying proton flux in hydrogenase-catalyzed reactions because the movement of H ions is involved in almost every essential step of the mechanism. However, because H_2 is highly diffusive, stable H isotopes have thus far not been widely used in studying biological H_2 production. Our proof-of-concept experiment provided the first efficient method to quantify the fractionation factors of the hydrogenase-catalyzed H_2 production process.

After establishing the method to measure the fractionation of hydrogenase-catalyzed reactions, I utilized this approach to determine the fractionation pattern for a number of [NiFe]- and [FeFe]-hydrogenases (Chapter 3). I ascertained the isotope fractionation patterns for each of the three reactions catalyzed by hydrogenases: H_2 production, H_2 consumption, and H_2-H_2O exchange. The measurements and analyses were used to facilitate our understanding of hydrogenase catalysis under physiological conditions where three reactions can occur simultaneously. In addition, the fractionation factors determined for a specific reaction (i.e. production, consumption, or H_2-H_2O exchange) for different hydrogenases can be used as signatures in studying H_2 metabolism in complex microbial communities where multiple hydrogenases coexist. In essence, the amount of H_2 in a microbial community is the composite of quantifiable contributions from different hydrogenases. Using a multiple component mixture equation (as exemplified in the work published by Kreuzer et al.[1]) and the fractionation factors for each hydrogenase, one can potentially quantify the fractions of H_2 produced or consumed by different hydrogenases in a microbial community.

Our analysis of the hydrogen production results indicated that all six hydrogenases displayed normal isotope effects, which indicated that the H_2 produced was severely depleted in ^2H relative to the substrate water. This result was consistent with the fact that deuterons formed stronger and less labile hydrogen bonds during H_2 production. More importantly, the fractionation factors for each class of hydrogenases appeared to cluster, which was consistent with the difference in active site structures between [FeFe]- and [NiFe]-hydrogenases. In our analysis, the three [NiFe]-hydrogenases ($\alpha = 0.27 - 0.40$) turned out to be statistically smaller than the three [FeFe]-hydrogenases ($\alpha = 0.41 - 0.55$). The results from the H_2 production study support our original hypothesis that fractionation factors can be used as signatures for different hydrogenases in the study of H_2 source partitioning in a complex microbial community where there are multiple hydrogenases.

In addition, the isotope fractionation patterns for H_2 consumption and H_2-H_2O exchange were also determined. In our analysis, the fractionation factors determined for H_2 consumption were approximately 0.88, consistent with metal-hydrogen binding studies in various M (η^2-H_2) complexes which displayed normal equilibrium isotope effects. The fact that the fraction factors were similar was surprising to us. We predicted that because of the distinct active site structures of [FeFe]- and [NiFe]-hydrogenases, that H_2 consumption would have different fractionation factors. We hypothesize that 0.88 is a net fractionation factor, and that steps other than H_2 oxidation (e.g. H_2 diffusion, H_2 consumption step, proton transfer, electron transfer, etc.) must be masking the true fraction factor. Nevertheless, the fractionation factors of the H_2 consumption process indicated that hydrogenase-catalyzed H_2 consumption exhibited a normal isotope effect, with hydrogen reacting faster than deuterium. Interestingly, we observed no obvious isotope

fractionation in the H_2-H_2O exchange experiments during the three-hour period of the reaction. Thus, under our reaction conditions, H_2-H_2O exchange is not occurring to a significant extent.

In addition to the study of purified hydrogenases, we also quantified the isotopic fractionation of purified fungal nitric oxide reductase, an enzyme that produces N_2O via the reduction of NO. Fungal nitric oxide reductases are generally called P450nor because of the involvement of a P450 heme in the active site. In this study, we used gas chromatography-isotope ratio mass spectrometry (GC-IRMS) to measure the $\delta^{15}N$, $\delta^{18}O$, $\delta^{15}N^{\alpha}$, and $\delta^{15}N^{\beta}$ of N_2O generated by purified fungal P450nor from *Histoplasma capsulatum*. These isotope values can provide us the information needed for both the calculation of fractionation factors and site preference values as well as the clarification of the reaction mechanism. First, the isotope values were used to calculate the fractionation factors, which indicated that O and N^{α} displayed normal isotope effects during enzymatic NO reduction. However, bulk N and N^{β} showed inverse isotope effects. Importantly, the observed inverse isotope effect in N^{β} provided support for reversible binding of the first NO in the proposed P450nor reaction mechanism. In addition, the isotope values were used to calculate site preference values, which is the difference between the $\delta^{15}N^{\alpha}$ and $\delta^{15}N^{\beta}$. The site preference value is a key index for identifying the sources and sinks of N_2O. In our experiments, however, we found that in contrast to the results reported from pure microbial culture studies, the site preference value was not constant in our purified enzyme analyses. These results suggested that site preference for microbial cultures can vary depending on the growth conditions, which may complicate source tracing during microbial denitrification.

Our study of the P450nor was well received by the scientific community, which prompted us to initiate a collaboration with a computational chemist. The information from the fractionation patterns determined in our P450nor studies was shared with Professor Nicolai Lehnert at The

University of Michigan. It is hoped that his expertise in computational modeling of the thermodynamics and reaction intermediates in N_2O biosynthesis[2] can be combined with our observed fractionation factor values in P450nor catalyzed NO conversion,[3] which will shed light on the details of the P450nor reaction mechanism.

Very recently, experiments using a similar approach were designed and initiated to determine the fractionation patterns for bacterial nitric oxide reductase. In addition to fungal P450nor, this enzyme is also a major player in microbial N_2O generation.[4] The analysis of this enzyme will not only contribute to our understanding of N_2O cycling in the environment, but also to the mechanism of bacterial N_2O biosynthesis.

In summary, we have demonstrated that stable isotopes can be a powerful tool in studying enzyme catalysis. In particular, the study of isotopic fractionation patterns of purified enzyme-catalyzed reactions can provide important information about reaction mechanisms (Chapter 2, 3, and 4) as well as intracellular metabolic homeostasis (Chapter 4).

BIBLIOGRAPHY

BIBLIOGRAPHY

1. Kreuzer-Martin, H. W.; Ehleringer, J. R.; Hegg, E. L., Oxygen isotopes indicate most intracellular water in log-phase *Escherichia coli* is derived from metabolism. *Proc. Natl. Acad. Sci. U.S.A.* **2005,** *102* (48), 17337-17341.

2. McQuarters, A. B.; Wirgau, N. E.; Lehnert, N., Model complexes of key intermediates in fungal cytochrome P450 nitric oxide reductase (P450nor). *Curr. Opin. Chem. Biol.* **2014,** *19* (0), 82-89.

3. Yang, H.; Gandhi, H.; Ostrom, N. E.; Hegg, E. L., Isotopic fractionation by a fungal P450 nitric oxide reductase during the production of N_2O. *Environ. Sci. Technol.* **2014,** *48* (18), 10707-10715.

4. Baggs, E. M., A review of stable isotope techniques for N_2O source partitioning in soils: recent progress, remaining challenges and future considerations. *Rapid Commun. Mass Spectrom.* **2008,** *22* (11), 1664-1672.